Diss. ETH Nr. **18142**

A dissertation submitted to the
SWISS FEDERAL INSTITUTE OF TECHNOLOGY
ZURICH
for the degree of
DOCTOR OF TECHNICAL SCIENCES

Assessment of methods to reduce tonal emission from high voltage transmission lines during and after precipitation

presented by
CLAUDIA ROERO
Dipl. Physics, Turin University, Italy
born on the 29th of November,1976
citizen of Italy

Zürich, December 2008

Accepted upon recommendation of
Prof. Dr. Klaus FRÖHLICH, examiner
Prof. Dr. Josef KINDERSBERGER, co-examiner

Certainly, if I know a drop of water
in all its internal determinations as a thing in itself,
and if the whole concept of any one drop is identical with that of any other,
I cannot allow that any drop is different from any other.
But if the drop is an appearance in space,
it has its location not only in the understanding (under concepts)
but in sensible outer intuition (in space)
and the physical locations are there quite indifferent
to the inner determinations of the things.

Gottfried Wilhelm von Leibniz

Acknowledgments

Without the help of a long list of people I would not have been able to write down this thesis. I am incredibly grateful to the many people who have gone out of their way to help me with these long, difficult years at ETH.

First of all, I want to express my gratitude to Prof. Dr. Klaus Fröhlich for his suggestions, hints, observations and interest in my work, but above all for his constant confidence in me.

Many thanks to Prof. Dr. Josef Kindersberger for having contributed in refining and enriching this thesis, for his efficient review of the work.

This work would not have been possible without the precious help and continuous support of Dr. Timm H. Teich, and I am also very grateful to him for the care with which he reviewed my thesis and a big amount of manuscripts in these years; and for conversations that clarified my thinking on every step of the project. Thank you also to the other members of the CONOR project, Dr. Ueli Straumann, Dr. Micha Semmler and Hans-Jürg Weber for their constant constructive criticism. A special thanks goes to Charles Sigrist, Heiko Vögeli and Henry Kienast for their efficient assistance with all technical problems.

I want to thank all the colleagues at the High Voltage Laboratory, their friendship and professional collaboration meant a great deal to me. In particular, I would like to thank my former office mates Stefan and Manfred for their moral and professional support. A special thanks to Karin, thanks for "being there", thanks for the nice conversations and for the massages.

The support of the work by EnBW (D), APG (A), Illwerke AG (A), PSEL (CH) and BUWAL (CH) has been greatly appreciated. I wish also to thank Mr. A. Biedermann, Dr. D. W. Bahnemann and Mr. V. H. Selzer for the provision of coatings and materials for the laboratory experiments.

A special “thank you so much” goes to my Italian friends in Zürich: Chiara, Maria and Paola for their moral support, to Flavio, Luca, Valerio, Davide and Francesca for making me laugh a lot.

Thanks also to all my best friends from Asti, Claudia, Rosaria, Donato, Elena, Maurizio, Silvia and Valentina, for their saint-like patience every time.

I want to thank my parents Giorgio and Teresa, my brother Marco and my favorite aunt Carla, who supported and encouraged me a lot through all these years.

Finally, I owe a special thanks to Stefan. Without his encouragement, support and motivation when we were just colleagues and his endless love, patience and understanding since we are together, this work would not have been finished.

Thanks again to all of you.

Zurich, December 2008 Claudia Roero

Contents

Abstract

Existing overhead transmission lines have been upgraded to higher voltage levels for economical reasons. Excessive tonal noise from wet high voltage lines has locally become an acute problem and sensibility to the problem has increased in the past few years within a general awareness to environmental problems. Network operators face the problem by taking into consideration the possibility to modify lines or take other measures to achieve noise reduction. Tonal noise has been recognized as a foul weather problem, particularly annoying during nighttime when the background noise is low. During and after precipitation, AC high voltage lines emit two kinds of noise: a wide-spectrum hissing, mostly in the kHz range, and an almost pure tone, called tonal noise, at twice mains frequency ($2f$ = 100 Hz in Europe), in some places at levels apparently unacceptable to local residents.

To assist efforts to elucidate the processes involved in the generation of tonal acoustic emissions from high voltage conductors, the project CONOR (COrona NOise Reduction) was started. The work of CONOR was directed at finding the real causes of the tonal emission and to propose and assess economically viable solutions for its reduction. In particular, the work presented here concentrates on the assessment of methods to quantify the effectiveness of such solutions.

Tonal emission from high voltage lines, which residents recognize as a foul weather problem, has been traced to a discharge mechanism where charges are injected into the air nearby and act upon the neutral gas. This charge injection takes place from particular sites of elevated electrical field strength such as blemishes on conductors and other hardware surfaces and - most importantly - water drops. Thus, a possible way to reduce tonal emissions is to keep everywhere field strengths low to avoid discharge inception. In this context, conductor arrangements and bundle configurations have been considered. An alternative way is to eliminate or reduce the number of water drops to speed up the drying of the line. Previous investigations demonstrated that the use of ultra-hydrophilic coatings and thus the reduction of the population of deformable water drops on the conductors by encouraging runoff and drying can provide a significant reduction of sound emissions produced by overhead high voltage transmission lines during and after wet weather conditions;

the effects are particularly pronounced after the cessation of rain. However, the coatings used in those investigations had not been proved to persistently show hydrophilic behaviour on high voltage conductors in active use over many years. Therefore, the main factors that influence the ageing of coatings applied to high voltage lines have been analyzed in this work which concentrates on describing a method to quantify the effectiveness of the use of such hydrophilic coatings and to provide a classification of properties which a suitable coating for high voltage lines must have.

The first step in evaluating a coating is to observe the behaviour of single sessile water drops resting on that coating in an electric field. A new set-up for detailed optical investigation of drop deformation was used and has proved in this context its capability to yield significant information on the parameter dependence of deformation of water drops in an electric field. These investigations showed that the voltage at which instability is reached depends strongly on the shape of the water droplet and thus on the surface contact angle - which in turn is controlled by the surface properties. The voltage at which a water drop elongates in the direction of the electric field increases strongly with a reduction in zero-field contact angle and decreases with increasing drop volume. This underlines the beneficial effect of hydrophilicity of conductor surfaces in reducing wet weather discharge activity from high voltage conductors. AC investigations showed the different oscillation modes and resonances of water drops in the frequency range of particular interest (100 Hz). Records of motion sequences for different size drops in an AC field demonstrated that the resonance frequency of water drops does not only depend on the volume of the water drops and on the applied electric field strength, it also depends on the surface properties of the materials on which the drop sits.

The following step in the quantification of the efficacy of a coating to be used to cover high voltage lines, is to be the evaluation of the drop populations and their development on different surfaces. The combination of the study of the behaviour of the water drop population and of the single drop deformation is meant to assist in the approach to a method to assess the lifetime of the coatings. Since drop populations on electrically stressed surfaces have to the best of the author's knowledge not been described in literature, their change with time, geometry, applied electric field strength and surface properties have been investigated here. A method to measure the drop size distributions which allows a geometric drop size classification during rain and at different times after the cessation of a rain period is proposed. Investigations showed that the application of an electric field to the line yields an alteration of the drop size distribution, as drops of particular sizes may undergo resonant deformation.

A major task in the context of the evaluation of coatings is then the development of a methodology that mimics and/or accelerates the effects of weathering of coatings applied to real high voltage cables which would come about in service over many years. Although in general it is very difficult to duplicate all of the variables associated with a coatings environment, to test future performance of the coatings, continuous environmental testing and accelerated weathering have been successfully performed and planned. A method to establish the long-term stability and effectiveness of various coatings applied to high voltage lines has been proposed and tested in order to single out the coating which most persistently shows hydrophilic behaviour.

Analysis of the various coatings applied to a choice of substrates indicates that a silica based hydrophilic coating and a TiO_2 based super-hydrophilic preparation have a potential for long life when applied to high voltage conductors. However, the hydrophilicity of the silica based coatings appears inferior compared with that of the titania based one because it does not have the photocatalytic properties and thus the associated self-cleaning effect expected with anatase TiO_2.

Kurzfassung

Zur Erhöhung der Übertragungskapazität werden Betriebspannungen existierender Hochspannungsleitungen erhöht. Als Folge davon sind örtlich begrenzt bei nassen Leitungen Probleme mit zu hoher tonaler Schallemission aufgetreten. Hinzu kommt auch, dass die Empfindlichkeit der Bevölkerung gegenüber Umweltbelastungen in den letzten Jahren stark zugenommen hat. Netzbetreiber sehen sich genötigt, lokal Massnahmen zu ergreifen, um die Schallemission der Leitungen zu verringern. Das könnte mit erheblichen Kosten verbundene Umbauten erfordern, falls keine günstigeren Lösungen gefunden werden.

Die Schallemission der Leitungen ist im allgemeinen ein Schlechtwetterproblem; der Schall wird als besonders störend zur Nachtzeit empfunden, wenn andere Hintergrundgeräusche niedrige Pegel haben. Bei Wechselspannung emittieren Hochspannungsleitungen während und nach Niederschlag zwei Arten von Lärm: Ein rischendes oder knatterndes Geräusch mit einem breitbandigen Spektrum überwiegend im kHz - Bereich und ein tonales Geräusch bei der doppelten Netzfrequenz, 100 Hz in Europa. Die Pegel von letzterem können lokal als unerträglich empfunden werden.

Das Bemühen um Abhilfe verlangt zunächst einmal das Verstehen der Prozesse, die den Lärm verursachen. Zu diesem Zweck wurde in Zusammenarbeit von Industrie, Behörden und der Hochschule das Projekt CONOR (CORona NOise Reduction) ins Leben gerufen. Ausser mit dem Verständnis der Vorgänge befassten sich die Projektarbeiten auch mit der Suche nach wirtschaftlich vertretbaren Abhilfemassnahmen und der Einschätzung von deren Wirksamkeit unter verschiedenen Bedingungen.

Beide Arten von Lärmemission - breitbandig und niederfrequent tonal - haben ihren Ursprung in Entladungsprozessen. Die Mechanismen sind aber verschieden. Die *tonale* Emission lässt sich auf die Bewegung von Ionen im elektrischen Feld zurückführen, die ihren Impuls auf neutrale Gasmoleküle übertragen. Die Ladungsinjektion findet an Orten erhöhter elektrischer Feldstärke statt, das können einmal Stellen mechanischer Schäden an Leitungen und Armaturen sein, vor allem aber Wassertropfen. Eine Massnahme zur Vermeidung

tonaler Emission wäre es, die Feldstärken überall so niedrig zu halten, dass die Einsatzfeldstärke elektrischer Entladungen nicht erreicht wird. In diesem Zusammenhang wurden Bündelgeometrien und Leiteranordnungen untersucht. Ein anderer Weg wäre die Unterdrückung oder wenigstens die Verringerung der Tropfenbildung auf der Leitung und eine Beschleunigung des Abtrocknens nach Niederschlag. Vorangehende Untersuchungen haben gezeigt, dass stark hydrophile Leiteroberflächen das Vorkommen der Wassertropfen auf die Unterseite der Leitungen beschränken. Das Abtropfen fördern und das Abtrocken sehr erheblich beschleunigen, so dass die gesamte Schallemission - vor allem nach Aufhören des Niederschlags - beträchtlich verringert wird. Die Dauerhaftigkeit der bei jenen Studien benutzten Oberflächenbehandlungen war nicht bewiesen - schliesslich müssen die guten Eigenschaften bei praktischem Einsatz über viele Jahre erhalten bleiben und dabei intensiven elektrischen Entladungen widerstehen können. In dieser Arbeit werden daher nicht nur die Anfangseigenschaften der Leiteroberflächen untersucht, sondern auch die Faktoren, die eine Alterung bewirken können. Dazu werden Methoden zur Klassifizierung der Eigenschaften angegeben und Forderungen an die Oberflächenbehandlungen gestellt.

Der erste Schritt in der Evaluation einer Oberfläche ist die Beobachtung des Verhaltens einzelner Wassertropfen auf einer horizontalen Fläche unter dem Einfluss des elektrischen Feldes. Ein neuer Aufbau zur optischen Untersuchung der Deformation von Wassertropfen im Feld wurde in Betrieb genommen und lieferte signifikante Informationen über die Parameterabhängigkeit des Tropfenverhaltens. Es zeigte sich, dass die Spannung, bei der Instabilität auftritt, stark von der Form des Tropfens abhängt, also von den Oberflächeneigenschaften, die sich im Kontaktwinkel manifestieren. Die Spannung, bei der der Wassertropfen in Richtung des Feldes verformt wird, nimmt stark zu bei Verringerung des Randwinkels (ohne Feld gemessen) und bei Reduktion des Tropfenvolumens. Dieses Verhalten unterstreicht die Nützlichkeit einer gut hydrophilen Leiteroberfläche zur Unterdrückung von Entladungsaktivität bei nassem Wetter. Untersuchungen mit Wechselspannung zeigten die verschiedenen Schwingungsmoden und Resonanzen der Wassertropfen bei niedrigen Frequenzen insbesondere nahe bei 100 Hz. Aufnahmen der Bewegungsfolgen von Tropfen verschiedenen Volumens bei Wechselspannung unterschiedlicher Frequenz zeigten, dass die Resonanzfrequenz nicht nur von Volumen und Feldstärke abhängt, sondern auch von den Oberflächeneigenschaften des Substrats.

Der nachfolgende Schritt in der Quantifizierung der Wirksamkeit der für Hochspannungsleiter vorgesehenen Oberflächenbehandlung war eine Untersuchung der Tropfenpopulationen und deren zeitlicher Veränderung auf verschiedenen

Oberflächen. Die Kombination der Studien des Verhaltens der Tropfenpopulationen mit den Kenntnissen über die Deformation einzelner Tropfen soll die Bemühungen um die Entwicklung einer Methode zur Einschätzung der Beständigkeit von behandelten Oberflächen unterstützen. Nach bestem Wissen des Autors sind Tropfenpopulationen auf mit elektrischen Feldern beaufschlagten Oberflächen bisher nicht in der Literatur beschrieben, ihre Veränderlichkeit bezüglich Zeit, Geometrie, angelegter Feldstärke und Oberflächeneigenschaften wird hier untersucht. Es wird eine Methode vorgeschlagen, die Tropfengrössenverteilung zu messen und einer geometrischen Grössen - Klassifikation zu unterwerfen - sowohl während des Regens als auch für verschiedene Zeiten nach dem Aufhören des Niederschlags. Die Untersuchungen zeigen, dass die Tropfengrössenverteilungen durch Anlegen eines elektrischen Feldes verändert werden - Tropfen einer gewissen Grösse unterliegen Deformation in Resonanz.

Eine wichtige Aufgabe im Zusammenhang mit der Erprobung von Oberflächenbehandlungen ist die Entwicklung von Methoden, die die Belastungen nachahmen, denen die Leiteroberflächen bei realen Hochspannungsleitungen bei Einsatz über viele Jahre ausgesetzt wird. Entsprechende Vorschläge werden hier angeboten, die Methoden sollen helfen, die besten Oberflächenbehandlungen auszuwählen, die beständige, sehr gute Hydrophilie bieten.

Die zahlreichen untersuchten Oberflächenbehandlungen führen zu dem Schluss, dass sich bezüglich leichter Verarbeitung und guter und beständiger Hydrophilie sich zwei Beschichtungsmaterialen für Anwendung auf Hochspannungsleitern qualifizieren, eines auf SiO_2 - Basis, das andere auf Basis von TiO_2 (Anatase), das den zusätzlichen Vorteil photokatalytischer Wirksamkeit zeigt, so dass gegenüber organischen Verunreinigungen ein selbstreinigender Effekt erwartet werden darf.

1 Problem statement

Electrical energy is transported across the countryside by means of *high voltage* lines because the line losses are much smaller than with *low voltage* lines. When the electric field on the surface of any conductor (i.e., surface gradient) exceeds the breakdown strength of air, about 30 kV/cm, corona discharges occur. These discharges generate light, audible noise, radio noise, and cause also some energy loss. Audible noise from conductor corona may locally infringe noise standards, while radio noise from conductor corona may interfere with communication or navigation systems. "Corona loss"is one of the reasons why the transmission of electrical energy between two points is considered to be not perfect. However, in general, corona loss is significantly lower than resistive loss. Nevertheless, at higher voltages, high altitudes and during foul weather, corona loss can actually become quite significant.
Noise emissions and corona loss from most high voltage lines are considered unproblematic in dry weather. However, in foul weather conditions water drops on the line may led to intense discharge activity. With AC lines two types of acoustical noise may result: crackling/hissing (in the kHz range and efficiently picked up in A-weighted sound pressure measurement) and an almost pure tone at twice mains frequency ($2f$ = 100 Hz in Europe) classed as *tonal* noise [1] and perceived as particularly annoying especially during the night when the hum may become the dominating noise in the locality.
At the early days of line corona studies, considerable investigations have been done concerning audible noise from equipment such as transformers and switchyards [2] and the focus was on the hissing noise at high frequencies. Corona noise levels are characterized by a frequency spectrum covering a wider band than other environmental noises. Sensibility to noise emissions has increased in the past few years within a general awareness to environmental problems [3]. So far, the electric power supply industry encounters locally the problem of an increasing number of complaints about unacceptable noise levels, in particular tonal noise [1], by people living close to transmission lines. Theoretical and experimental studies have been carried out to predict this type of audible noise, but, while high frequency noise has been successfully linked to discharge activities, the origin of tonal noise was still under investigation.
A research team of High Voltage Laboratory of the ETH Zurich initiated in 2002 the project CONOR (COrona NOise Reduction) to establish the cause

of tonal emission from high voltage lines, as the hypothesis widely put forward in the literature appeared not very credible. The solution of this problem should facilitate the prediction of tonal noise levels the choice of transmission lines which produce less noise and thus cause less annoyance to people living near such lines. Once the processes involved have been understood, the aim was to propose and assess economically viable methods for effective reduction of tonal emission and to be able to calculate and predict tonal noise levels at any of a broad range of meteorological conditions. The four principal goals of CONOR can be summarized as:

1. Comprehension of the mechanism of tonal noise emission.

2. Provide a method to compute tonal noise levels in dependence of bundle geometry, phase configuration, operating voltage and weather conditions.

3. Assessment of measures to reduce tonal noise and their experimental verification.

4. Development of a methodology to verify and quantify the effectiveness of the measures.

The first two points and part of the third are presented in another doctoral thesis [4], where a method to compute the $2f$ emissions is given. What is still lacking is the correlation with rainfall intensity and the dependence on other climate conditions, such as snow, fog and hoar frost. In the work mentioned it is also pointed out that $2f$ emissions are firmly associated with electrical discharges from sites of elevated field strength and from protrusions such as are constituted by water drops. Thus, one method to reduce the electric field strength in the relevant places is the use of larger bundle geometries, as reported in the literature and as investigated in detail in [4]. Furthermore, a way to reduce the formation of water drops which will be subjected to deformation has been found to be the use of a special hydrophilic surface preparation to cover the high voltage lines [5, 6, 7, 8]. What it is still missing is a method to quantify the effectiveness of the use of such hydrophilic coatings and that is the principal aim of this work. To achieve this aim, the following questions have to be answered:

- What is the behaviour of single water drops under electric field on various surfaces and conductor types?

- What does the drop population look like on different conductors carrying different coatings?

- What are the preliminary investigations that need to be done to establish whether a certain coating would be suitable to cover high voltage lines?
- Once a coating is confirmed as potentially good for high voltage lines, can a general method be developed to investigate its effectiveness with respect to all parameters of interest (e.g. geometry, age, material and stranding of the conductor)?

2 State of the art

This chapter offers the basis to a better understanding of the work. It summarizes important information already known in the literature, that is necessary to built a method to analyze and quantify properties of hydrophilic coatings applied to high voltage lines.

2.1 Corona noise from high voltage lines

The principal aim of this section is to provide the description of the general characteristics of corona noise and its manifestation. As the application of hydrophilic coatings to conductor should prevent or at least reduce the corona-generated noise, focus here is to describe its properties and the problems the noise can cause. In addition, the role of parameters that influence corona noise is clarified.

2.1.1 Corona discharge

Under *homogeneous* field conditions, exceeding a certain critical value of density reduced field strength E/N invariably leads to complete breakdown. However, if the field is strongly divergent, a self-sustained "partial"discharge can exist without necessarily leading to flashover. Such discharges are arrested as a consequence of field geometry and/or space charge buildup.
High voltage transmission lines represent structures with highly inhomogeneous fields normally laid out and operated in such a way that a breakdown will not occur. However, conditions may be encountered under which local low power discharges cannot be entirely avoided without incurring a cost penalty due to over-generous dimensioning. Any discharges on a high voltage installation - especially on an AC overhead line - have undesirable effects: acoustical noise (AC), radio influence (interference) (RI), energy loss and - though less important - gas chemistry and conductor corrosion [9, 10]. In order to have an idea how to minimize detrimental effects, one has tried - for a long time - to understand the processes controlling corona in the hope to gain insights which can be utilized in improved line design. Early investigations using merely a point-plane setup led to the recognition that space charge at the highly stressed electrode leads to a (nearly) constant surface field strength

almost irrespective of applied voltage above the inception level. To be closer to the transmission line geometry, cylindrical conductor - plane and coaxial cylinder configurations have been used for in-depth investigations, in addition to full scale test lines.
Corona modes come in at least seven different forms and transitions between these, all strongly influenced by a number of parameters: conductor size, its configuration and surface properties, conductor spacing [11], overall applied voltage, surface field strength of the highly stressed electrode (usually the conductor) and its derivative dE/dr, ambient air density, radial current density at the particular corona type, frequency or polarity of the applied voltage.

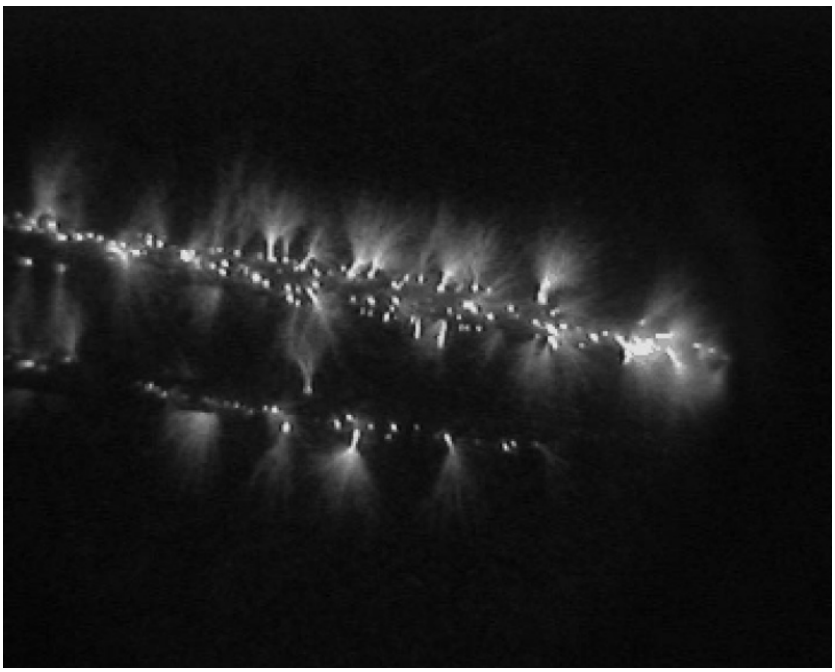

Figure 2.1: Manifestation of corona discharge on a bundled conductor viewed by a UV image converter.

Inspection of Figure 2.1 gives already a vague idea that quite different forms of corona may co-exist at the same time, particularly with a heterogeneous array of water drops on the conductor surface. The ionization zone manifest itself by light emission, much of it in the UV, from nitrogen molecules excited by electron impact. The active discharge space need not be as extensive as in that illustration, it may have only mm dimensions.
So far, the physical corona phenomena have mostly been described for dry conductors. What appears to be a very complete list has been given by Trinh [9] based on his studies which involved ocular observation, current measurement and time-resolved light emission picked up by photomultiplier. In the following, a much abbreviated summary of Trinh's listing will be given.

Negative DC corona For negative DC corona three types are listed:

1. Trichel streamers: These originate from short range electron avalanches with copious feedback presumably by positive ions. The electrons survive on their radial track only until they enter a zone in which attachment is greater than ionization, thus building up a negative ion population which will screen the cathode spot of origin and thereby choke the discharge. The current measurement shows a regular sequence of fast rise pulses, repetition kHz to MHz depending on geometry and voltage. The tail of these pulses (current and light emission) shows a weak persisting component indicating the short term establishment of a glow. Increase in voltage leads to an increase in frequency, not in amplitude, and an increase in the number of active sites.

2. Negative pulseless glow: This "miniature"glow discharge may be reached with increase of voltage or even found co-existing with Trichel streamers or toggling between the two forms, developing out of the short term glows of Trichel pulses. Once established, the pulseless glow constitutes a very stable discharge form, in appearance characterized by a contraction of the base of the "fan"previously seen with the Trichel streamer pulses (mm dimensions).

3. Negative streamers: With further increase in voltage, there is increased removal of negative ions until then restricting the extension of the discharge, so that the positive column can proceed further into the gap and by construction form a streamer channel. This mode is not observed with AC corona (see below).

Positive DC corona
For positive DC corona four types are listed:

1. Burst corona: Sporadic electrons originating in the gas space near the positive electrode form growing avalanches manifesting themselves by a faint glow on the anode surface and by small positive pulses (5 μs); positive space charge terminates the discharge which may then re-occur in another nearby spot.

2. Onset streamers: A typical streamer development with relatively high current pulses, say 30 mA/100 ns: the positive ion tail of an inward electron avalanche "attracts"further avalanches and thus lets the streamer channel proceed away from the anode. In this way a large number of filamentary channels develop and extend put into the gap, all originating from a common stem (see Figure 2.2 [12]). This form of discharge is possibly much enhanced by electron detachment from negative oxygen

ions in the high field near the anode. The discharge is terminated by its own residual positive space charge.

3. Positive glow: With voltage further increased, space charge removal at the anode becomes even more effective and thus allows intense ionization by electrons detached from negative ions. The current is steady with superimposed pulses at a high frequency, the appearance is a thin luminous sheath covering the anode.

4. "Breakdown streamer"(as these can exist without producting breakdown, Hermstein (in discussion to [13]) suggested the name "positive brush streamers"): With the further increase in voltage and thus a better clearing of space charge at the anode, streamers once more appear: There are local streamer spots of intense ionization activity moving slowly over the anode surface, and with further removal of positive space charge the streamers can grow radially and may cross the gap. This does not necessarily constitute breakdown as the filamentary region may not be highly conducting.

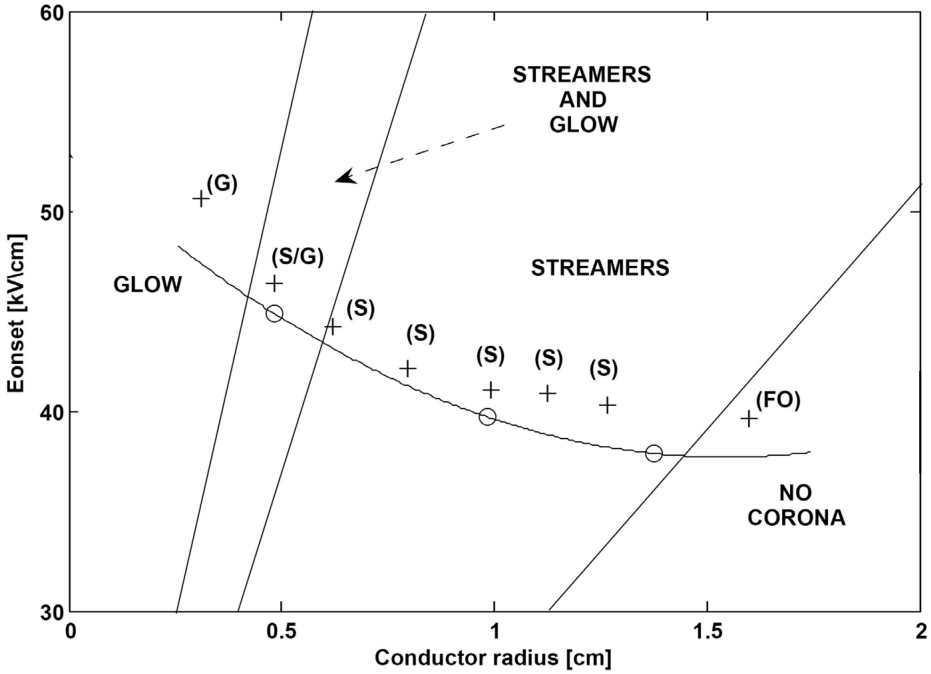

Figure 2.2: Corona onset fields and discharge forms. (G) = glow. (S) = streamers. (FO) = flashover. + = positive corona. ○ = negative and AC corona [12].

AC corona

AC corona for large gaps may undergo same modification from the DC processes from ions not absorbed by the electrodes but left in the gap from the

previous half-wave and drawn back into the active discharge space. Because of the time dependence of the applied voltage, several different corona forms may be observed during a single cycle.
AC coronas with short gaps, in which all charges will be absorbed by the electrodes in each half-cycle, show the same corona forms in sequence which would be found in DC corona. However, with long gaps, ions from one half cycle will persist into the next and modify the space charge field accordingly. Four corona modes can commonly be distinguished: Trichel streamers, negative glow, positive glow (which seems to be favored) and positive "breakdown"streamers. Negative streamers cannot develop because their onset field is greater than the breakdown field in the positive half-cycle.
It is obvious that the very heterogeneous surface condition of a highly stressed conductor *with water drops* in a multitude of shapes and sizes will also give rise to a multitude of corona modes (Figure 2.2) during each cycle so that it appears difficult to extract much more information than geometry and magnitude of charge injection.
The widespread idea of constant onset field is in need of some modification. Waters [14] have measured onset fields with space charge on model conductors of realistic dimensions (1.59 to 2.75 cm dia.) during the positive half-wave the actual onset field remains, after an initial drop of $5-8\%$, practically constant with an increase of applied field (by 20…25%), during the negative half-wave the onset field is considerably and increasingly reduced with an increase of applied field and current. The inception field is decreasing with increasing conductor radius - this is also evident in the map of corona modes from the same authors in Figure 2.2.

2.1.2 Problems caused by corona

Under perfectly dry conditions, most high voltage transmission lines are relatively free from corona and associated noise. However, although conductors are designed to minimize corona discharges, surface irregularities constituted by damage, insects, raindrops rime or snow may locally enhance the electric field intensity sufficiently for corona discharges to occur [1].
As already said, corona discharges can produce audible and radio noise, representing a power loss. Their action on atmospheric particles, associated with production of ozone O_3 and NO_x, can contribute to conductor ageing and to insulation damage. Corona discharge may also generate electromagnetic interference.
The corona noise level generated by overhead transmission lines depends on various parameters, such as:

- atmospheric conditions,

- line length (of minor importance except for total energy loss),
- altitude (air density),
- bundle conductor composition (size of conductors and their configuration),
- surface field strength,
- surface properties of the conductors.

The corona noise changes with atmospheric conditions and also environmental conditions that cannot be defined accurately and are uncertain in nature. It is thus convenient to represent this change with a probabilistic model, which takes into account uncertainties (by suitable averaging) of the parameters mentioned above. The influence of different weather conditions on corona noise are represented in Figure 2.3 [15]. There is a clear evidence that higher noise levels are produced by heavy rainfalls.

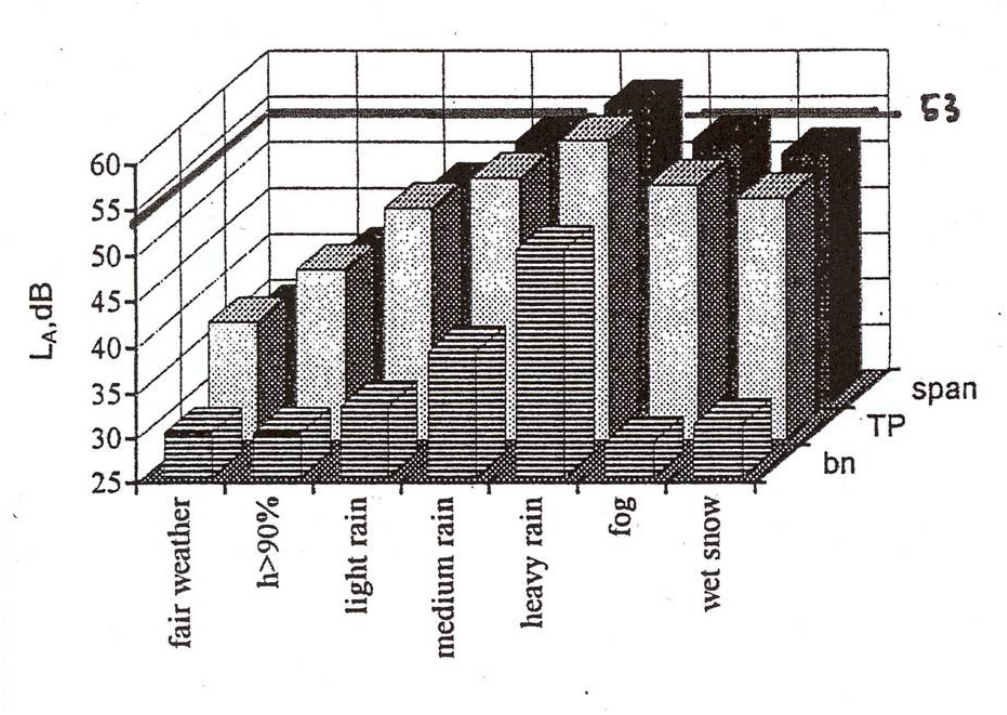

Figure 2.3: A-weighted noise measured at a distance of 15 m from a conductor for different weather conditions for the middle of the span and for the axis of TP-type (tension-pole) supports for the line of 400 kV. bn = background noise [15].

2.2 Acoustic emissions from high voltage lines

To understand how the application of a hydrophilic coating could promote a significant reduction of noise, it is important to know whether $2f$ emission originates from corona discharges and ion clouds or from oscillating drops acting as acoustical membranes. Here, the different explanations of the $2f$ emission given in the literature are presented. When research on audible noise commenced, focus was on investigating radio interference (RI) and A-weighted acoustical noise, with weighting geared to perception by the human ear. The results of the investigations aimed to explore the origin of A-weighting AN emissions are also presented in this paragraph.

2.2.1 Type of acoustic noise

During and after precipitation, AC high voltage lines emit two types of acoustic noise [1]:

- in the kHz range, a crackling/hissing noise originating from brush discharges predominantly during the positive half-cycle of the conductor voltage,
- at 100 Hz, twice mains frequency, a pure tone which is considered particularly annoying especially during night time.

The typical frequency spectrum of audible noise from an AC transmission line during rain is represented in Figure 2.4.

2.2.2 Earlier studies on noise from high voltage installations

Early investigations of AN from lines under wet weather conditions [16], using both model conductors [17, 18] and bundle conductors [19, 20, 21], investigated radio interference (RI) as well as AN. Tonal noise was also noticed in some of these experiments [22, 21, 2, 17], but it was sometimessimply attributed to transformers and switchyard noise. Focus was on managing the hissing/crackling noise at high frequencies, while low frequency noise was considered not a significant problem [2]. Some investigations [21] took note of the pure tone emission at twice mains frequency and recorded some values in dependence upon configuration [21], but their further evaluations were only based on A-weighted noise. The conclusion was that at a given field strength there is no unambiguous relationship between such AN and bundle configuration (number and diameter of conductors).

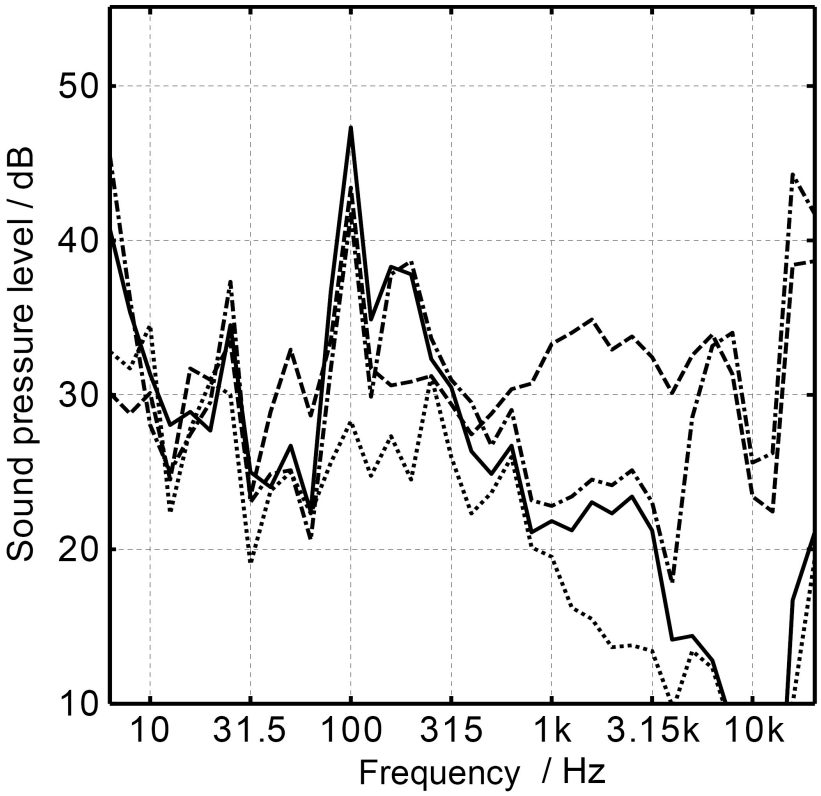

Figure 2.4: Frequency spectrum of audible noise of the third-octave bands.

Numerous studies on the subject included investigations on the effect of field strength on the conductor surface [17], of conductor diameter [21] and of the number of conductors in a bundle [20, 21, 17, 19]. Some studies introduced also the effect of surface condition of conductors and the relative orientation of the maximum electric field with respect to gravity on noise emissions [20].

2.2.3 Origin of tonal emissions

Tonal noise is the low frequency humming part at twice main frequency ($2f$) of what is generally referred to as audible noise of high voltage transmission lines [1]. With AC transmission lines, wet weather conditions are associated with intensive discharge activity during the positive half-cycle (brush discharges can be linked to wide-band noise emission), while only a very small contribution is given by the Trichel pulse discharges during the negative half-cycle [16, 17, 19]. An explanation of $2f$ is that discharges produce ion density near transmission lines with consequent transfer of momentum between ions and neutral molecules [1, 23]. Measurements of ion densities near ground level under a line demonstrated no correlation with the emission of tonal noise [24].
For this reason one had to look for a different explanation of the tonal $2f$

emissions. When the research of CONOR started it was believed [6, 5] that the oscillation of water droplets is the dominant cause of the *2f* (100 Hz) emission. Experiments made to measure ionic space charges failed [24] and the assumption made was that the vibrating drops in the AC field would act as oscillating membranes, thereby emitting tonal noise [6]. This idea was supported by the interpretation of an experiment where the freezing of water drops led to a sharp decrease of tonal noise emissions [5]. The problem has been then revisited by Straumann [25, 4] and clear evidence for a discharge mechanism with ionic space charges was found. An experiment with model conductors prepared with metallic protrusions has shown that tonal noise is emitted not only from wetted conductors with water drops deformed by the electric field, but also from conductors with rigid protrusions. Thus, the periodic ($2f$) drop deformation is assumed to be a source of charge injection into the immediate surroundings of the conductor.

2.2.4 A-weighted sound level

A-weighted noise is the sound level expressed in decibel as measured on a sound level meter using the A-weighted filter network. The A-weighting curve is illustrated in Figure 2.5. The C-weighting curve illustrated has a much broader spectrum than that of the 'A' weighting curve and it is often used to ascertain the acoustic emissions of machines.

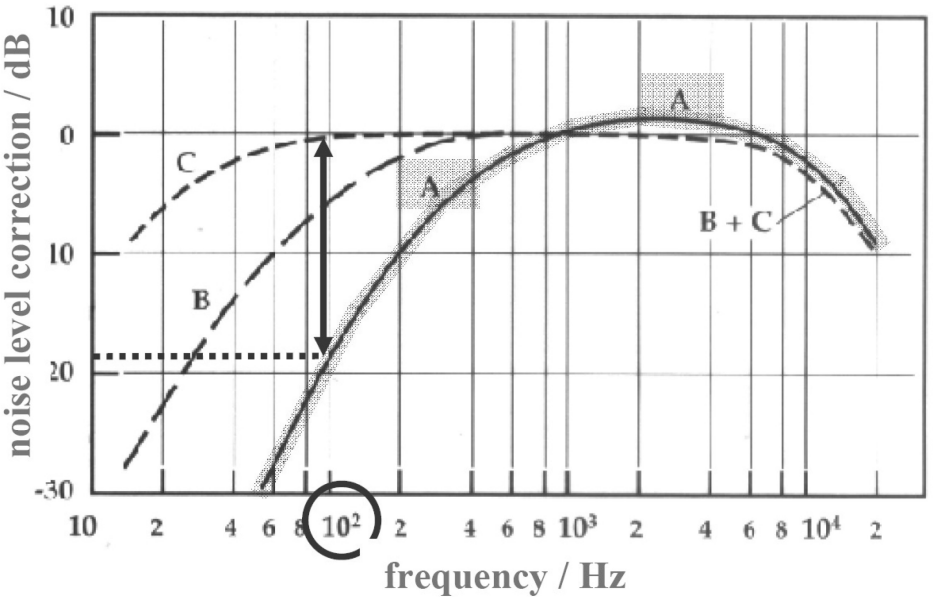

Figure 2.5: Frequency-Weighting Curves. The A, B and C weightings mainly differ in the degree of sensitivity at lower frequencies, relative to 100 Hz. The least sensitivity to lower frequencies is provided by the A-scale, the most by the C-scale.

As shown in Figure 2.5, the A-weighted filter de-emphasizes the very low and very high frequency components of the sound in a fashion similar to how a person perceives or hears sound, thus achieving a good correlation with the evaluation of acceptable and unacceptable sound levels.
In the past, sound pressure level has been measured widely by A-weighting. However, since A-weighting underestimates the impact of the low-frequency noise, it has been stated that it predicts annoyance of community noise rather poorly.
Molino and colleagues [26] reported psychoacoustic studies of the aversive effects of corona noise from high voltage lines. The corona noise from high voltage lines was recorded, reproduced for human listeners in a simulated living room and the human response to the noise was measured in the room. It has been found out that, despite its low sound level, corona noise appears to be more annoying to people than might be expected on the basis of physical measurements of the sound.
As already stated, audible noise from high voltage lines depends strongly on conductor surface conditions, in particular on rain rate [20], on field strength applied [17] and on bundle geometry.
The dependence of A-weighted sound level on rain rate is well described by the empirical model of Kirkham and Gajda [27] presented in the next paragraph.

2.2.5 The influence of rain rate on noise emission

Noise emission from high voltage lines has been recognized as a foul weather problem. It is important to know by which rain rate transmission lines emit how much noise. An ab-initio model of Kirkham and Gajda [27, 28] has proposed saturation of A-weighted noise with respect to rain rate from a threshold rain rate value that is of the order of 1 mm/h.
The final formula for the generated power (in decibels) of the model is:

$$P = 10\log\left(C_1(G-G_0)^{2.4}\left(1-\exp\left(-K_2(G-G_0)^{4/3}\tau\rho\right)\right)\right) \tag{2.1}$$

where

$$C_1 = W\frac{C_3C_4}{4\frac{1}{(\gamma C')^{2/3}}} \tag{2.2}$$

$$K_2 = 4\frac{1}{(\gamma C')^{2/3}}B \tag{2.3}$$

C_1: The parameter C_1 (Equation 2.2) has only influence on the saturation level. The relation between C_1 and the noise level is linear.

K_2: The parameter K_2 (Equation 2.3) has only influence on the saturation rain rate.

$G - G_0$: Represents the difference between the average electric field strength and the corona onset field strength G_0 and has influence on both the saturation noise level and the saturation rain rate [28].

B: Describes the relation between the rain rate and the number of drops on the conductor.

τ: τ is the drop lifetime on the conductor surface and thus describes the wettability of the conductors. It has influence on the saturation rain rate.

C_3: The probability that a drop shows corona activity is proportional to Towsend's first ionization coefficient, α.

C_4: C_4 Describes the energy density in the plume associated with the active drop.

W: W is the active area of the conductor, on which the electric field strength is high enough to cause corona activity when wet.

γ: Describes the geometric shape of the plume.

C': Describes the energy density necessary to sustain the plume.

This study provides thus a quantitative presentation of saturation in dependence upon surface field strength and rain rate (Figure 2.6). In Figure 2.6 it can be observed that for light rain rate the A-weighted sound level increases monotonously with $\sim$ 10 dB per rain order of magnitude and saturates to a constant level with higher rain rates.
It has here been found [4] that the 100 Hz sound level increases monotonously with rain rates up to 100 mm/h or beyond. This means that the 100 Hz and the A-weighted emissions are due to two different mechanisms and, thus, the model of Kirkham and Gajda appears to be not suitable for the calculation of the tonal *2f* noise emission [4].

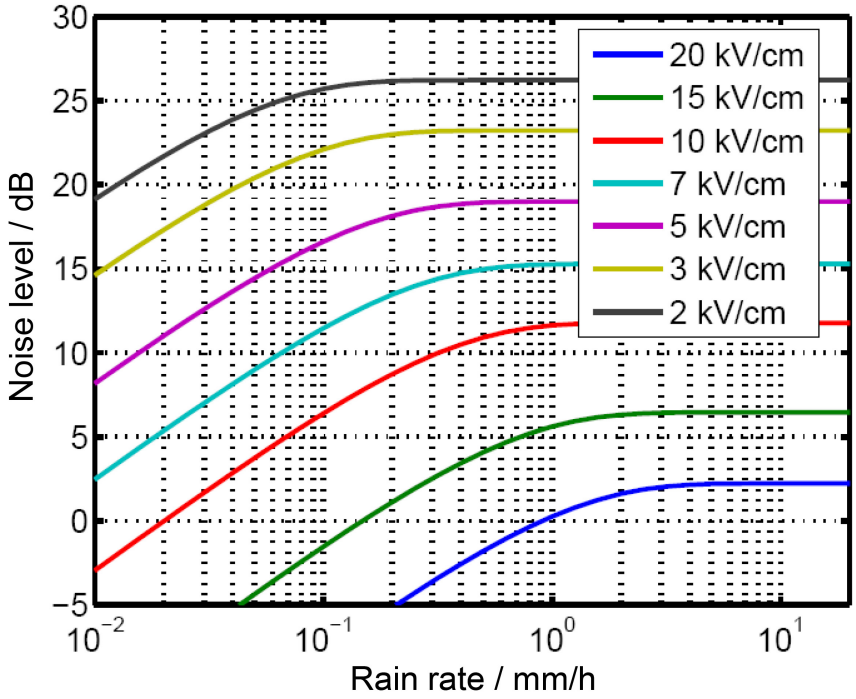

Figure 2.6: Variation of audible noise with rain rate by different electric field strengths $G - G_0$ with the parameter $K_2\tau = 0.4$ and $C_1 = 10^{-1/2}$ based on the empirical model of Kirkham and Gajda [29, 27].

2.3 The analysis of water drop shape

An important step in the characterization of coatings applied to overhead high voltage lines is the study of the properties of single sessile water drops with and without the application of an electric field. In this paragraph, the parameters and the methods necessary to describe the shape of a liquid drop on a certain surface are presented. Furthermore, to classify different surfaces, a criterion from the literature is also given.

2.3.1 Water drop on a surface

The spherical shape of a free drop is a result of intermolecular forces between the molecules of which it is made [30]. A molecule located within the drop is equally attracted in all directions by the molecules surrounding it, and so the total force exerted on it is zero. However, a molecule located near the drop surface is attracted only by its inner neighbors, and so feels a resultant force in the direction of the neighboring molecules. This effective attraction of a molecule on the surface creates surface tension [30].
Surface tension is a physical quantity measured in units of force per unit length, or equivalently in units of energy per unit area, and it expresses the

amount of energy necessary to enlarge the surface by one surface unit [30]. Since the sphere has the lowest surface area per given volume, it is easy to understand that this is also the state with the lowest surface energy, and that is what causes the drop to take on a spherical shape.
Surface tension at the interface of two materials depends on their mutual properties, and not just on one of them. When a liquid drop is placed on a surface, the behavior of the drop depends not only on characteristics of the liquid, but also on characteristics of the material of which the surface is made.

2.3.2 The concept of contact angle

Contact angle measurements have been widely used in surface studies [31]. Contact angle, θ, is defined as the angle, specified in degrees, between the surface and a tangent drawn to the surface of the drop from the contact point (triple point) on the supporting surface.
The important concept is that the shape of the drop reveals information about the chemical bonding nature of the surface [31]. This bonding will determine its wettability and drop adhesion. The contact angle is a useful quantity to characterize the bonding.
The contact angle can be considered in terms of the thermodynamics of the materials involved. Wettability is determined by the balance between adhesive forces between the liquid and solid and cohesive forces in the liquid. Adhesive forces cause a liquid drop to spread. Cohesive forces cause the drop to ball up. The contact angle is determined by the competition between these two forces. Young [32] formulated the relationship between the equilibrium contact angle θ and the three surface tensions: the surface tension between the liquid and the solid surface γ_{SL}, between the surface and the air γ_{SV}, and between the liquid and the air γ_{LV}. At equilibrium the three lateral forces acting on the drop are balanced as the drop does not move:

$$\gamma_{LV}\cos\theta + \gamma_{SL} - \gamma_{SV} = 0 \tag{2.4}$$

The Young equation relates the cosine of the angle θ to the three surface tensions:

$$\cos\theta = \frac{\gamma_{SV} - \gamma_{SL}}{\gamma_{LV}} \tag{2.5}$$

The contact angle can vary between $\theta = 0^\circ$ and $\theta = 180^\circ$. The conditions of good wetting ($< 90^\circ$) and partial-wetting ($> 90^\circ$) are illustrated in Figure 2.7. Complete wetting (also referred to as spreading) is obtained at an angle of 0° and complete non-wetting occurs at an angle of 180°. The intermediate case of $\theta = 90^\circ$ is achieved when $\gamma_{SV} = \gamma_{SL}$ in the Young equation (Equation 2.5).

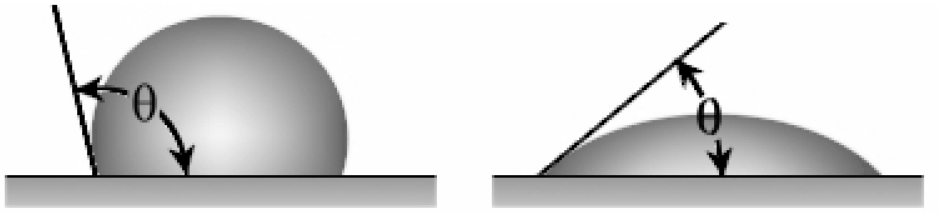

Figure 2.7: Water drop on a surface. Left: large contact angle, poor wetting, low solid surface free energy. Right: small contact angle, good wetting, high solid surface free energy.

2.3.3 Hysteresis

For any given solid/liquid interaction there exists a range of contact angles which may be found. The value of static contact angles are found to depend on the recent history of the interaction. When the drop has recently expanded the angle is said to represent the *advanced* contact angle [31]. When the drop has recently contracted the angle is said to represent the *receded* contact angle [31]. These angles fall within a range with advanced angles approaching a maximum value and receded angles approaching a minimum value. If the three phase (liquid/solid/vapor) boundary is in actual motion the angles produced are called dynamic contact angles and are referred to as *advancing* (θ_a) and *receding* (θ_r) angles. The general physical relation between the advancing and receding contact angle and the static contact angle θ is : $\theta_r \leq \theta \leq \theta_a$.
The difference between the maximum (advanced/advancing) and minimum (receded/receding) contact angle values is called the contact angle hysteresis. A great deal of research has gone into analysis of the significance of hysteresis [33]. Several authors have discussed critically contact angle analysis [34, 35] and contact angle hysteresis related to surface heterogeneity, roughness and mobility. For surfaces which are not homogeneous there will exist domains on the surface which present barriers to the motion of the contact line. For the case of chemical heterogeneity these domains represent areas with different contact angles than those of immediately surrounding surface. For example, when wetting with water, hydrophobic domains will pin the motion of the contact line as the liquid advances, thus increasing the contact angles. When the water recedes the hydrophilic domains will hold back the draining motion of the contact line, thus decreasing the contact angle. From this analysis it can be seen that, when testing with water, advancing angles will be sensitive to the *hydrophobic* domains and receding angles will characterize the *hydrophilic* domains on the surface.

2.3.4 Hydrophobicity and hydrophilicity

A drop with a large contact angle characterizes *hydrophobic* surfaces. This condition is exemplified by poor wetting, and poor adhesiveness; the solid surface free energy of the solid material is low. A drop with a small contact angle characterizes *hydrophilic* surfaces. This condition reflects better wetting, better adhesiveness, and the surface energy of the solid material is higher.
In industrial applications, contact angle is a primary tool used to measure cleanliness. Organic contaminants may prevent wetting and result in larger contact angles. As a surface is cleaned and treated to remove contaminants, the contact angle will typically decrease as wetting improves. The roughness of a surface improves the wettability for hydrophilic surfaces (see Figure 2.8). In this case a drop will seem to sink into the hydrophilic surface. On the other side, it is energetically too expensive to wet a rough hydrophobic surface. The result is an increased water-repellency.

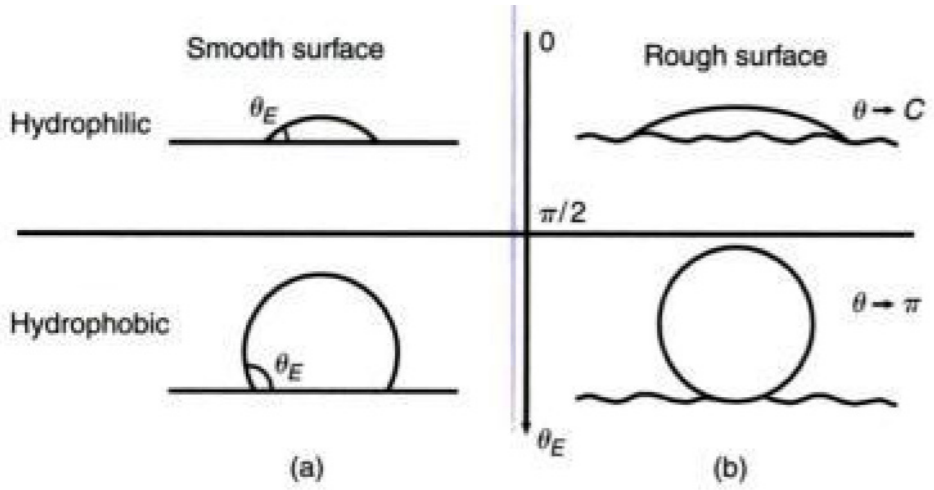

Figure 2.8: Influence of the roughness on the contact angle. Smooth surface (a); rough surface (b). Hydrophilic substrate becoming even more hydrophilic with a rough surface (top); hydrophobic substrate becoming "super-hydrophobic"(bottom).

A droplet on an inclined superhydrophobic surface does not *slide* off; it rolls off. When the droplet rolls over a contamination, the particle is removed from the surface if the force of absorption of the particle is higher than the static friction force between the particle and the surface. Usually the force needed to remove a particle is very low due to the minimized contact area between the particle and the hydrophobic surface. As a result, the droplet cleans e.g. a the leaf by rolling off the surface.
Seven wettability classes (WC) have been defined [36] for a fast and easy

check of the wettability of insulators. A surface with the WC value 1 is the most hydrophobic surface and a surface with the WC value 7 is the most hydrophilic surface (Table 2.1).

WC	Description
1	Only discrete droplets are formed. $\theta_r \approx 80^\circ$ or larger for the majority of droplets.
2	Only discrete droplets are formed. $50^\circ < \theta_r < 80^\circ$ for the majority of droplets.
3	Only discrete droplets are formed. $20^\circ < \theta_r < 50^\circ$ for the majority of droplets. Usually their contact area is no longer circular.
4	Both discrete droplets and wetted traces from the water runnels are observed (i.e. $\theta_r = 0^\circ$). Completely wetted areas may measure $> 2\text{cm}^2$. Together they cover $< 90\%$ of the tested area.
5	Some completely wetted areas $> 2\text{cm}^2$, which cover $< 90\%$ of the tested area.
6	Wetted areas cover $> 90\%$ of the area, i.e. small unwetted areas (spots/traces) are still observed.
7	Continuous water film over the whole tested area.

Table 2.1: Criteria for the determination of wettability class (WC) [36].

2.3.5 Methods to measure the contact angle of a drop

For experimental investigations of drop behaviour measurement techniques are necessary, which allow one to determine drop shape, size, surface tension, temperature and other properties. Photographic and video observation techniques allow one to determine the shape and the size of drops. Video techniques based on periodic phenomena allow one to study the temporal evolution of shape and size.
One of the most common methods for measuring the contact angle is the sessile drop method, which involves depositing a liquid drop on a horizontal solid surface and measuring the angle between the solid surface and the tangent to the drop profile at the drop edge [37] (Figure 2.7). Two different approaches can be used to measure contact angle: goniometry and tensiometry.
Goniometry involves the observation of a sessile drop of test liquid on a solid

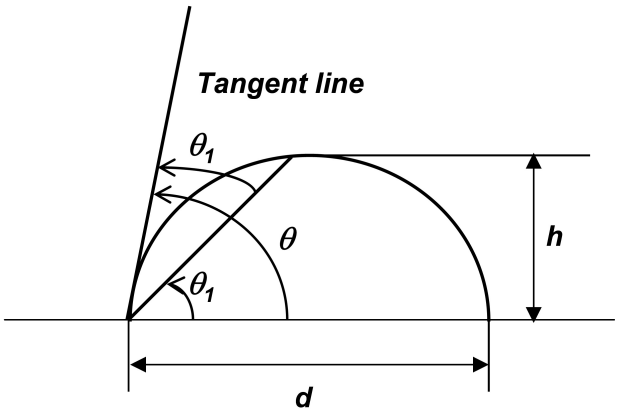

Figure 2.9: The $\theta/2$ method calculates the contact angle from the angle (θ_1) between the drop base line and the line passing through the apex of the drop as shown in the figure. Based on the assumption that the droplet profile forms a segment of an arc, $2\theta_1 = \theta$.

substrate and it includes the use of a light source, a sample stage, lens and an image capture device. The contact angle can then be measured directly by using Equation 2.6 or 2.7 relating the height *h* and the diameter *d* of the drop to the angle obtained. This method is called the half angle method ($\theta/2$ method) and it calculates the contact angle θ from the angle between the droplet base line and the line passing beyond the apex of the droplet. The method is based on the assumption that the droplet profile forms a segment of an arc "a partial sphere"and that the drop is symmetric about a central vertical axis (this means it is irrelevant from which direction the droplet is viewed), see Figure 2.9.

$$for\ \theta < 90^\circ\ :\ \theta = 2\arctan(2h/d) \tag{2.6}$$

$$for\ \theta > 90^\circ\ :\ \theta = 2\pi - \arccos[(2h/d) - 1] \tag{2.7}$$

Therefore, if the droplet becomes non-spherical due to gravity, an inaccurate measurement will result. Generally, small droplets within a few micro liters are used for contact angle measurement to reduce the effect of gravity to an acceptable level. For bigger drops, one has still the choice to assess the contact angle by measuring the angle formed between solid surface and the tangent by means of a goniometer.
Tensiometry involves measuring the forces of interaction as a solid is contacted with a test liquid. If the forces of interaction, geometry of the solid and surface tension of the liquid are known, the contact angle may be calculated. This approach will not be used for the investigations presented here.
The sessile drop method is the most widely accepted method for determining the contact angle due to the simplicity of obtaining fairly reliable data. However, the assignment of the tangent line which will define the contact angle is a factor which can limit the reproducibility of contact angle measurements.

Conventional goniometry relies on the consistency of the operator in the assignment of the tangent line. This can lead to significant error, especially subjective error between multiple users. Contact angles are very sensitive to contamination and solid surface roughness. Furthermore, contact angles are also very sensitive to external factors such as temperature and humidity and may affect the results and thus recording the environment during the measurement is very important [38].
Special instruments remove the subjective problem by using computer analysis of the drop shape to generate consistent contact angle data [39]. It is also important to point out that sessile drop measurements require good focus and a very clearly defined baseline. Reflection images, particularly when the contact angle is close to 90°, also pose a challenge. In fact, computer evaluated measurements may not correctly separate the true image from the reflection on the surface.
For the analysis of the wettability of a surface the so called 'sliding method' can be used also [40]. This method measures the contact angle of a droplet attached on a tilted solid surface. When a droplet is attached to a solid surface and the solid surface is tilted little by little, the droplet will lunge forward and finally slide downward. The angles formed at the front and the rear of the droplet lunging forward are the advancing angle and the receding angle mentioned before. The tilting angle of a solid surface when the droplet starts sliding downward is called the sliding angle. This method presents various data, not only the advancing and receding contact angles, but also the sliding angle and adhesive work of the liquid against the solid.

2.3.6 Evaporation of a water drop on a surface

The evaporation of water drops on a surface is a very important parameter to be considered in the evaluation of drop shapes [38]. The evaporation of a sessile droplet has been studied by Birdi and Winter [41], who obtained the evaporation rate by measuring the change of weight of droplets of water on a glass surface and concluded that for most of the time the evaporation rate remains constant. The role of geometrical parameters of droplets during evaporation has been investigated by Diogo [42]. The conclusion was that contact angle measurements are strongly influenced by the time t between positioning the drop on the surface and making the measurement. This has also been stated by other authors [43, 38].

To be able to determine the evaporation rate of a water drop it is important to identify the critical geometrical parameters and solve an analytical relationship. These parameters are (see Figure 2.10): the contact angle, the droplet

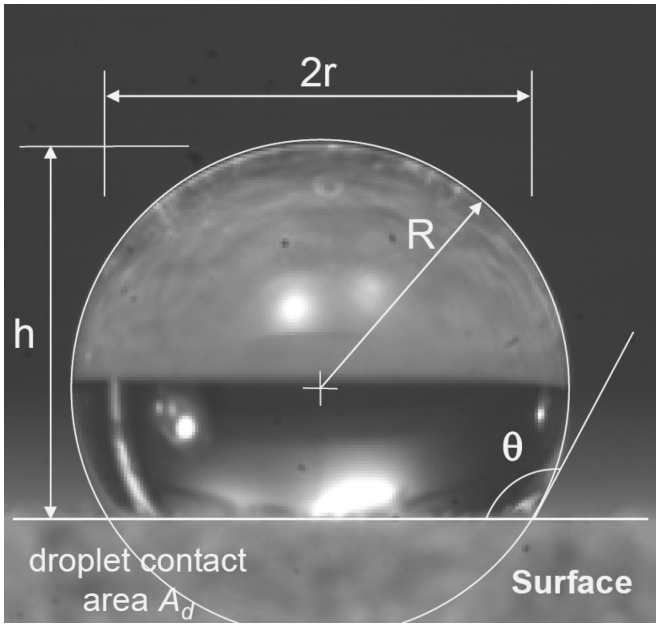

Figure 2.10: Physical quantities determining the drop shape [42].

radius (R), the base or contact radius ($r = Rsin\theta$), the free drop area ($A_s = 2\pi Rh$), drop base area ($A_b = \pi r^2$) and drop volume ($V_l = \pi/3(3R - h)h^2$). To predict the evaporation rate a model with the assumption that no hysteresis takes place has been built [42]. The input data are the initial volume (V_{l0}), initial contact angle (θ_0), initial base radius (r_0) and initial evaporation rate (I_0). Then, the following geometrical analytical relation is used:

$$V_l = f(\theta, r) \Rightarrow V_l = \frac{-\pi \cdot r^3}{3} \cdot \frac{(\cos\theta + 2) \cdot (\cos\theta - 1)}{(\cos\theta + 1) \cdot \sin\theta} \tag{2.8}$$

$$\theta = f(V_l, r) \Rightarrow \tag{2.9}$$

$$\theta = 2 \cdot \arctan \left[\sqrt[3]{\frac{6 \cdot V_l}{\pi \cdot r^3} + \frac{\frac{-6 \cdot V_l}{\pi \cdot r^3} + \sqrt{\left(\frac{6 \cdot V_l}{\pi \cdot r^3}\right)^2 + 4}}{2}} - \sqrt[3]{\frac{\frac{-6 \cdot V_l}{\pi \cdot r^3} + \sqrt{\left(\frac{6 \cdot V_l}{\pi \cdot r^3}\right)^2 + 4}}{2}} \right]$$

$$r = f(V_l, \theta) \Rightarrow r = -\sqrt[3]{\frac{3 \cdot V_l \cdot (\cos\theta + 1) \cdot \sin\theta}{\pi \cdot ((\cos\theta)^2 + \cos\theta - 2)}} \tag{2.10}$$

2.4 Behaviour of single water drops on high voltage lines

In Section 2.2 it has been concluded that tonal noise emitted from high voltage lines during and after precipitation originates from sources of charge injection provided by water drops subjected to periodic deformation. Thus, deformation of water drops of different size in the electric field leading to instability and resulting in electric discharges has to be of interest due to its role in the origin of $2f$ emission. In particular, for the characterization and understanding of the performance of coatings applied to high voltage lines, the electrodynamic behaviour of water drops should be taken into consideration. The behavior of water drops in an electric field is well explained in the literature, as reported in this paragraph, but it will be seen that the influence of surface conditions on the deformation and instabilities of water drops has not been satisfactorily clarified.

2.4.1 Instability of water drops in an electric field

The deformation and instabilities of water drops in high electric fields have long been a subject of interest for many researchers. The maximum electric charge a water drop can have is limited by two factors:

- The electrostatic forces must not exceed the value at which the drop becomes unstable [44], when it would form a Taylor cone and eject highly charged water droplets.
- The electric field at the apex of the drop must not exceed the value at which it would initiate corona from the drop.

The coupling of instability and corona depends on air density [45], at low air densities the discharge may set in with fields not yet effecting instability. The critical electric field strength at which an uncharged water drop immersed into an uniform electric field becomes unstable depends on drop radius and surface tension. This critical electric field strength has been found experimentally and theoretically. The first calculation of the critical electric field strength has been made by Lord Rayleigh, who stated a stability criterion for a droplet of liquid in an electric field [44]. If the electric field at the surface of the drops is high enough they become elongated in the direction of the electric field. Eventually the deformation becomes so large that the drop is mechanically unstable [44] and this results in ejection of liquid in a very fine water filament of a diameter of a few μm from the apex [46, 47]. This ejection has been beautifully photographed [48] (see Figure 2.11) revealing that the thin water

jet emerges from an elongated surface ending in a cone whose vertical angle appeared to be approximately 90°. This angle was later calculated and experimentally proved to be 98.6° [49] and has since been called the Taylor angle or Taylor cone angle.

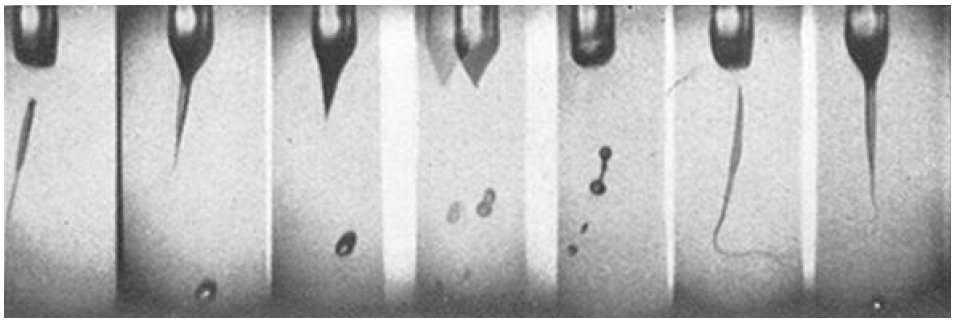

Figure 2.11: Ejection of droplets of liquid charged to 6 kV. The apparatus used for getting the electrified surface consisted of a vertical glass tube, 0.92 mm diameter, joined from its upper end to a reservoir of liquid. A drop of liquid at the lower end of the small glass tube was the part under observation. Time interval between the separate exposures: $\sim$ 1/800 of a second. The pictures are to be followed from right to left. [48]

The electrodynamic instability of a water drop in a uniform electric field is described by a critical electric field strength E_{cr} [V/m] [46, 49]:

$$E_{cr} = c\sqrt{\frac{\gamma}{\varepsilon_0 r}} \tag{2.11}$$

where r [m] is the radius of the drop, γ [N/m] is the surface tension (γ of water at room temperature is $7.28 \cdot 10^2$ N/m) and c is a constant. The constant c has been estimated both theoretically and experimentally and is about 0.453 [50]. The formula points out that the smaller a drop is the higher is the electric field, which takes it to instability

If a free water drop is charged, it can also become unstable in absence of an *external* electric field. The maximum charge that a drop can have without becoming unstable is equal to the Rayleigh charge Q_R [C] [44]:

$$Q_R = 8\pi\sqrt{\gamma\varepsilon_0 r^3} \tag{2.12}$$

If the charged drop is in an external electric field, the critical electric field is reduced nearly linearly with the charge Q of the drop according to the following formula [51]:

$$E_{cr_{charged}} \approx E_{cr} \cdot \left(1 - \frac{Q}{Q_R}\right) \tag{2.13}$$

Thus, the critical electric field expressed in V/m for a charged drop is

$$E_{cr_{charged}} \approx 0.453 \cdot \left(1 - \frac{Q}{Q_R}\right) \cdot \sqrt{\frac{\gamma}{\varepsilon_0 r}} \tag{2.14}$$

The critical electric field necessary for the disintegration of a water drop has been calculated on the basis of experimental studies on water drops falling in a vertical field [52, 53]:

$$E_{cr_{charged}} = 4.08 \cdot 10^4 \frac{(1 - 1.76 \cdot 10^9 Q)}{\sqrt{r}} \tag{2.15}$$

It has been found that the electric field necessary for disintegration of a negatively charged water drop is larger than for an uncharged water drop and that it increases with increasing negative charge on the water drop [52].

2.4.2 Corona discharges from a water drop

A water drop in a strong electric field deforms to a conical shape and disintegrates producing corona discharges [49, 54, 55]. Numerous studies [56, 57, 58, 59, 60] have confirmed the link between the deformation of the water drop in an electric field and the generation of corona pulses. English [56] reviewed the works done by Macky [46] and Zeleny [48] on the disruption of water drops in an electric field and concluded that the corona onset depends critically on the radius of curvature of the drop.
As was mentioned above, when disintegration occurs there is ejection of small drops from a big one and the resulting ejected water droplets are highly charged. In DC fields, this can result in intense oscillation of the liquid with repeated corona pulses, leading to emission of tonal AN [61]. With AC fields, the maximum of the deformation lags the applied voltage [62] giving rise to an electrical discharge whenever the field is sufficiently high to produce instabilities [48, 62]. The deformation is nearly the same for either polarity [62]. However, the appearance of positive corona pulses differs from that of negative pulses.
When a large positive water drop point emits small positively charged droplets, the field is great enough to produce streamers. On further increasing the electric field, a stable regime is reached and it is characterized by positive streamers and burst pulse corona generating positive space charge. The appearance of such a space charge then reduces the field at the surface of the drop below the value for disruption. With the disappearance of streamers, the ordinary

burst pulse corona with characteristic surface glow occurs, increasing in area over the point surface. With a further increase of the field, the water surface is again disrupted generating intermittent streamers and strong burst pulse corona.
With a large negative water drop point the resulting pulses are of two types: Trichel pulses [63, 64] corresponding to a regularly repeating series of discharges from the negative point and streamers from the positive end of the ejected droplet [56].
Onset electrical field strength E_c to initiate corona discharge depends on drop sizes, atmospheric gas density, temperature and absolute humidity, and is reduced for larger drops.

$$E_c = \frac{Q_c}{4\pi\varepsilon_0 r^2} \tag{2.16}$$

By sufficient reduction in gas density the discharge mechanism changes from electrodynamic instability to pure corona loss, since the corona process is pressure dependent. By a pressure below 500 hPa, which corresponds to an altitude of ca. 4.5 km, the loss of charge by corona is dominant [56, 45].

2.5 The evaluation of the drop population

After the provision of information on single water drops sitting on a conducting surface, a further step to approach the analysis of usefulness of coatings is the assessment of the drop size distribution. Only drops of particular sizes may undergo *resonant* deformation and thus it is of paramount importance to know what kind of drop population different surfaces present with and without application of an electric field. This paragraph offers an overview of the common methods used for the determination of particles/drops size distribution and their advantages and disadvantages.

2.5.1 Drop size analysis

The measurement and the analysis of particle and droplet size distributions are important in electrostatics research, but the accuracy has always been a problem. So far, although investigated by numerous researchers, each technique presents its own limitations and a generally valid solution applicable under actual and reproducible conditions does not exist [65]. In particular, particle shape - as water drops assume different shapes under the influence of an electric field - plays a significant role in measuring particle size [66, 67].

For a water drop, it is conventional to use diameter to describe its size. Calling $d_1, d_2, ..., d_n$ the diameters for n drops, the mean size can be defined by [67]:

$$Mean\ diameter = \sqrt{\sum_{i=1}^{n} \frac{d_i^2}{n}} \tag{2.17}$$

Techniques based on the photographic evaluation of drop size have been developed and appear to be the most reliable, since they allow a direct measurement of the drop size.

2.5.2 Manual evaluation methods

Normally pictures are printed out and evaluated manually in conformity with the chosen measurement techniques. On the picture then the two edge coordinates of a virtual square box around each drop are manually identified and stored in the PC where the diameters are then evaluated. These evaluations have the severe disadvantage that the manual identification of each drop is extremely time consuming and strongly dependent on the operator for their reliability. Moreover, in order to have an evaluation with minimal statistical significance, a high enough number of particles need to be evaluated, see [68, 69].

2.5.3 Automated evaluation methods (image processing)

Many studies have been carried out to obtain automated evaluation of the drop size and thus to permit a more rapid counting and sizing of water drops. Several types of optical measuring instruments for drops and particles have been developed in recent years. Generally, the parameters of major interest are the droplet sampling rate, the ability to process the data in a real or delayed mode, and the capability to record the droplet spatial configuration [70]. To be able to count and size individual drops, sensors could also be utilized, but the risk is the neglect of small drops [71].
Although various studies concerning the possibility of an automated evaluation of the size of the droplets have been conducted, many of them require anyway the human intervention and refer to particular conditions when the pictures are suitable for being easily evaluated. Automated processing of the image of droplets is in general not easy because it requires as input high-quality pictures of droplets. This condition can only be achieved providing suitable illumination of the droplets on the surface and taking into account the complexity of the video images with overlapping drops, reflexes and undefined background. At the present time a method for obtaining well-defined

pictures which can be automatically processed in digital form has not yet been developed.

2.5.4 Models for the identification of the drop population

In general, water drops on a conductor are *lognormally* distributed [72], where the mean diameter d and the width of the distribution depend on the rain rate ρ.
Under the condition that all parameters depend on the rain rate and that this dependence is expressed for example by: $a = c\rho^x$, $\mu = \mu_0 + \mu_1\rho$ and $\sigma = \sigma_0 + \sigma_1\rho$, for $c = 50$, $x = 1/5$, $\mu_0 = 0.1$, $\mu_1 = 0.01$, $\sigma_0 = 0.25$ and $\sigma_1 = 0.01$, the following hypothetical distribution $P(d)$ results:

$$P(d) = \frac{a}{\sqrt{2\pi}\sigma r}\exp\left(-\frac{(\ln(d)-\mu)^2}{2\sigma^2}\right) \tag{2.18}$$

When high voltage is applied, the large pendant drops on the underside of the conductor oscillate, become instable and lose water. The diameter of the water drops appear to be *normally* distributed.

$$P(d) = \frac{a}{\sqrt{2\pi}\sigma}\exp\left(-\frac{(d-\mu)^2}{2\sigma^2}\right) \tag{2.19}$$

Like in the lognormal case, the dependence of parameters on rain rate can be $a = c\rho^x$, $\mu = \mu_0 + \mu_1\rho$ and $\sigma = \sigma_0 + \sigma_1\rho$, where $c = 50$, $x = 1/5$, $\mu_0 = 1.5$, $\mu_1 = 0.01$, $\sigma_0 = 0.5$, and $\sigma_1 = 0.01$.
To estimate the number of active drops, it is necessary to give a diameter window $[d_1, d_2]$, in which the considered drops lie. To estimate this number, the integral on the distribution of water drops has to be calculated:

$$n(\rho) = \int_{d_1}^{d_2} P(d, \mu(\rho), \sigma(\rho))dd \tag{2.20}$$

At the end, the number of drops which are responsible for tonal emissions is obtained as a function of the rain rate in the form of a polynomial number described by the parameter x:

$$n(\rho) = B\rho^x \tag{2.21}$$

2.6 Analysis of coatings

To assess a coating, it is important to know its chemical and physical formulation in order to be able to forecast its wettability and adhesion and thus to know in advance which kind of failures the coating may encounter during its active use over many years. The purpose of this paragraph is to give an understanding of the mechanism of how coatings work and therefore, how they can fail. In particular, the properties of two special hydrophilic coatings that seemed promising will be described.

2.6.1 Formulation of coatings

Most conventional coating materials consist typically of four basic ingredients, namely a binder, pigments, solvents, and additives [73]. Some coatings may not have all of these ingredients.
A coating's binder is the 'glue' which holds it together, and which is principally responsible for providing adhesion to the substrate [74]. With few exceptions, the binder is nearly always organic, consisting of natural resins or man-made polymers. A fundamental aspect of binders is their viscosity, which is a material's resistance to flow. A coating must be low enough in viscosity to be applied by conventional equipment (brush, roller, spray or dipping) and high enough in viscosity so as not to sag or drip. It must maintain, for the time after application, a suitable viscosity such that the coating can flow and level, which is necessary to eliminate the imperfections such as brush marks but also so that the coating can thermodynamically wet the substrate (critical in achieving good adhesion)[73].
Pigments can affect a coating's corrosion resistance, physical properties, and appearance [73]. The many types of pigment are divided into inorganic and organic. Inorganic pigments consist of particles which are dispersed in paints [74]. They can contribute to all three of the pigment functions (corrosion resistance, physical properties and aesthetics). Two of the most common inorganic pigments are titanium dioxide (TiO_2) and iron oxide (FeO). TiO_2 is the most widely used white pigment, particularly for exterior coatings. It has a high refractive index, which means that it has excellent hiding strength, and also (in the form of rutile) provides a measure of stability against the ultraviolet rays of sunlight, which can degrade many coating binders. There are two common crystal forms of TiO_2: rutile and anatase [74]. Titanium dioxide in the anatase form is a photocatalyst under ultraviolet light and would degrade organic binders and substrates. As TiO_2 is exposed to UV light, it becomes increasingly hydrophilic; thus, it can be used for anti-fogging coatings or self-cleaning windows, as will be explained in next Section.
Organic pigments are in general fairly complicated organic molecules. They

are seldom used in primers or heavy duty industrial paints. Extender pigments are relatively low-cost inorganic pigments which provide little color or corrosion resistance, but which are used to provide bulk and to adjust density and flow properties. They can also affect physical properties such as hardness, permeability and gloss. They consist, for the most part, of silica/ silicates, calcium carbonate and barytes. Silicas fall into two broad types, i.e. natural and synthetic. The synthetic silicas are used in small amounts, and are perhaps better considered as additives. The three major natural silica pigments are crystalline silica, amorphous silica and diatomaceous silica. All are chemically inert, hard, and have low specific gravities and refractive indexes.
Most coatings require solvents to dissolve the binder and to modify the viscosity so that the coating can be applied by conventional methods [75]. Solvents serve in aid of the flow and levelling of the coating, as well as the wetting of the substrate and evaporate after the coating has been applied. Solvents are generally thought of as organic liquids, although in a latex paint the main solvent is water. The rate of evaporation of solvents is also very important. The rate of solvent evaporation can have a major influence on the properties of the coating.
Additives are various chemicals, typically added in small amounts, which can greatly affect the properties of a coating [74]. These include surfactants, anti-settling agents, coalescing agents, anti-skinning agents, catalysts, defoamers, ultraviolet light absorbers, dispersing agents, and plasticizers.

2.6.2 Super-hydrophilic coatings

One possibility to obtain low contact angles (hydrophilic surfaces) is the use of particular thin films on the materials surface. For example, thin layers of photocatalytically active metal oxides or sulfides can be applied. In the last years, TiO_2 coated materials have been of increasing interest [76].
If a surface coated with TiO_2 of the anatase type is exposed to UV light, very low contact angles are obtained ($< 1^\circ$). This material have the unique property of 'attracting' rather than repelling water and for this reason it is called a super-hydrophilic material. The water lies flat on the surface in sheets instead of forming droplets. When the illumination is stopped, the super-hydrophilic behavior of the TiO_2 surface is retained for a while, maybe for several days, depending on the coating as will be seen in Chapter 6. Furthermore, UV illumination of titanium dioxide leads to the formation of powerful agents with the ability to oxidize and decompose many types of bacteria and organic materials. This emphasizes the fact that super-hydrophilic properties with the photocatalyst can be used for many products and applications, using the anti-fogging and self-cleaning properties [76].

Compared with traditional advanced oxidation processes, the technology of photocatalyst has numerous advantages which make it competitive:

- low consumption of energy and consequently low costs,
- the reaction is quite fast at mild operating conditions (room temperature, atmospheric pressure),
- easy to set up and operate,
- no need for post-processes,
- no environmental hazard from the catalyst.

2.6.3 Thin-film deposition coatings

Special thin-film deposition techniques can also be used in the preparation of hydrophilic samples. Thin-film deposition methods include: CBD (Chemical Bath Deposition), evaporation (PVD: Physical Vapor Deposition), sputtering (PVD), plasma CVD (Chemical Vapor Deposition), thermal CVD, photo CVD and Sol-gel process [77].
Chemical vapor deposition (CVD) is a chemical process used to produce high-purity, high-performance solid materials. In a typical CVD process, the substrate is exposed to one or more volatile precursors, which react and/or decompose on the substrate surface to produce the desired deposit.
The Sol-gel process is a process for making glass/ceramic materials [77]. The Sol-gel process involves the transition of a system from a liquid (the colloidal "sol") into a solid (the "gel") phase. The Sol-gel process allows the fabrication of materials with a large variety of properties: ultra-fine powders, monolithic ceramics and glasses, ceramic fibers, inorganic membranes, thin film coatings and aerogels. The sol is made of solid particles of a diameter of few hundred nm, usually inorganic metal salts, suspended in a liquid phase. In a typical sol-gel process, the precursor is subjected to a series of hydrolysis and polymerization reactions to form a colloidal suspension, then the particles condense in a new phase, the gel, in which a solid macromolecule is immersed in a solvent.

2.6.4 Concept of ageing

Aging is a process of irreversible change of properties. In [78] ageing is defined as the totality of time in which a material shows irreversible chemical and physical modification. Transferring this concept to ageing of coatings for

high voltage lines, this means an irreversible change of the surface often manifesting itself in change of its wetting properties.
A demand on a coating is that it adheres well to the substrate, has a good cohesive strength or integrity, resists weathering and chemical deterioration, and impedes the permeability of harmful or corrosive agents.
There are a number of reasons why a particular coating may fail [75]. It is fairly common to ascribe these failures to one of four causes, namely misapplication of the coating, defective coating, the wrong choice of coating, or exposure to an unanticipated environmental excursion. While it is true that coating failures fall into one of these four categories, or perhaps a combination of them, there are still more fundamental forces that can cause coatings to fail. For a coating to fail, it may have to be stressed; there are many forms of stress [75]. There are factors and forces which can stress a coating, such as sketching deformation of the substrate, chemical attack, degradation by ultraviolet light, and even the fundamental tendency for all closed systems to reach a state of equilibrium. If the degree of stress exceeds that which might normally be expected of the particular service in which the coating has been placed, then it is probably correct to say that the coating failed because of this unexpected stress. If the coating were poorly designed or misapplied, and subsequently failed under the normal stress of the environment, the stress should not be blamed for the failure.

2.6.5 The ageing of hydrophobic coatings

The ageing of hydrophobic surfaces is an important factor for polymeric insulating surfaces, as reported in many papers [43, 79, 80, 81, 82]. Insulating materials under service conditions can lose their hydrophobic properties when stressed by several environmental factors, e.g. rain, condensation, fog, snow, ice, salt, dust, pollution, temperature changes, wind discharges and solar radiation. A very important ageing factor is the humidity which causes in combination with electric stress a change of the conditions on the insulating surface. Ageing of the solid insulating material can occur both, on the surface and inside the material. In the presence of humidity, the characteristic of hydrophobic surfaces causes formation of single drops with large contact angles, which can unfortunately change when an electric field is applied. As a result of ageing the contact angles of the drops decrease and the covered surface becomes more wettable (decrease of hydrophobicity).
Discharges due to deformation of water drops on the surface of polymeric insulators are considered to be one of the ageing mechanisms responsible for the failure of insulators [80]. Thus, optical investigation has been used to observe the formation of water drops and the development of discharges between wa-

ter drops on the insulator surfaces. It has been observed that the discharges create a number of radicals and ionized species which may chemically react with the insulator surface and thus alter the original properties of the insulator materials [83]. The situation is further aggravated by the high temperature of some discharges which then thermally degrade the insulator surface [80].

2.6.6 Weather and UV stress

The most important stress to which a coating is exposed is probably the weather stress. Conditions in various parts of the world and also in one location show very large variations, such as seasonal, geographic and weather variations from year to year. Apart from contaminated industrial atmosphere and acid rain, the simple elements of weather - heat, light and moisture - can be very destructive to coatings.
The primary cause of weather-induced coating degradation is the energetic ultraviolet (UV) radiation component of sunlight [73]. The UVC ($\lambda < 280$ nm) region is the most energetic and destructive. Fortunately, such radiation is entirely absorbed by the earth's atmosphere though a certain amount originates from electrical discharges which can contribute to coating and insulator degradation in high voltage installations in the open air. A small amount of UVB ($280 - 320$ nm) radiation reaches the earth's surface, while about 6% of the total radiant energy reaching the earth's surface falls in the UVA ($320 - 400$ nm) region. Nevertheless, this can be sufficient to cause substantial damage to organic coatings. Photodegradation of organic coatings is caused by the absorption of energetic ultraviolet light, which either breaks chemical bonds directly, or results in the formation of free radicals, which can effect bond breaking or bond formation. Either process will result in changes in the physical properties of the coating, usually for the worse. Most organic bonds do not absorb UV light at frequencies above approximately 280 nm, and therefore are not directly damaged by sunlight. Unfortunately, most resins used in coatings contain small amounts of peroxide and ketone impurities, which can absorb sunlight to form free radicals [73] and initiate a process of photooxidation.

2.6.7 Methods to evaluate the ageing of coatings

How good a coating material looks and performs when initially applied is not necessarily an indicator of future performance. A coating should perform well both just after cure and well into the future. Developing methodology that will mimic and/or accelerate the effects of time, weathering, and environment can be a difficult task. The industries developed a variety of standardized tests which can often provide reliable indicators of future performance. However, it

is important to realize no test can duplicate all of the variables associated with a coatings environment and these tests can not guarantee future behaviour.
Two major categories for future performance testing are accelerated weathering and environmental testing [84]. These tests consist in analyzing life data of a product's sample operating under normal conditions in order to quantify the life characteristics of the product and make predictions about all of the products in the population. For a variety of reasons, manufacturers may wish to obtain reliability results for their products more quickly than they can with data obtained under normal operating conditions. Instead, they may use quantitative accelerated life tests to capture life data for the product under accelerated stress conditions, which cause the products to fail more quickly.
There are numerous international standards for accelerated ageing tests available [85, 86]. These tests include electrical, thermal, mechanical and environmental factors as single- sequential- or multifactor load. The practice in [85, 86] covers the accelerated ageing testing of electrical insulating materials to derive the thermal endurance characteristics. Although these procedures have been developed for use with electrical insulating materials, they can also be used also for the assessment of materials not intended for use as electrical insulation, such as coatings applied to HV lines. However, tests accredited under such standards require much effort and are very expensive and, therefore, a new procedure that allows testing of coatings applied to overhead lines with less effort had to be developed.

2.7 Precipitation

In Section 2.2 the rain rate has been mentioned as important parameter influencing the noise emissions. Moreover, in Section 2.4 it has been discussed how the size of water drops plays a decisive role in the appearance of corona discharges. For these reasons, it is important in the ageing analysis of a coating to know the frequency with which precipitation occurs, the classification of typical rain rates and of typical water drop sizes in the particular regions of interest.

2.7.1 Definition of precipitation

Precipitation is water released in the atmosphere from clouds in two forms: liquid (rain and drizzle) and solid (sleet, snow, hail and rime by sublimation). It is the primary connection in the water cycle that provides for the delivery of atmospheric water to the earth. In temperate regions most precipitation falls as rain. Mean annual precipitation is a climatological characteristic of a region, while knowledge of other precipitation characteristics such as intensity,

duration and precipitation form (like rain and snow) are of great interest to determine the amount and timing of runoff.

2.7.2 Type of falling precipitations

Six different types of precipitation are defined here:
Rain is liquid precipitation that reaches the surface in the form of drops that have a diameter greater than 0.5 mm. The intensity of rain is determined by the accumulation over a given time. Intensity of rain is classified as in the Table 2.2.
Sleet originates from snow at higher level which partly thaws at temperatures above zero and thus presents itself as a mixture of water and snow ("wet snow", slush).
Drizzle is liquid precipitation that reaches the surface in the form of drops that are less than 0.5 mm in diameter.
Snow is an aggregate of ice crystals which form into flakes and that forms at temperatures below freezing. The intensity of snow is determined by the accumulation over a given time. If the snow falls through a layer that is a little above freezing and the snow partially melts to form sleet.
*Hail*is dense precipitation ice that is that least 5 mm in diameter. It forms due to seed ice crystals and supercooled water that freeze or stick to an embryo hail stone.
Rime, "hoar frost", is due to crystalline sublimation of water vapour on surfaces (such as HV conductors).

Type of rain	**Intensity [mm/h]**
very light	< 0.25
light	0.25 - 1.0
moderate	1.0 - 4.0
heavy	4.0 -16.0
very heavy	16.0 - 50
extreme	> 50

Table 2.2: Classification of rain intensity [87].

Precipitation does not fall in the same amounts throughout the world, in a country, or even in a city. For example, according to data from *Regierungsrat des Kantons Zürich* [88] and from *Meteo Schweiz* [89], in Zurich no precipitation to a maximum of 1 mm/h falls in 92% of the time, at about 5% of the time

between 1 and 3 mm/h, and at 2% of the time a precipitation with intensity between 3 and 8 mm/h falls. Higher rain rates like 8 mm/h and more occur with a frequency of only 0.4%. An example of the distribution of a typical rain rate in Switzerland is represented in Figure 2.12.

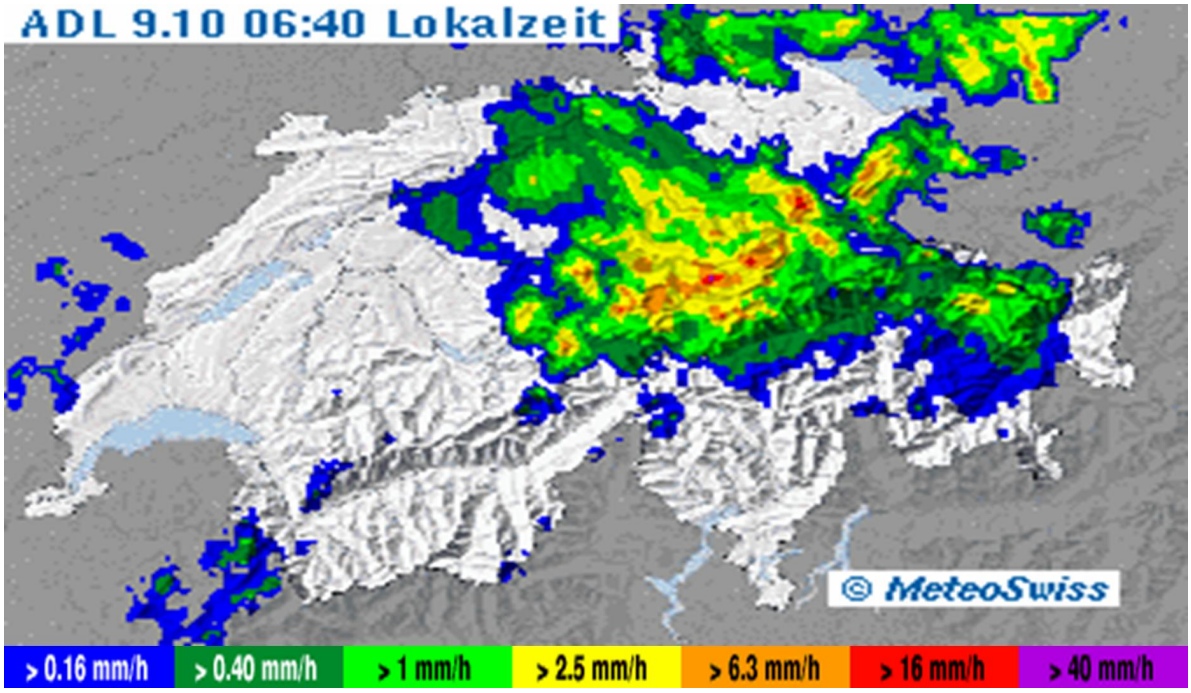

Figure 2.12: Typical instantaneous rain rates in Switzerland [89] at 06:40 on 9th October 2003.

2.7.3 Size of raindrops

Rain represents a very variable atmospheric parameter. Many of its characteristics depend on drops size, which is usually described through the drop diameter d assuming spherical drops.
For precipitation to happen, first tiny water droplets must condense on even tinier dust, salt, or smoke particles, which act as nuclei. Water droplets may grow as a result of additional condensation of water vapour. If enough collisions occur to produce a droplet which can have a fall velocity which exceeds ca. $v \approx 20\,\mathrm{cm/s}$, then it will fall out of the cloud as precipitation. Small raindrops, those with a radius of less than 1 mm, are spherical. As droplets collide and grow in size, the bottom of the drop begins to be affected by the resistance of the air through which it is falling. The bottom of the drop starts to flatten out until at about 2-3 mm in diameter the bottom is quite flat with an indention in the middle. When droplets reach about 4-5 mm dia., the indentation in the bottom greatly expands forming something like a parachute with two smaller droplets at the bottoms. The parachute does not last long, though, and the

large drop breaks up into smaller drops.
Typical rain drop size is given in Table 2.3. Also the corresponding volume is given, assuming a spherical shape of the drops.

Art of raindrops	Diameter d [mm]	Volume V [μl]
Small raindrops	0.1	$0.5 \cdot 10^{-3}$
Typical raindrops	1	0.5
	3	14.2
	4	33.5
Big raindrops	6	113.1

Table 2.3: Typical size of raindrops [87].

2.8 Assessment of measures to reduce corona noise

The central topic of this work is to find a method to judge the efficiency of measures against emission of tonal noise from high voltage lines. In particular, the effectiveness of hydrophilic coatings and their noise-reducing properties are investigated here. In this paragraph, the other possible measures to mitigate $2f$ emissions will also be briefly listed, since a combination of one or all of them with the use of a special hydrophilic coating could represent the optimal solution. Thus, the method sought should also quantify the efficacy of hydrophilic coatings when applied to different conductor types (e.g. changing the surface properties) and the effects due to different electric field strength.
From the literature it is well known that corona noise increases with increasing electric field strength, increasing conductor surface area (at a given field strength) and increasing number and radial size of protrusions, and with intensity of rain. Thus, corona noise can be reduced in three ways:

- reducing the electric field strength by changing the bundle and conductor geometry;
- changing the type and state of conductor;
- using an artificial hydrophilic coating on the conductor surface.

These measures have also been investigated in another doctoral thesis [4]. Further methods assessed for noise reduction are reported in the literature [90].

2.8.1 Electric field strength and bundle geometry

A well known method to reduce corona losses and thus the tonal emission during and after precipitation is reducing the electric field strength [19]. If the voltage of a transmission line is increased without changing the line design, the electric field at the surface of the line conductors will increase and this may lead to higher levels of corona.
A reduction of the electric field strength can be achieved using a larger size of conductor or using a number of conductors in a bundle. The higher the number of evenly placed conductors, the smaller is the surface electric field. Equations for the maximum field strength on the surface of a bundle (Figure 2.13) are given by Equation 2.22 [91].

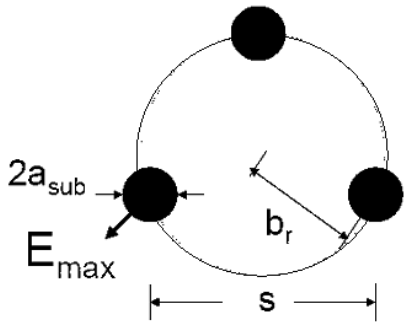

Figure 2.13: Conductor bundling.

$$E_{max} = \left(\frac{V_0}{n a_{sub} \ln \frac{2d}{a_{gmr}}} \right) \left(1 + a_{sub} \frac{(n-1)}{b_r} \right) \tag{2.22}$$

where n is number of subconductors, V_0 the applied voltage and:

$$b_r = \frac{s}{(2\sin(\frac{\pi}{n}))} \tag{2.23}$$

$$a_{gmr} = b_r \left(\frac{n a_{sub}}{b_r} \right)^{\frac{1}{n}} \tag{2.24}$$

Investigations on this subject [2, 17, 20, 21, 3], although not definitive in character, have indicated that the audible noise levels associated with conductor bundles of high voltage lines may reach fairly high levels. Control of such levels by means of a suitable choice of the bundle characteristics (number and diameter of the subconductors) seems to be less easy than in the case of radio interference [92].
Corona losses for a limited number of conductor arrangements (single and

bundles) in dependence upon geometries, applied voltage and ageing have been assessed 1953-1957 in an open air trial line installation [93]. In laboratory tests the effects of changes in size and number of subconductors in the bundles were considered in 1968 [2]. The set-up consisted of tubular conductors of undefined surface condition which were exposed to very heavy rain (60 to 600 mm/h) and the resulting corona was studied from various points of view: visual observation, photography, noise measurement with three different weightings and spectral analysis. The results were that audible noise levels increase with size of conductor *for the same gradients* and with the number of subconductors in a bundle *for the same gradients* and subconductor size. Although the emission of significant *2f* emission from the lines themselves had been pointed out about two decades earlier [22], the existence of tonal noise at twice mains frequency was nevertheless later [2, 21, 17] still ascribed to transformer and general switchyard origin. At that time, it was thought that the only important noise emission from a point of view of annoyance of the public was that at higher frequencies around 1 kHz and above.
The effects of conductor diameter [21] and of the number of conductors in a bundle [20, 21, 17, 19] on field strength on the conductor surface [17], have been investigated [94] and an attempt has been made to optimize bundles by non-uniform arrangement of the conductors [20]. The conclusion was that lowering the maximum field strength to minimize AN by increasing the number of conductors in a bundle (4, 6, 8) can bring considerable practical difficulties, for example with stringing and increasing ice load.

2.8.2 Type and state of the conductor

Tonal emissions could change depending on the type of conductors utilized. Some studies [20] introduced consideration of the surface conditions of the conductors and the relative orientation of the maximum electric field with respect to gravity. Furthermore, the intensity of rain was varied and the drying phase after rain was investigated [20] and it was found that surface conditions can play an important role in light rain or during the drying period.
There are different types of overhead conductors in use for transmission and distribution, such as aluminium alloy conductors, aluminium conductors steel reinforced, hollow conductors and gap conductors. The various combinations and modifications of these conductor types provide a wide variety of possible conductor system designs. The usual conductors are stranded. This lead to a higher surface field strength than with a smooth cylindrical conductor of the same diameter; in general, it is assumed that the field enhancement by stranding is about 1/0.82.
Some conductors are designed to present a smooth outer surface and marginally

reduced overall diameter. This smaller diameter can reduce the ice and wind loading encountered during severe weather.
The surface of a conductor must be relatively clean and smooth, however, special surface treatments or finishes may be required to reduce noise emissions. For instance, a possible way to reduce noise from high voltage lines is represented by the sandblasting process, which consists of treating the surface of the conductors with a spray of abrasive sand. This sandblasting gives rise to the formation of microscopic roughness.

2.8.3 Coatings for high voltage cables

The use of an artificial film on a conductor surface can reduce the number of water drops on the conductor and thus reduce considerably the corona noise under wet conditions.
The first proposal of using hydrophilic coatings to reduce noise emissions from high voltage lines has to be attributed to the research team of the Cavi Pirelli S.p.A. [7]. The invention proposed consisted of a conductor coat for overhead high voltage lines, composed of one or more electrically conductive materials and at least one hydrophilic material. The conductor thus prepared had the characteristics that during rainfall or significant humidity corona noise is suppressed or drastically reduced as compared to the same conductor without a hydrophilic material. The inventors demonstrated that noise associated with wet conductors can be suppressed, or at least, drastically reduced by means of covering the conductors with a mixture of composition indicated above. All the mixtures comprise a plastic resin or resin-rubber base (PVC, polyethylene, nitrile rubber, ethylene rubber, viny-acetate rubber etc., various additives such as anti-oxidants, plasticizes and lubricants). Tests carried out to verify if the invention worked successfully were conducted in an anechoic chamber and an acoustically insulated chamber, where the conductors were placed and kept under electrical tension and where the outside atmospheric conditions could be simulated. In the chamber the intensity of the noise emissions was measured. The hermetic coating at the conductor has the added advantage that the storage of water between the strands is avoided - there is then a faster recovery of quiet conditions after rain.
Another proposal to use a film of a hydrophilic compound came from a Japanese patent [8] in which the surface of the aluminum conductor was first roughened by blasting and then provided with a hydrophilic film, such as boehmite film, an anodic oxide film, a chromate film or a chemical conversion film. For the tests, samples of aluminium conductors were prepared under various conditions and the attenuation of audible noise levels measured. The samples were energized, and water sprayed at a rate of 30 mm/hour. Some samples

were subjected to a blasting treatment; results showed excellent noise levels of 39 dB. However, when the same samples have been left in a room under relatively poor conditions for six months, the noise level was degraded to 58 dB. Other samples having the protective film of wetting agent or of a hydrophilic nature on the hydrophilic film on the conductor surface, retained excellent noise levels for a prolonged period of time after long time storage.

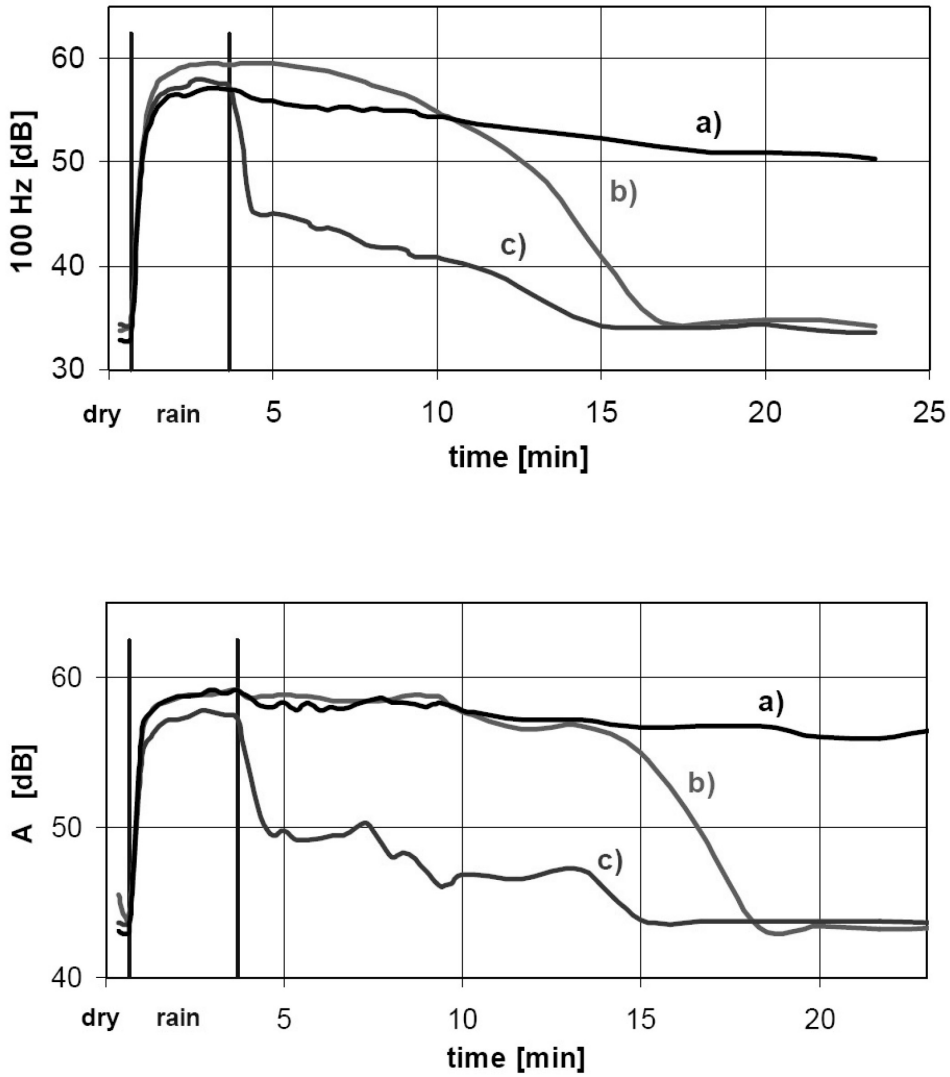

Figure 2.14: 100 Hz and A-weighted AN during and after "heavy rain"for three conductors of different surface state: a) hydrophobic, b) sandblasted c) highly hydrophilic [6].

Some more recent investigations [6, 5] taking into account both A-weighted and tonal noise have indicated that hydrophilic coating, particularly with inclined sections of line, could alleviate the situation after cessation of heavy rain by assisting runoff, eliminating drops except on the underside of conductors and generally speeding up the drying of the line. Since the methods used for testing different conductors and to measure noise emission are similar to the method acquired for the present work, the detailed technical description of the setup will be given in the next chapters.
These investigations showed that (Figure 2.14) with a strongly hydrophilic conductor there is a rapid initial decay of noise on cessation of rain, followed by a slower but still very marked further decay to very low levels indeed. However, the coating used at that time in these laboratory tests could not be expected to stand up to the elements for long and thus further research of a suitable coating for high voltage lines remained open.

3 Research goal

To find a method to quantify the effectiveness of the use of hydrophilic coatings to cover high voltage transmission lines and thus their noise-reducing effect, one has to consider different steps. In fact, there are different phenomena tied together which need to be initially investigated individually and then assembled into an overall picture.
As seen in Chapter 2, Section 2.6, the ageing processes of coatings are well established and many investigations have already been carried out. However, in order to build a method capable of testing the efficacy of coatings in the particular case in which they are applied to high voltage lines, more knowledge about the physical mechanisms involved, the ageing process and its influencing factors in such high voltage systems is necessary. Bearing this in mind and considering the state of the art as outlined in Chapter 2, the following scientific topics were identified:

- **Study of the behaviour of single sessile water drops in an electric field**
  To improve the understanding of the ageing phenomenon and thus to be able to deliver a method for the quantification of coatings, it seems advisable to observe at first single drops on these. As mentioned in Section 2.4, several authors have studied the effects of water drop size, water resistivity and contact angle on the inception voltage, but only little is known about the dependence on the surface properties. It appears that, the behaviour of water drops located on hydrophobic surfaces is fairly well understood, due to an interest in the understanding of the ageing phenomena occurring on insulating surfaces of high voltage equipment, as seen in Section 2.6. However, the behaviour of water drops electrically stressed on hydrophilic surfaces has not been extensively investigated. Since the shape of the drops supplies more information about the status of the surface, the deformation and instabilities of the drops have to be measured and classified depending on the size of drops, on the type of surface and on the applied DC or AC electric field strength. For different drop sizes the effect of the surface property on the resonance phenomena of water drops has also to be analyzed.
  How does a single sessile drop behave under a AC or DC field on different surfaces (untreated, hydrophobic, hydrophilic)? Does a method

exist to calculate in an easy, economical and quick way the contact angle of water drops under high voltage on different surfaces? Which information does the instability and deformation of a single water drop bring for the characterization of a coating?

- **Evaluation of drop population as function of time, geometry, surface properties and electric field at the conductors**
  Considering that the ensemble of water drops forms the most important discharge source and that discharge activity might significantly affect the properties of coatings, the drop populations and their development on different surfaces must be included in the steps to evaluate comprehensively the efficacy of coatings on high voltage lines. Since drop populations on electrically stressed surfaces have not been described so far (see Section 2.5), their change with time, geometry, applied electric field strength and surface properties have also not been investigated. After having identified the drop population on different surfaces without the application of voltage, the behaviour and life of water drops on various surfaces and under the influence of the electric field has to be described. In Section 2.5 it has been pointed out that a perfect method to obtain well-defined pictures of water drops on a surface which can be automatically processed had not been developed. Therefore, to find out automatically the drop population on the conductors, a tool that allows a more rapid counting and sizing of the drops has to be brought about.
  What is the drop population on high voltage lines during and after periods of rain? Does a method exist to establish in an easy, economic and quick way the statistics of water drops on different high voltage conductors? What is the lifetime of water drops of different sizes?

- **Description of the stress factors that can lead to degradation of hydrophilic coatings**
  The basic mechanisms by which a coating can fail are only known for selected materials (see Section 2.6). Moreover, the description of the major factors and forces affecting the durability of the particular coatings applied to high voltage lines is missing. The different stress factors that could affect hydrophilic coatings need to be described.
  Which kind of coatings could be suitable to cover high voltage lines? What are the factors affecting the longevity of hydrophilic coatings applied to high voltage lines?

- **Development of a method to test hydrophilic coatings apart from their application to high voltage lines**
  There are a variety of miscellaneous methods for evaluating the change of the physical properties of coatings, as described in Section 2.6. There

is a collection of such test methods compiled by the American Society for Testing and Materials (ASTM) and by IEC; however, they require much effort and thus tend to be very expensive. A suitable method to quantify the effect of ageing of hydrophilic coatings with less efforts had to be developed.
Can an easy method be developed to investigate whether a hydrophilic coating would potentially be good to cover high voltage lines?

- **Description of ageing tests for hydrophilic coatings applied to high voltage lines**
  According to the providers of hydrophilic coatings, their product fulfil long-term durability requirements under normal conditions; however, for high-voltage conditions resulting in high electric fields and bombardment by ions, the suppliers have no experience to date. Such stresses on the coatings have to be tested. The possibility that the charged conductor would become polluted, accompanied by possible loss of the hydrophilic characteristics, has to be investigated.
  Can a suitable ageing test be developed for hydrophilic coatings applied to high voltage lines?

- **Development of a general method to evaluate the conditions of hydrophilic coatings applied to high voltage lines**
  A step by step method to quantify hydrophilic coatings and to check whether the coating failed has to be derived. The success of application of such coatings to high voltage lines, including their endurance throughout the service life of the line, has to be investigated by means of a tool.
  Can a general tool be generated to evaluate any kind of hydrophilic coating applied to high voltage lines? What are the limitations and shortcomings of such a method?

4 Behaviour of water drops in a DC and an AC field

In Section 2.4 the role of deformation of water drops in the electric field as the origin of $2f$ emission has been described. It had been concluded that periodically oscillating drops play a decisive role for the origin of tonal noise [95]. The assumption used here is that sessile water drop geometries reveal important information on the properties and on the eventual changes of the analyzed surfaces and so they have to be taken into consideration in the evaluation of coatings. Thus, to generate a method for the qualification and quantification of coatings applied to high voltage transmission lines, a thorough understanding of the electrodynamic behaviour of single water drops with and without exposure to electrical fields is necessary.
As seen in Section 2.4, the characteristics of deformation and instabilities of water drops in high electric fields have been thoroughly investigated during the last century or more. In this chapter it is studied how these characteristics are strongly linked to the surface conditions [96, 95]. The processes involved in their entirety, including the associated electrical discharges which could deteriorate the surfaces, required also further clarification and are subject to this part of the investigation. A record of all stages of time-dependent development of water drop instability was needed, aiming to catch step by step the ejection of a fine water jet which results from instability. For further characterization of surfaces, resonance effects with single water drops through AC investigations had also to be embraced.

4.1 The measurement of contact angle

For the characterization of a surface, it is at first necessary to measure the contact angle of a water drop on the surface. As seen in Section 2.3, several methods are currently available for measuring contact angles. Moreover, in Section 2.3, it has been pointed out that contact angle measurements can be troublesome and that data obtained may be very questionable as regards their accuracy and reproducibility. In some cases, errors may arise due to surface roughness or chemical heterogeneity, which impairs accurate measurements [39]. It is therefore an additional aim to investigate influences that arise with

contact angle measurements of water drops in an electric field. In particular, the influence of the measurement method, of the water drop size, of the surface roughness and of the measurement duration on the analysis of contact angle data shall be described.

4.1.1 Influence of the measuring technique

The first step to characterize a surface is placing a water drop of defined volume on the solid sample surface, which has to be always exactly horizontal. To apply reproducible uniform volume drops of deionized water, calibrated micropipettes were used. The volumes of the water drops used in the following experiments was in the range of $5-100\,\mu$l. Drop shape was recorded with a still camera or a high speed framing camera, and images were then processed by a computer and stored. It has been noticed that the uncertainty in the measurements depends mostly on the light-dark contrasts of the drop picture, in particular at the air-liquid-solid triple point, and on the method used for the evaluation.
For the purpose of this study, the sessile drop method was chosen. In most of the experiments described here static contact angles were measured; only if differently specified advancing and receding angles were also considered. Furthermore, since a drop does not necessarily behave symmetrically in the electric field, the contact angles have been separately determined at the left and at right sides; as result the average of the left and right values have been used. At this stage two methods, depending on the degree of drop picture quality, for contact angle measurements were chosen: manually and using a software.
Numerous problems have been encountered in the experiments carried out. It has been noticed that it is easy for the program to find the drop profile, but hard for it to find the correct baseline, which may be obscured in the image; furthermore the specimen may have been somewhat irregular. Conversely, it has been seen that it is easy for a person to locate the baseline but fitting a tangent to the drop profile is more difficult and the measurements appeared to be strongly subjective and a larger error has to be assumed.
Measuring contact angle with a software has the big advantage that it enables one to determine contact angles on solids rapidly and easily, as already said in Section 2.3. Many companies in the world sell costly systems [39] which provide a number of features that make the procedure for contact angle measurements easy and versatile. However, since for this study only approximate values of contact angles were required and considering that the use of such systems would present some difficulties under application of high voltage, that investment in costly systems would not have been justified. So, for a

more rapid but also a more economical method to analyze the image of a drop and, therefore, to assess contact angle, a suitable software has been developed. The program, a Matlab script (see Appendix B.1 for details), permits hands-free measurements using image acquisition and image processing techniques. Most commercial instruments do not allow the measurement of small contact angles and have only a spherical mode where the shape of the drop is approximated by a circle in the image. The program used here allows also the measurement of quite small contact angles and includes a more complex equation to better approximate the drop shape when it is no longer perfectly spherical. First the program reduces the grey-scale image of the drop to a set of equations describing the periphery, and then it obtains the intersection of the baseline with the tangent. Another possible way to obtain an approximate value of the contact angle using image processing is to fit a circle to the drop profile using a polynomial regression. The different steps in the processing technique are presented in Figure 4.1. The results of a comparison between

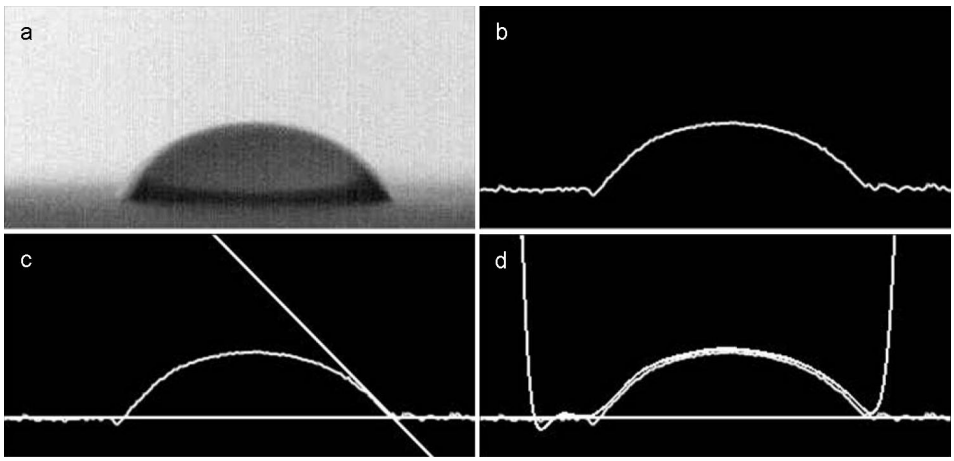

Figure 4.1: Routine image processing to calculate the contact angle of a water drop. 30 μl water drop. a) Original image, b) Black and white image and extraction of the contours c) Image with the base line and the tangent, d) Image with the base line and the fitted polynomial curve.

the methods described above for a 30 μl water drop on an aluminium glass bead blasted surface is presented in Table 4.1 and show that the measurement using the software produces a lower uncertainty (about 2°), while a larger error (4°) is encountered in measurements made manually. One can see that the mean value seems to show no significant difference for the first three different methods mentioned above. The value of contact angle obtained using the half angle method, i.e. assuming that the drop profile is represented by a portion of a perfect circle of defined radius and center, is also given in Table 4.1. This value results in a larger contact angle (by $\sim 7°$) compared to the values

obtained with the other methods, because the shape of this 30 μl drop is not particularly well approximated by a circle.

Methods	θ
baseline + fitted curve	$48.68^\circ \pm 2.8^\circ$
tangent drawn manually	$48.40^\circ \pm 4.0^\circ$
baseline + fitted tangent	$48.25^\circ \pm 2.1^\circ$
half angle method	$55.10^\circ \pm 1.0^\circ$

Table 4.1: Comparison between different contact angle measurement methods applied to the same drop image of a 30 μl water drop.

4.1.2 Influence of the surface roughness of the substrate

To check the influence of surface roughness on contact angle measurements, surfaces were variously prepared for each measurement: stainless steel polished (smooth surface), aluminium sandblasted and aluminium glass beads blasted. Coatings were obtained for assessment from commercial and institutional sources; for a detailed description of coatings applied to surfaces see Chapter 6. A commercial hydrophobic coating based on silica and a hydrophilic TiO_2 powder were applied to all the substrates mentioned.
The contact angles for different states (untreated, hydrophobic and hydrophilic) of the surfaces in the absence of high voltage are presented for a 50 μl drop in Figure 4.2. Contact angles were measured using the program mentioned in Section 4.1. It can be observed that when the surface is smooth (as in the case of stainless steel), the contact angle of the untreated state is much larger than in the case of a surface presenting a higher roughness. This means that with a sandblasted surface it is already possible to achieve a significant reduction in contact angle without coating. Applying an hydrophilic coating to all surfaces has in all cases shown a significant decrease in contact angle.

4.1.3 Influence of the drop volume

From the literature it is known that the size of drops also influences the value of the contact angle [97, 98]. Furthermore, as it will be reported in Chapter 7, only a size dependent fraction of the drop population contributes to tonal noise emissions. Therefore, the influence of the size of water drops shall

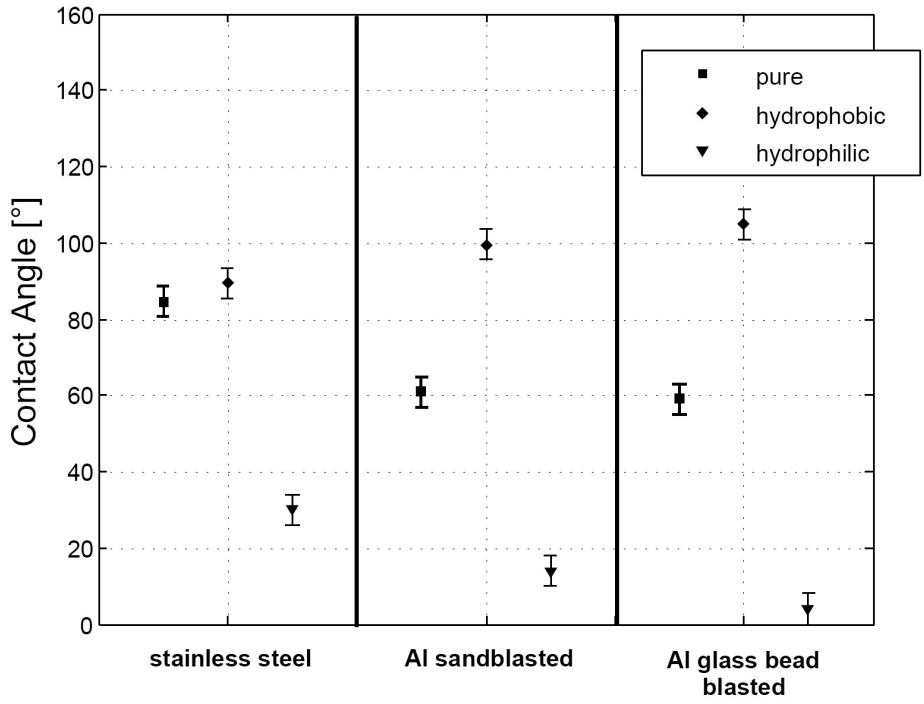

Figure 4.2: Contact angle for a 50 μl water drop on stainless steel, sandblasted aluminium, aluminium glass bead blasted surfaces carrying different coatings.

also be considered for the analysis of contact angle of water drops on different surfaces.
Table 4.2 shows the mean value of the contact angle in dependence upon water drop volume ($30 - 100\,\mu$l) for all the surface treatments considered: stainless steel, sandblasted and glass bead blasted aluminium surfaces and carrying hydrophobic and hydrophilic coatings. Contact angles were measured using the usual program, when possible, otherwise using the goniometry technique. For each contact angle value and for each considered surface treatment, ten measurements have been made and the mean value of the set of measurements is reported here. The results show that for the untreated surfaces the contact angle increases as the volume of drops increases. For hydrophobic and hydrophilic surfaces no particular trend can be observed; the lack of an observable trend with the hydrophilic surface may also be due to the larger error which is encountered when measuring small contact angles. There may also be some scatter due to the non-uniformity of the analyzed surfaces.

Surface treatment	100 µl	80 µl	50 µl	20 µl
Stainless steel	88.5°	88.0°	84.5°	82.0°
Stainless steel hydrophobic	90.5°	87.0°	89.5°	86.0°
Stainless steel hydrophilic (powder)	9.3°	14.3°	20.9°	25.5°
Stainless steel hydrophilic (SiO_2)	62.5°	63.0°	62.5°	60.5°
Al sandblasted	71.0°	65.5°	61°	59.5°
Al sandblasted hydrophobic	130.5°	119.5°	99.5°	115°
Al sandblasted hydrophilic	26.0°	21.0°	14.0°	9.5°
Al glass bead blasted	68.5°	58.0°	59.0°	48.5°
Al glass bead blasted hydrophobic	101.5°	104.0°	105.0°	100.0°
Al glass bead blasted hydrophilic	6.0°	5.0°	4.0°	-

Table 4.2: Contact angle for 100, 80, 50 and 20 µl water drops on stainless steel, sandblasted aluminium, aluminium glass bead blasted with surface treatment: untreated, hydrophobic and hydrophilic.

4.1.4 Influence of the measurement duration

To show the effect of the elapsed time linked with evaporation on the contact angle measurement, drops on sandblasted aluminium and stainless steel surfaces were investigated again without the influence of an electric field. Pictures were recorded at room temperature of 20°C and 40% relative humidity. The contact angle was then measured with both methods, i.e. manually and using the program.

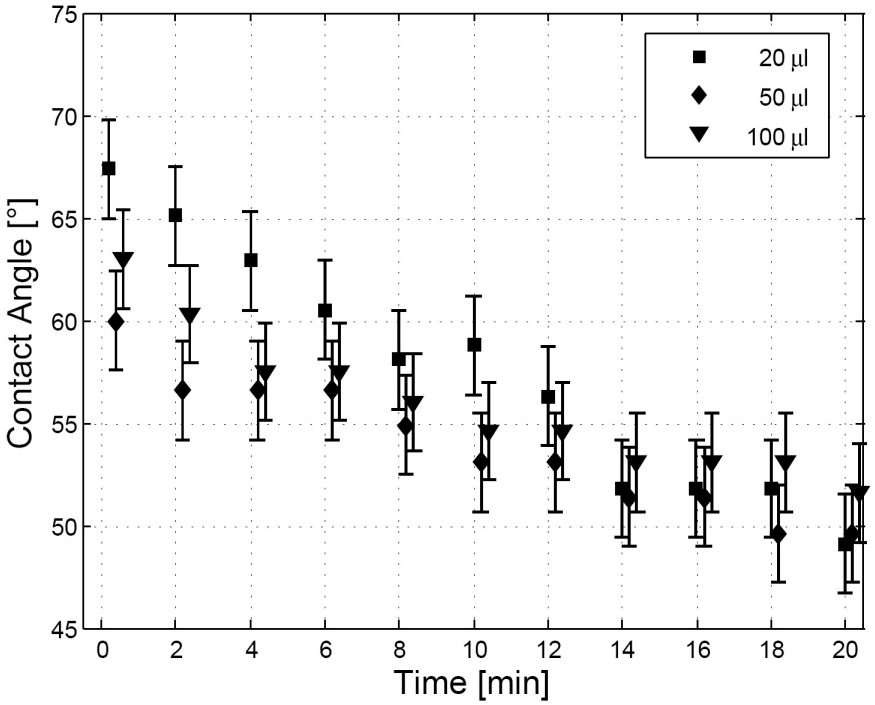

Figure 4.3: Contact angle versus elapsed time for 20, 50 and 100 μl drops on sandblasted aluminium surfaces.

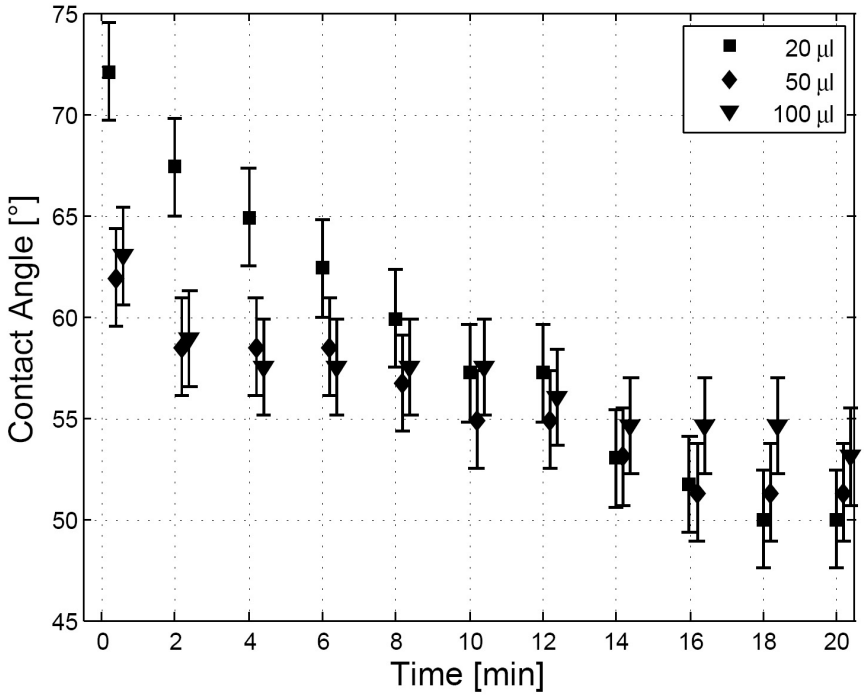

Figure 4.4: Contact angle versus time for 20, 50 and 100 μl drops on stainless steel surfaces.

Figures 4.3 and 4.4 illustrate the decrease of contact angle with time for three initial drop volumes (20, 50 and 100 μl) for a rough surface (sandblasted aluminium) and a smooth/polished surface (stainless steel). Within a few minutes the loss of volume due to evaporation - manifesting itself in a decrease of contact angle - is quite evident with both surfaces and with all drop sizes, as in [42]. At this point it can be stated that with both stainless steel and sandblasted aluminium surfaces, the time t elapsed until the contact angle is measured should be less than 2 minutes, in order not to influence the results significantly, in accord with [38]. This is a good choice, because, as will be explained in the next sections, the experiments with electric fields were carried out within 1.5 minutes including deposition of the drops and taking the normal security steps required before starting an experiment using high voltage. Moreover, in the present experiments the temperature of the electrodes on which the drops were positioned did not change during application of high voltage.
As shown in Figures 4.3 and 4.4, contact angle on the uncoated surface decreases a little with *increasing* drop size (with the surface considered here) but decreases more with *decreasing* drop volume.

4.2 Deformation and instabilities of single water drops on different surfaces

To assess coatings properties, the contact angles of water drops of controlled volume under high voltage on a series of surface preparations on stainless steel and aluminium have been determined. Untreated, sandblasted or glass bead blasted surfaces were investigated without any further treatment, with proprietary hydrophobic and moderately hydrophilic coating or with a titania-based preparation. Two parallel metal plates of defined dimensions and shapes (6.5 cm diameter, 90° Rogowski profile) were arranged with 1 cm gap. The upper electrode was always stainless steel without any treatment, while the lower one was varied to test different surfaces and coatings available. After each measurement the lower electrode was rubbed down with ethyl alcohol to restore uniform starting conditions. The test set-up and equipment for the measurement are described in more detail in the Appendix A.1. The arrangement of Figure A.1, supplemented as required by a framing camera, was used to study drop deformation and instability. The following results are documented with numerous video films made with the high speed camera using a recording time of 16 seconds and a recording rate of 2000 frames per second. The water drops were always illuminated indirectly, to avoid rapid evaporation.

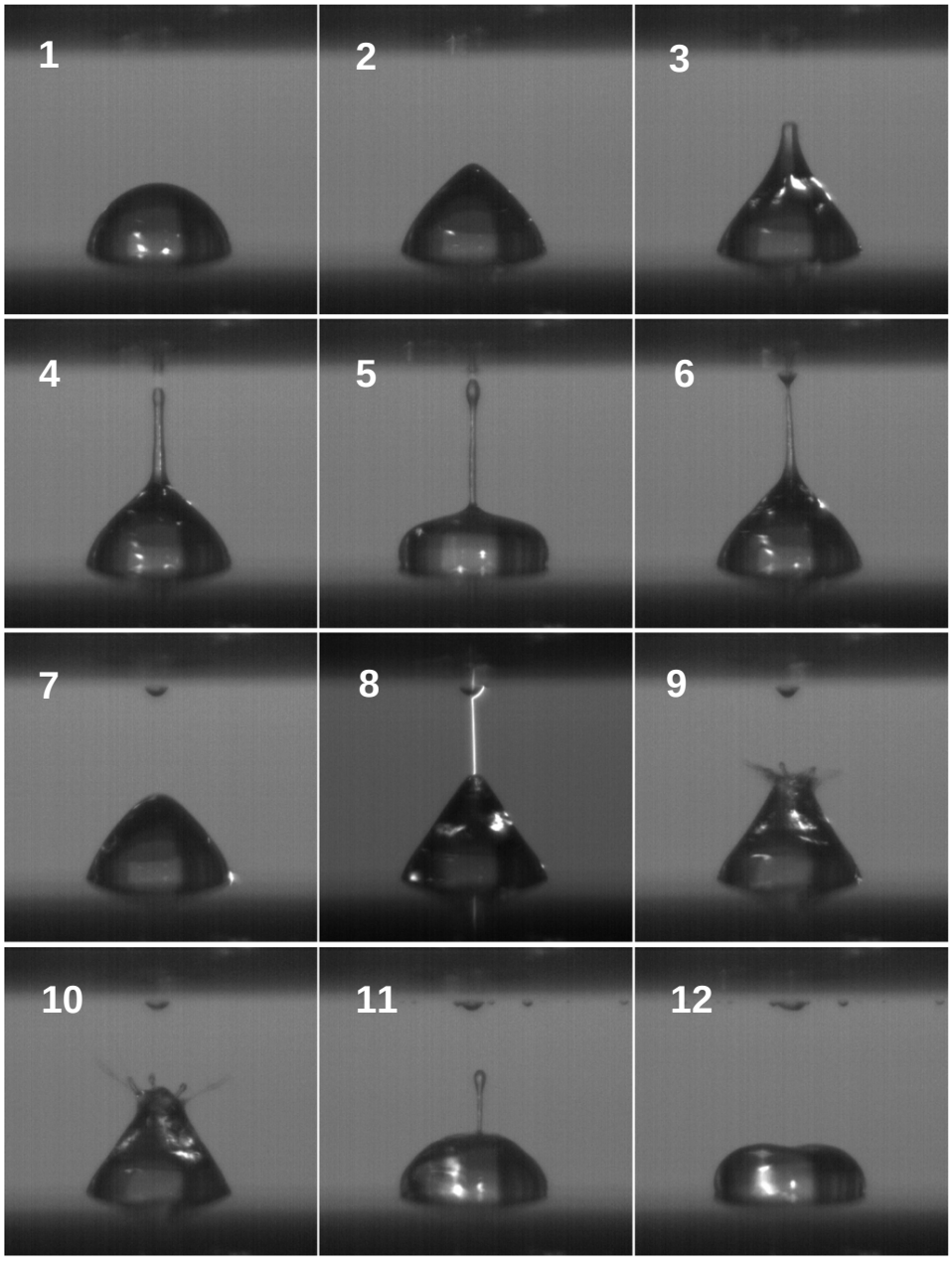

Figure 4.5: Applying a slow ramp voltage to the discharge gap results in a sequence of instabilities of the 100 μl water drop. Time between frames about 20 ms, untreated stainless steel surface, gap spacing 10 mm, instability onset about 10700 V. Picture Nr.8 shows a perfect Taylor cone, obviously leading rapidly to a flashover.

As the available recording times at high frame rates are only some seconds, a high voltage DC ramp is produced by controlling the high voltage source by a programmable function generator (see Figure A.1b in the Appendix). Feeding the discharge gap with such a ramp voltage will lead to repeated instabilities like those in Figure 4.5. Ejected water jets take charge with them and screen the droplet apex, which leads to droplet collapse followed by repetition of the process. The charged free droplets ejected migrate to the counter-electrode.

4.2.1 Instability voltage in dependence on drop size and surface properties

The behaviour of water drops on different surfaces when high voltage is applied is studied using the high speed camera and the contact angle measuring technique described in Section 4.1. The aim of this study was to characterize the behaviour of the drops in the electrical field and to find out typical and reproducible movements.
When high voltage is applied, water drops begin to deform from a certain value of the voltage which depends on the volume of the drops and on the surface properties. To see how water drops of different sizes behave under the influence of an electric field, experiments carried out with water drops of 30 μl, 50 μl and 100 μl positioned on an aluminium glass beads blasted surface coated with a hydrophobic preparation are represented in the sequences in Figures 4.6, 4.7, 4.8.
The deformation of a 50 μl water drop in the electric field on different surfaces in the parallel plate configuration is illustrated in the sequences in Figures 4.9, 4.10 , 4.11, 4.12, 4.13. The growing axial elongation of the drop with increasing field is quite evident.

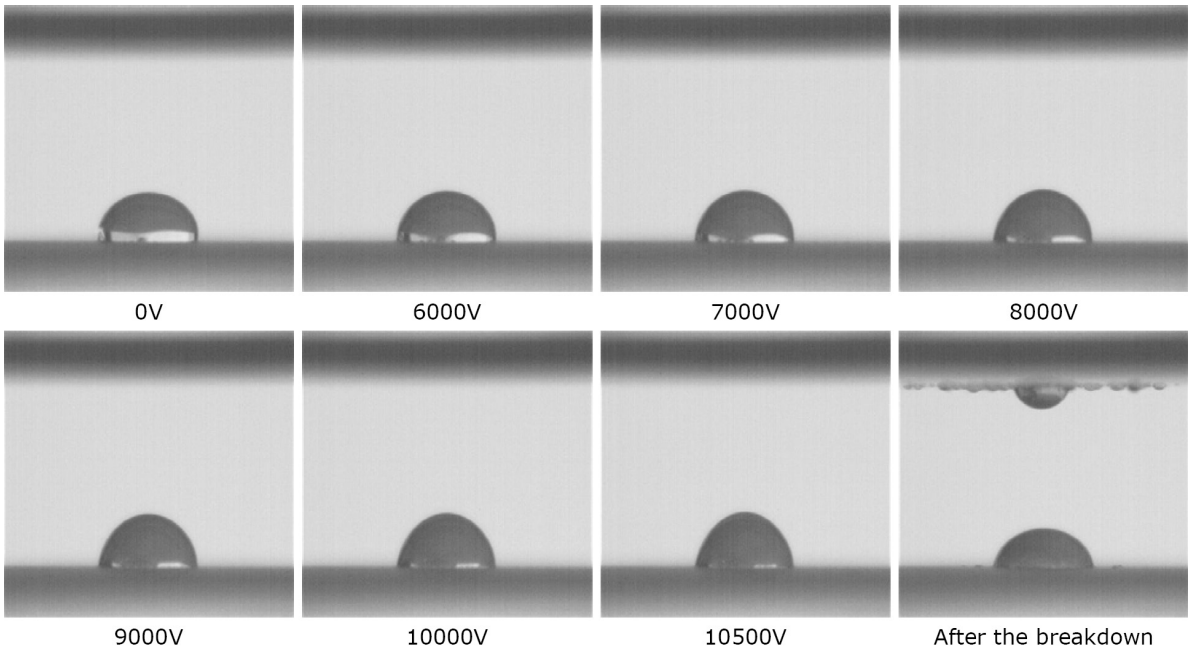

Figure 4.6: Deformation of a 30 μl water droplet by the DC electric field. Aluminium surface, glass beads blasted and subjected to a proprietary hydrophobic preparation. Gap spacing 10 mm. The sequence was terminated on reaching instability ($>$ 10500 V).

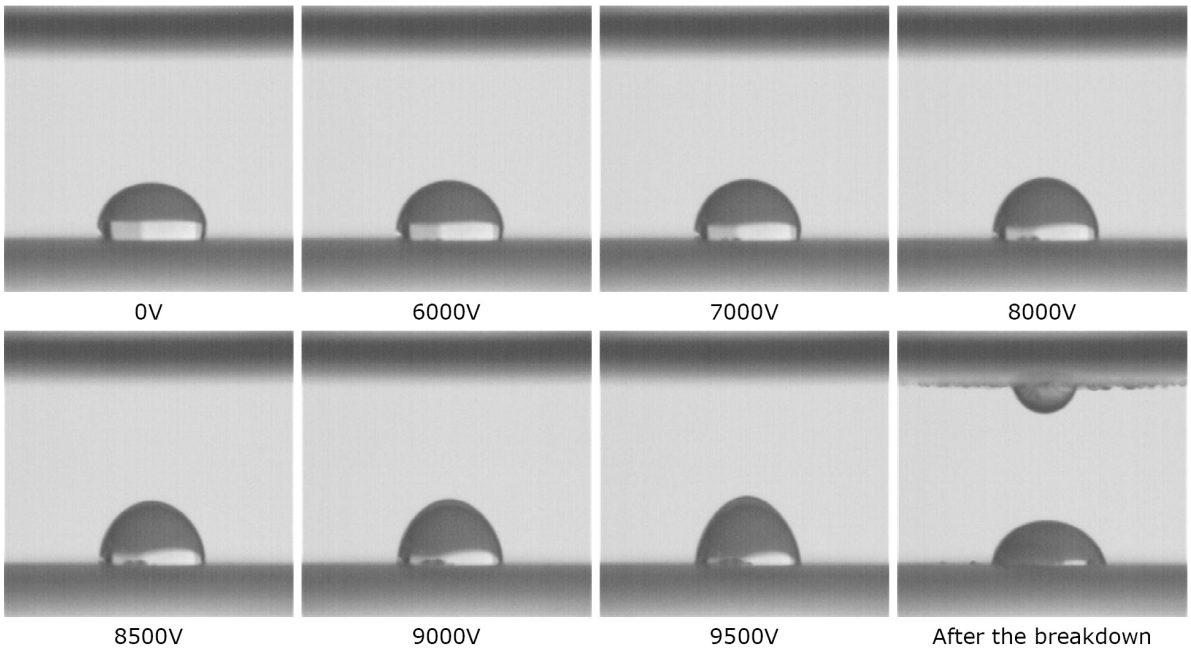

Figure 4.7: Deformation of a 50 μl water droplet by the DC electric field. Aluminium surface, glass beads blasted and subjected to a proprietary hydrophobic preparation. Gap spacing 10 mm. The sequence was terminated on reaching instability ($>$ 9500 V).

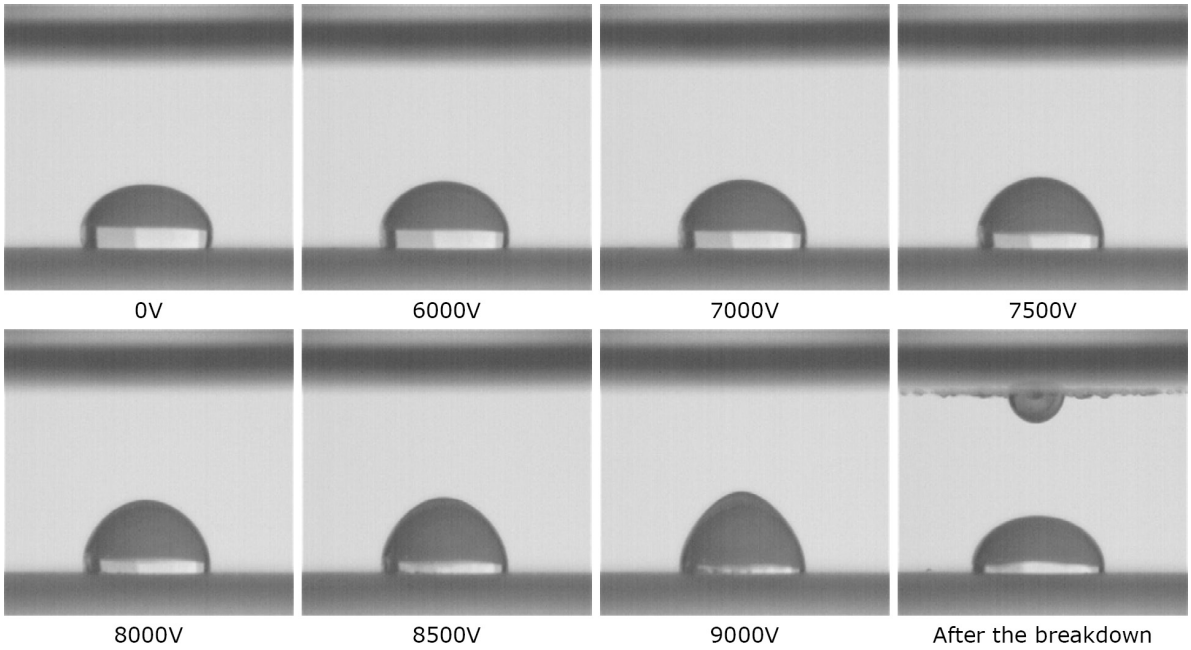

Figure 4.8: Deformation of a 100 μl water droplet by the DC electric field. Aluminium surface, glass beads blasted and subjected to a proprietary hydrophobic preparation. Gap spacing 10 mm. The sequence was terminated on reaching instability ($>$ 9000 V).

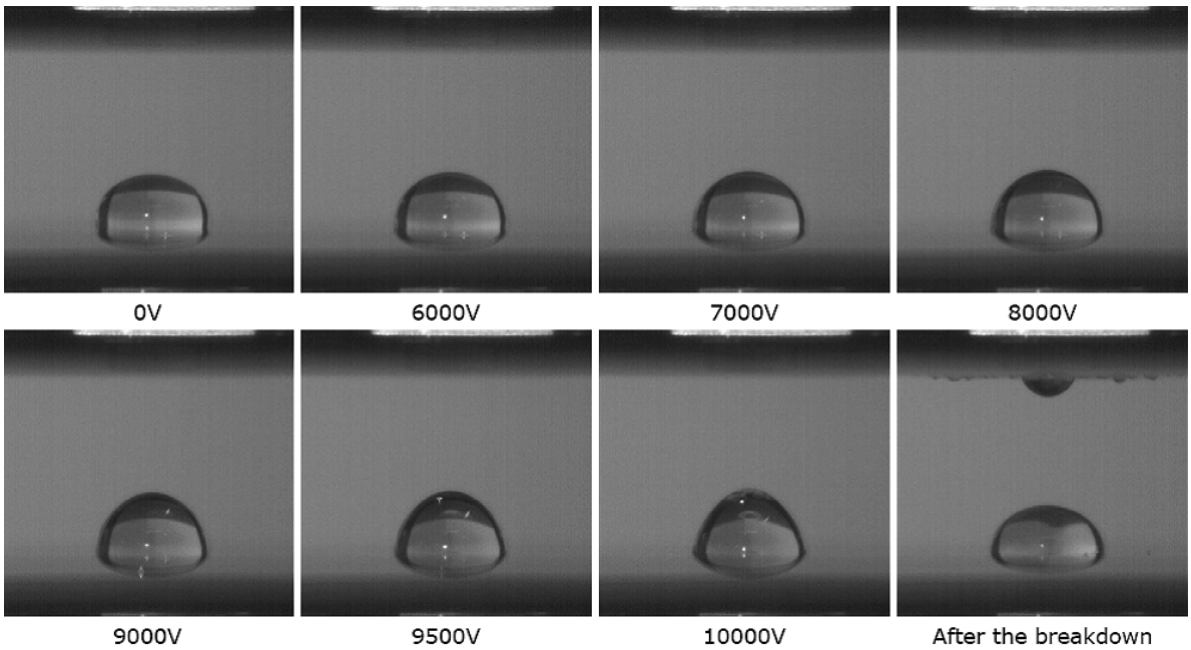

Figure 4.9: Deformation of a 50 μl water droplet by the DC electric field. Stainless steel surface and subjected to a proprietary hydrophobic preparation. Gap spacing 10 mm. The sequence was terminated on reaching instability ($>$ 10000 V).

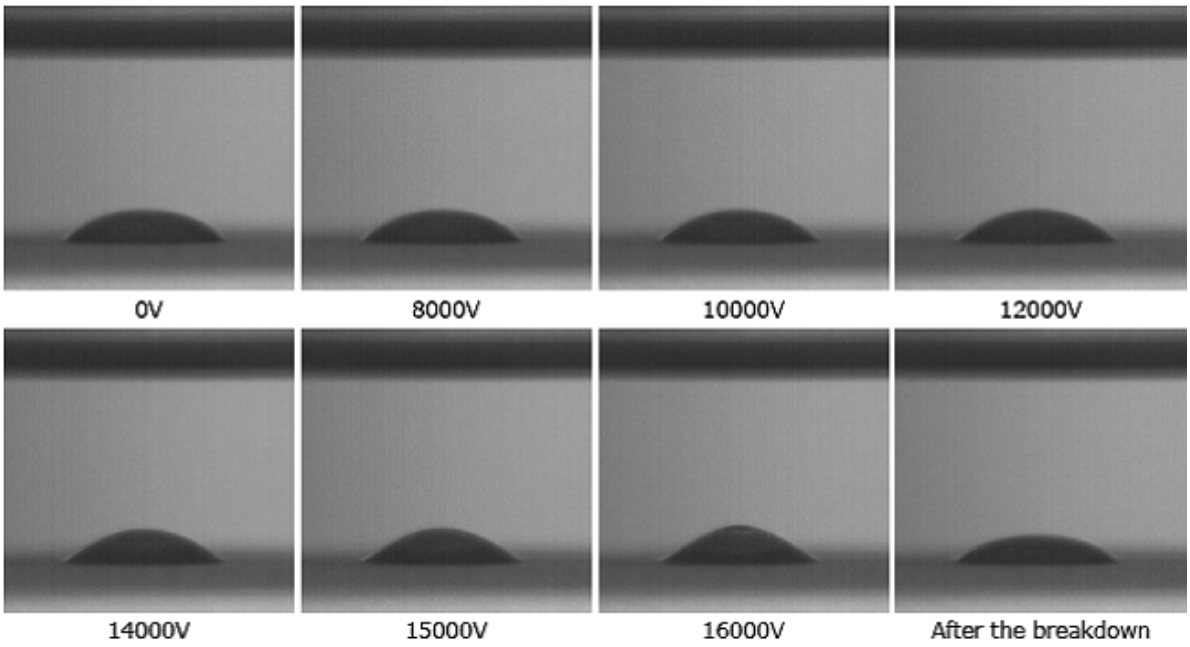

Figure 4.10: Deformation of a 50 μl water droplet by the DC electric field. Aluminium surface, sandblasted. Gap spacing 10 mm. The sequence was terminated on reaching instability (>16000 V).

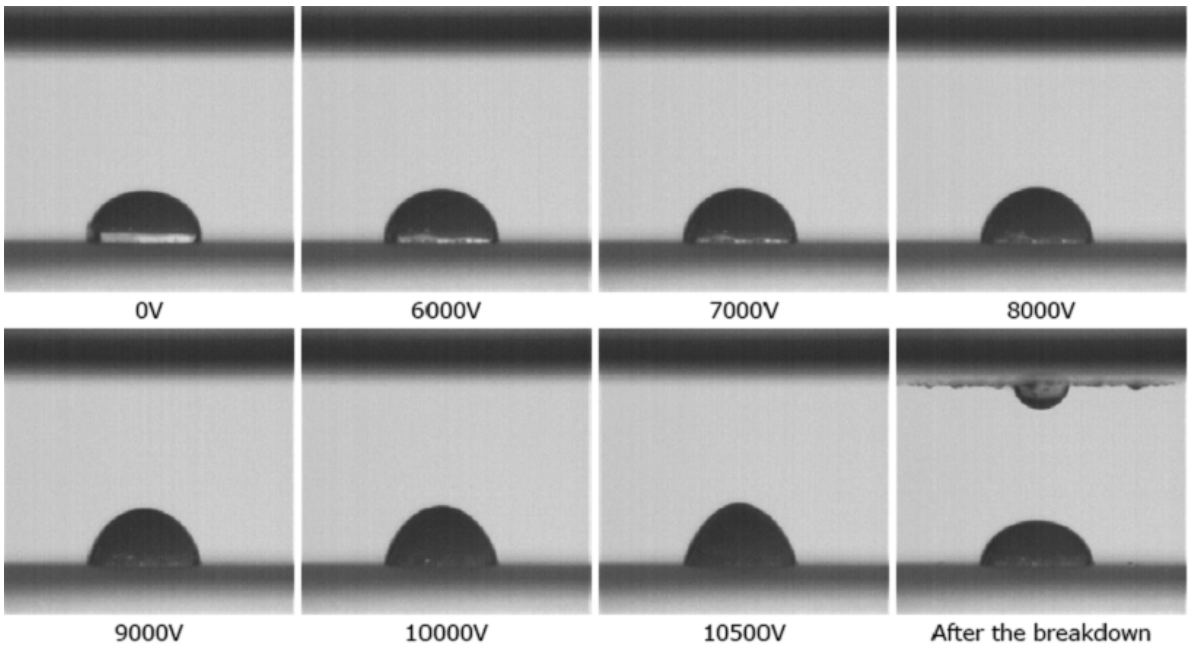

Figure 4.11: Deformation of a 50 μl water droplet by the DC electric field. Aluminium surface, sandblasted and subjected to a proprietary hydrophobic preparation. Gap spacing 10 mm. The sequence was terminated on reaching instability (> 10500 V).

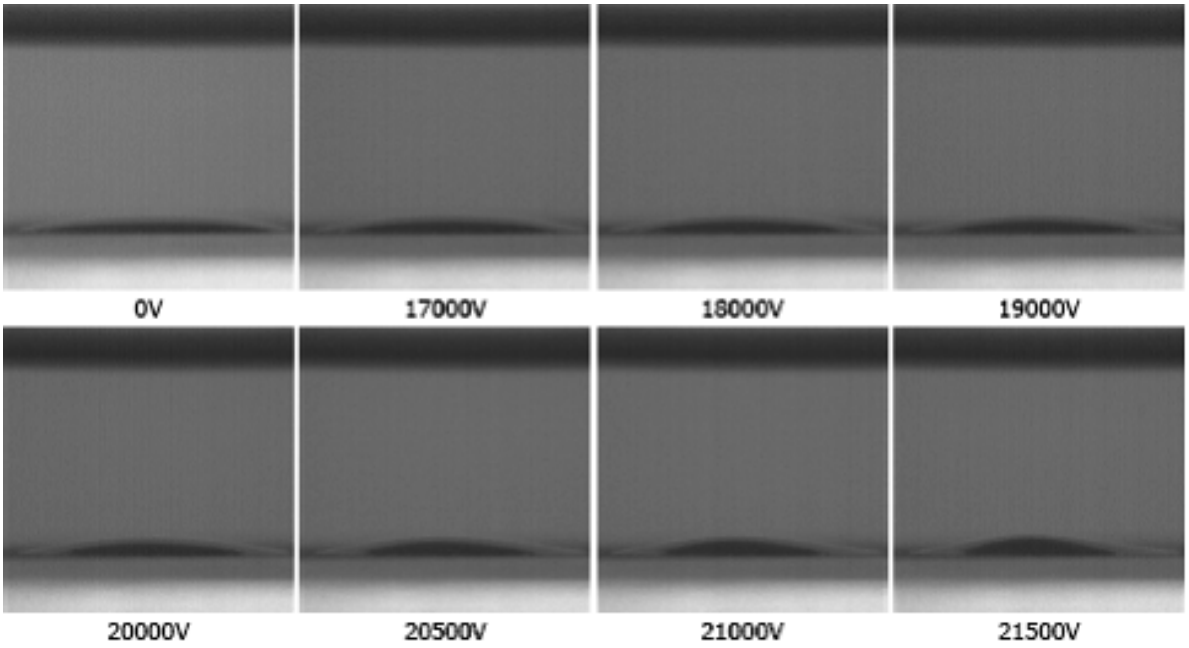

Figure 4.12: Deformation of a 50 μl water droplet by the DC electric field. Aluminium surface, sandblasted and subjected to a proprietary hydrophilic preparation. Gap spacing 10 mm. The sequence was terminated on reaching instability ($>$ 21500 V).

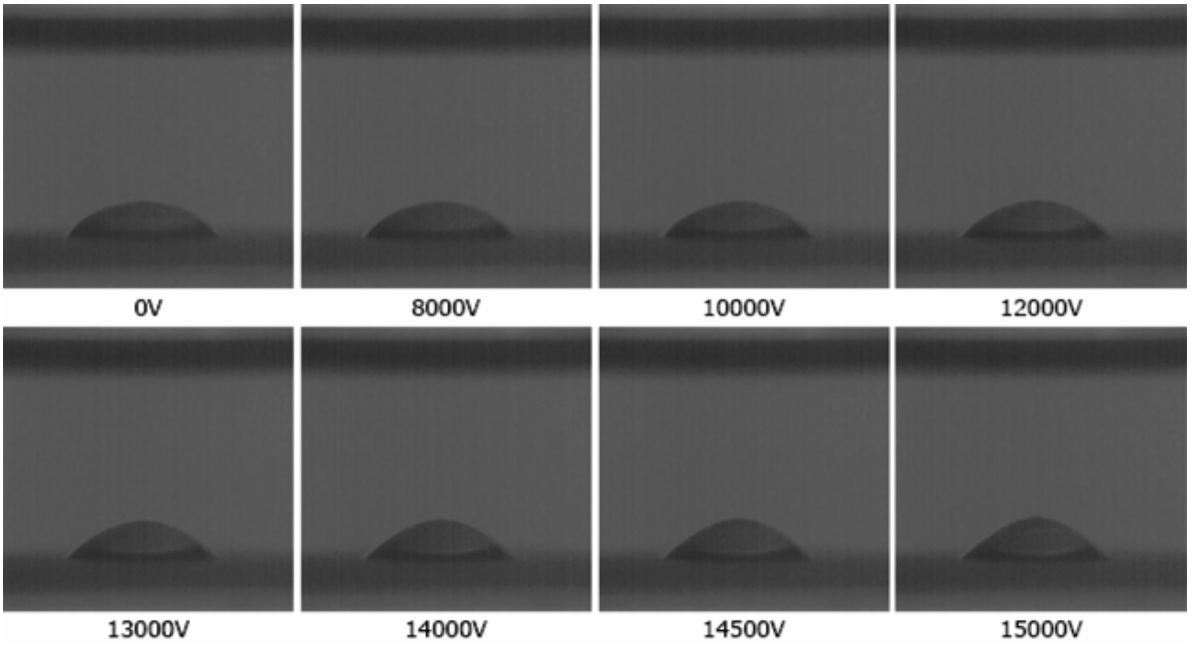

Figure 4.13: Deformation of a 50 μl water droplet by the DC electric field. Aluminium surface, polished and glass beads blasted. Gap spacing 10 mm. The sequence was terminated on reaching instability ($>$ 15000V).

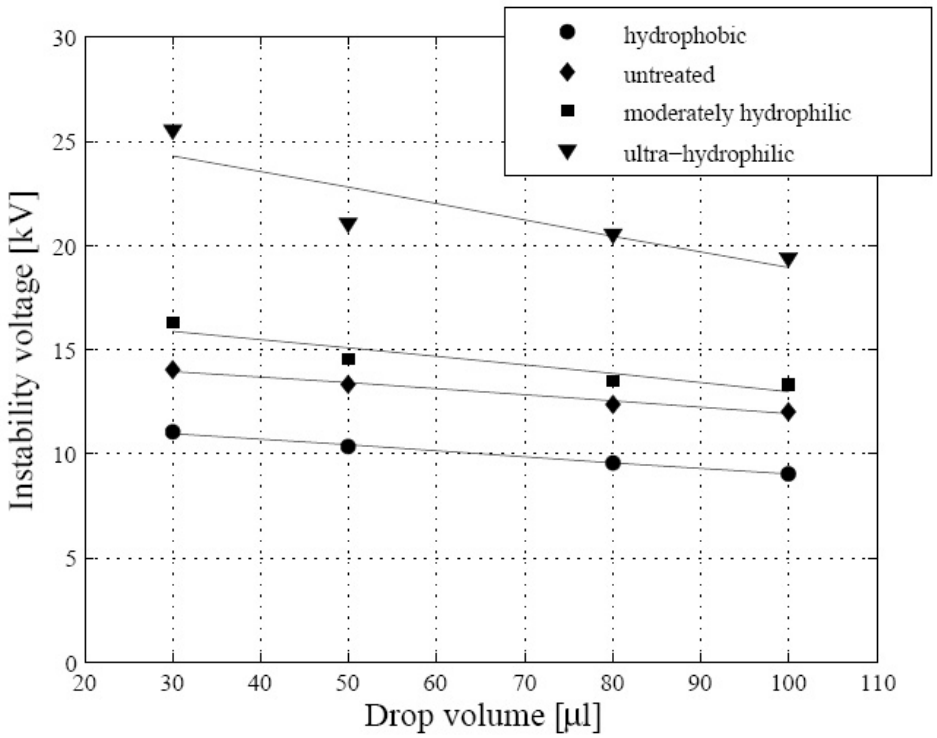

Figure 4.14: Instability voltage in dependence on drop size for various treatments of a sandblasted aluminium substrate.

These experiments reveal that voltage at which instability occurs depends clearly on the conductor surface and on the drop size (Figure 4.14). This result underscores that the critical global electric field at first instability can be significantly higher when the drop is flatter (lower contact angle) and, correspondingly, it is lower with a greater contact angle. Figure 4.14 illustrates also that the decrease of instability voltage with increasing drop volume in the range 30-100 μl is approximately linear with all surfaces considered.

4.2.2 Contact angle in dependence on applied voltage and surface properties

The deformation of the drop by the electric field brings an evident change in contact angle. The following figures show variations of contact angle as functions of voltage and drop size for a stainless steel electrode which was untreated (Figure 4.15) or made hydrophobic (Figure 4.16), hydrophilic using the SiO_2 coating (Figure 4.17) and hydrophilic using the TiO_2 powder (Figure 4.18). The values of contact angles for water drops in absence of voltage are reported in the Table 4.1.3 in Section 4.1.3. One can see that the contact angle decreases as the electric field distorts the drop. The drop has initially a higher contact angle, which then becomes somewhat smaller with increasing deformation of the drop. A comparison between the cases analyzed shows that variation of the contact angle has a similar tendency for both hydrophobic as well as hydrophilic surfaces, in the latter case, however, starting from noticeably different zero field contact angles depending on initial drop volume and having a marked onset of angle reduction only at significantly higher voltage (Figure 4.18).

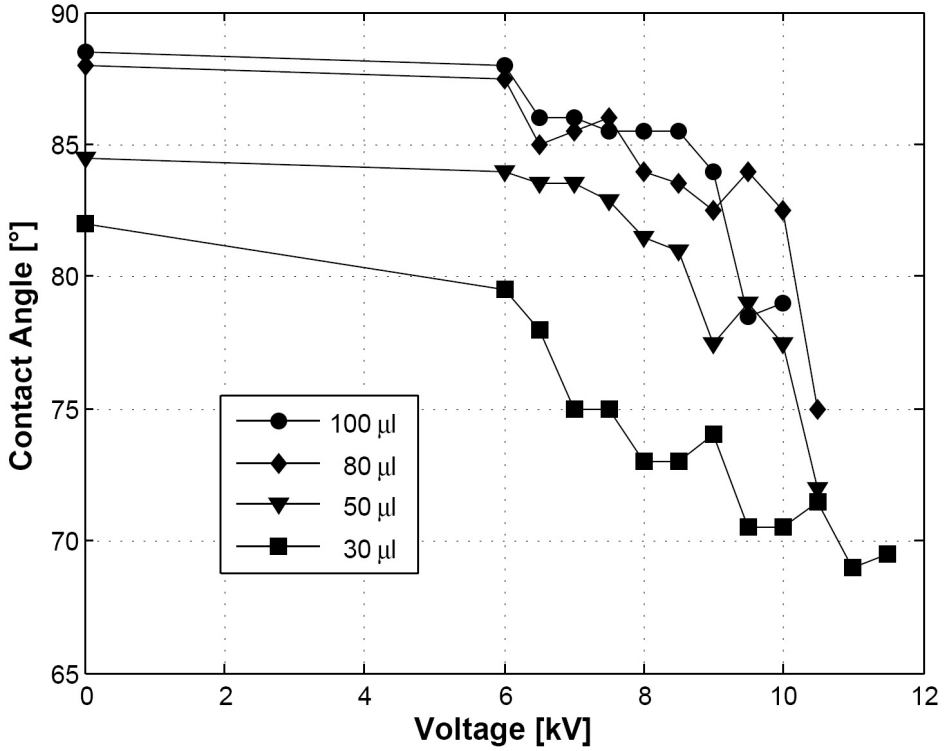

Figure 4.15: Variation of contact angle versus applied DC voltage for different drop sizes for a stainless steel electrode untreated.

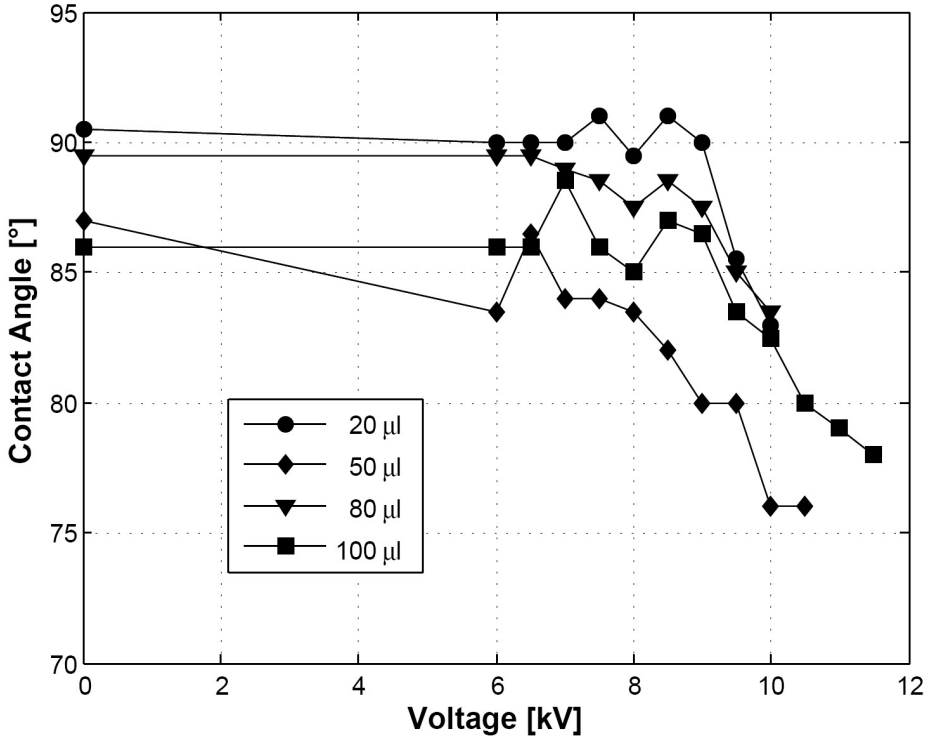

Figure 4.16: Variation of contact angle versus applied DC voltage for different drop sizes for a hydrophobic stainless steel electrode.

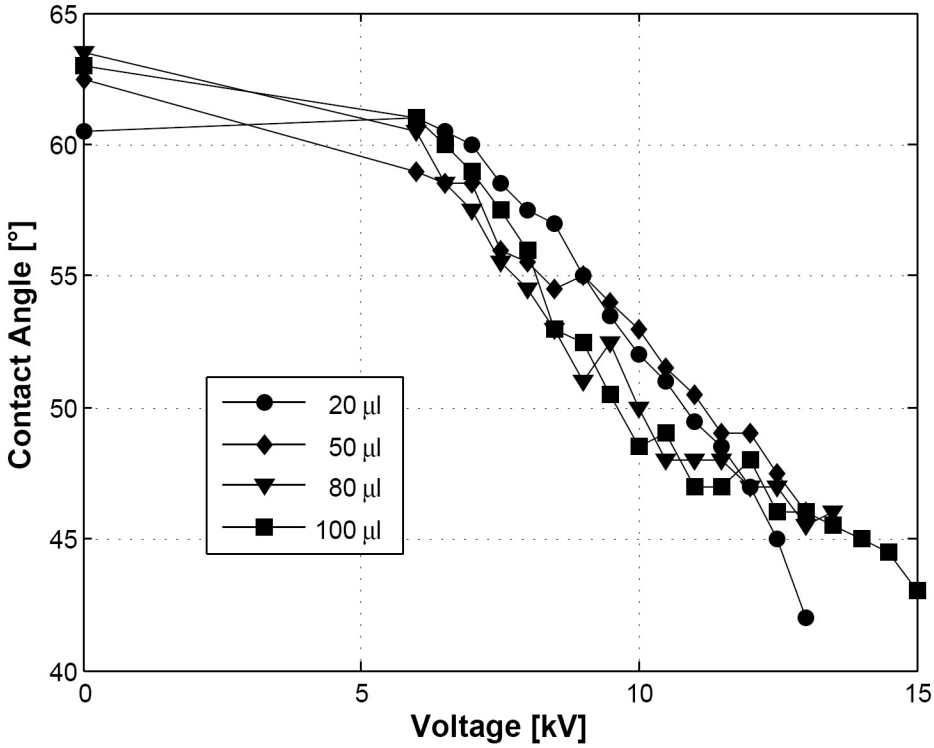

Figure 4.17: Variation of contact angle versus applied DC voltage for different drop sizes for a moderately hydrophilic stainless steel electrode.

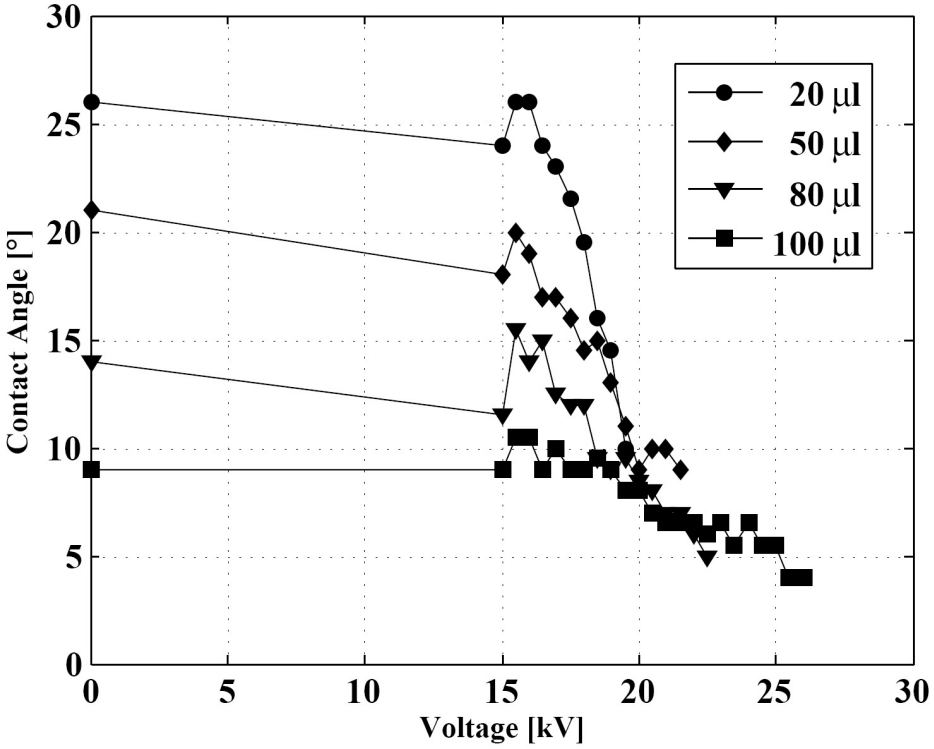

Figure 4.18: Variation of contact angle versus applied DC voltage for different drop sizes for a hydrophilic stainless steel electrode. Note that the reduction in contact angle in the bottom right figure sets in at about twice the voltage observed with the sample in Figure 4.16.

4.2.3 Inception voltage in dependence on contact angle

The investigations reported in the previous sections provide details on the instability of water drops in an electric field in dependence on drop size, surface condition and field strength. It is observed with all surfaces analyzed that the drop changed its shape becoming more pointed with increasing voltage but flatter at the base, which means that the contact angle decreases considerably. This behaviour begins here at ca.6 kV for hydrophobic as well as for untreated surfaces, then the decrease of contact angle is nearly linear with increase in voltage (Figures 4.15 and 4.16); while with more hydrophilic surfaces it becomes significant only at above ca. 16 kV (Figure 4.18).
Clearly the instability voltage depends on the contact angle, as shown in Figures 4.15, 4.16, 4.17 and 4.18. An evaluation of the entire series of contact angles measured leads to the plot in Figure 4.19, in which it is observed that with a decrease of contact angle from about 90° (hydrophobic surface) to about 5° (strongly hydrophilic) the instability voltage roughly doubles for a 100 μl drop. For 80 and 50 μl drops the same behaviour was observed, while for a 30 μl drop the instability voltage increased even by a factor of 3.

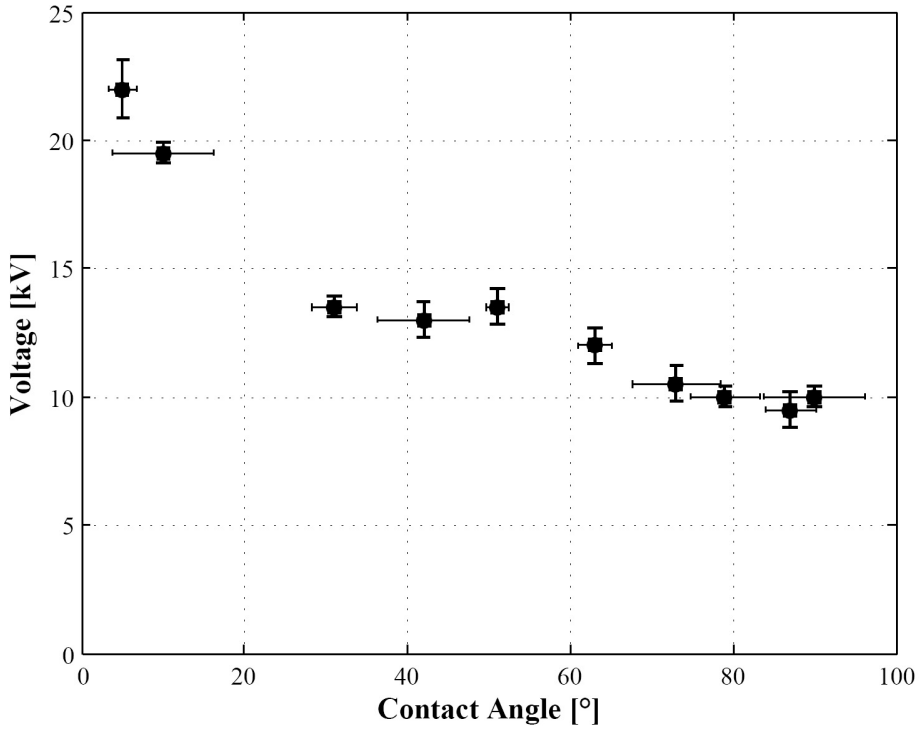

Figure 4.19: Instability voltage in dependence on contact angle; 100 μl water drop, 10 mm gap.

4.3 Discharge behaviour of sessile water drops

For the characterization and understanding of the performance of coatings applied to high voltage lines, the discharge behaviour of water drops should also be taken into consideration. As in the measurements mentioned in the previous sections, the drops can be deformed until discharge onset occurs. This has been studied for drops of 2 μl to 100 μl in three configurations:

1. Parallel plate arrangement as in Section 4.2, spacing 10 mm, 90° Rogowski profile electrodes;

2. as 1, but spacing to 50 mm, with a hemispherical 10 mm radius 'calotte' placed on the lower electrode; the single drops are placed at the apex of the calotte;

3. model conductor arrangement as described in [25] with the single water drop placed on top of the 20 mm cylindrical conductors.

In the first two small-scale setups, discharges from individual water drops were observed in terms of discharge current or UV light emission measured with high time resolution. The geometry changes of water drops were recorded by static and by high speed framing.

Discharge currents and light emission from the arrangement are measured with bandwidths from DC to $>$ 100 MHz. In order to register the passage of small water droplets ejected from drops reaching instability, a flat band of UV

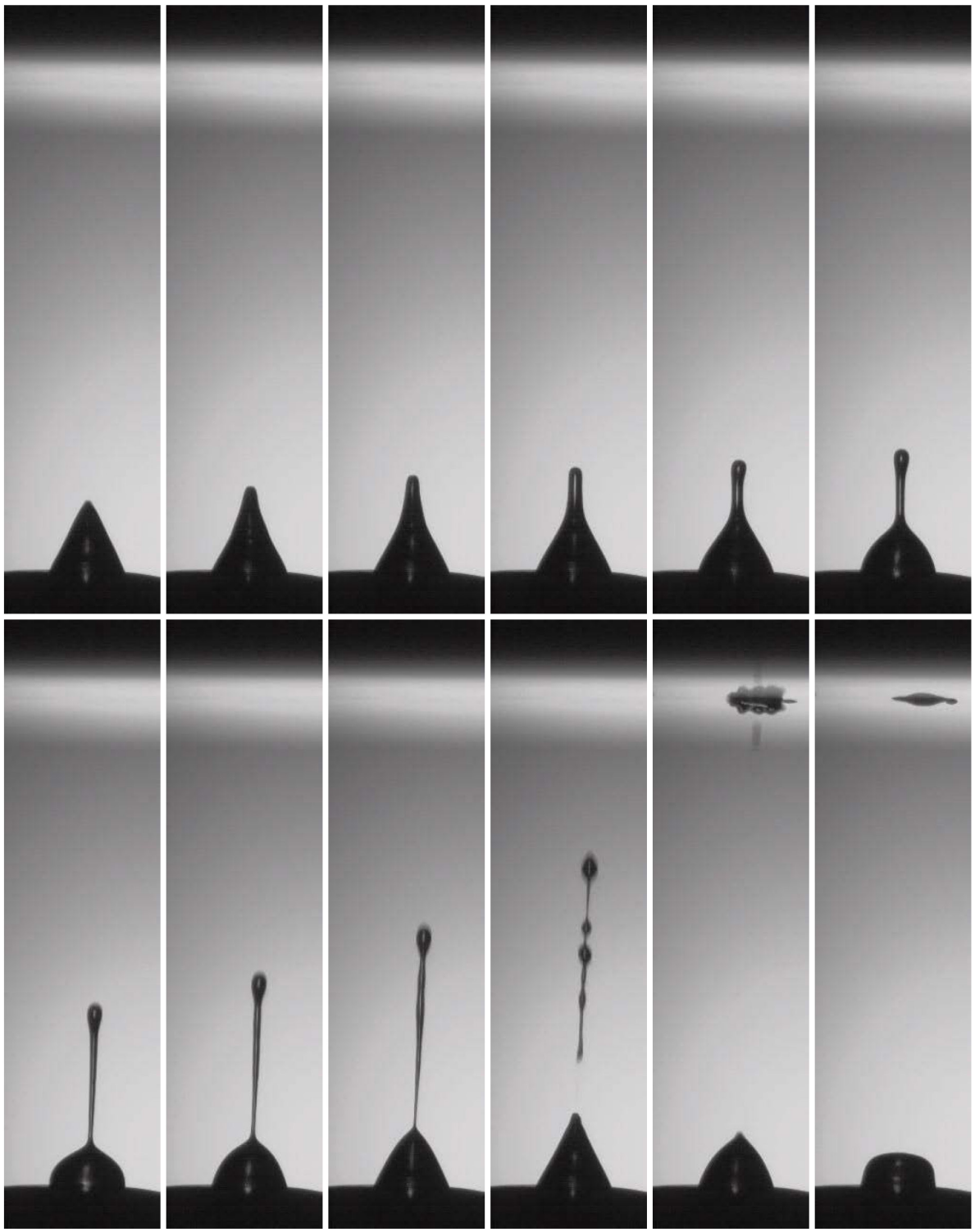

Figure 4.20: Deformation by the electric field of a 10 μl water drop placed on hemispherical 10 mm radius calotte, 50 mm spacing of the discharge gap homogeneous without the drop.

light is passed between the apex of the sessile drop and the (upper) counter electrode to which the ejected droplet will move on account of its charge.
Water drops of defined volume (2-100 μl) were placed on the hydrophobic surface of a metallic hemisphere of 10 mm radius residing centrally on the lower flat electrode of a 50 mm spacing homogeneous field discharge gap. Voltage of either polarity is increased to first discharge inception. The deformation and relative Taylor cone formation of a 10 μl water drop is represented in Figure 4.20. The image sequence demonstrates the ejection of a fine jet which coagulates into spherical droplets carrying electric charge and deposited on the anode. As inception is controlled by drop deformation/instability, the onset voltage is the same for either polarity and decreases with increasing drop size.

4.3.1 Negative water drops

With negative water drops, discharge onset produces a train of "packets"of fairly regular Trichel pulse sequences [54], each of which is initiated by Taylor cone formation and terminated by droplet ejection (Figure 4.21).
The "packet"repetition frequency (ca. 20-110 Hz) depends strongly on drop volume and is interpreted here in terms of resonant oscillation of the deformed drops. At a voltage kept constant the sequence comes to an end when the drop volume is sufficiently reduced so that the onset conditions are no longer fulfilled. The fast front of each current pulse representing the ionization period is associated with UV emission, while the scattered light signal produced by the passage of the ejected droplet is not associated with any appreciable current as the charged droplet motion is too slow to produce a readily measurable current signal.
The droplet resulting from the jet ejection must be very small as it is not visible in the video record and is also not seen as a deposit on the anode. In contrast to metal points which produce continuous sequences of Trichel pulses, here the pulse groups occur in fast and slow sequences with repetition intervals of 1-2 ms and 30-40 ms depending on drop size (see Figure 4.22).

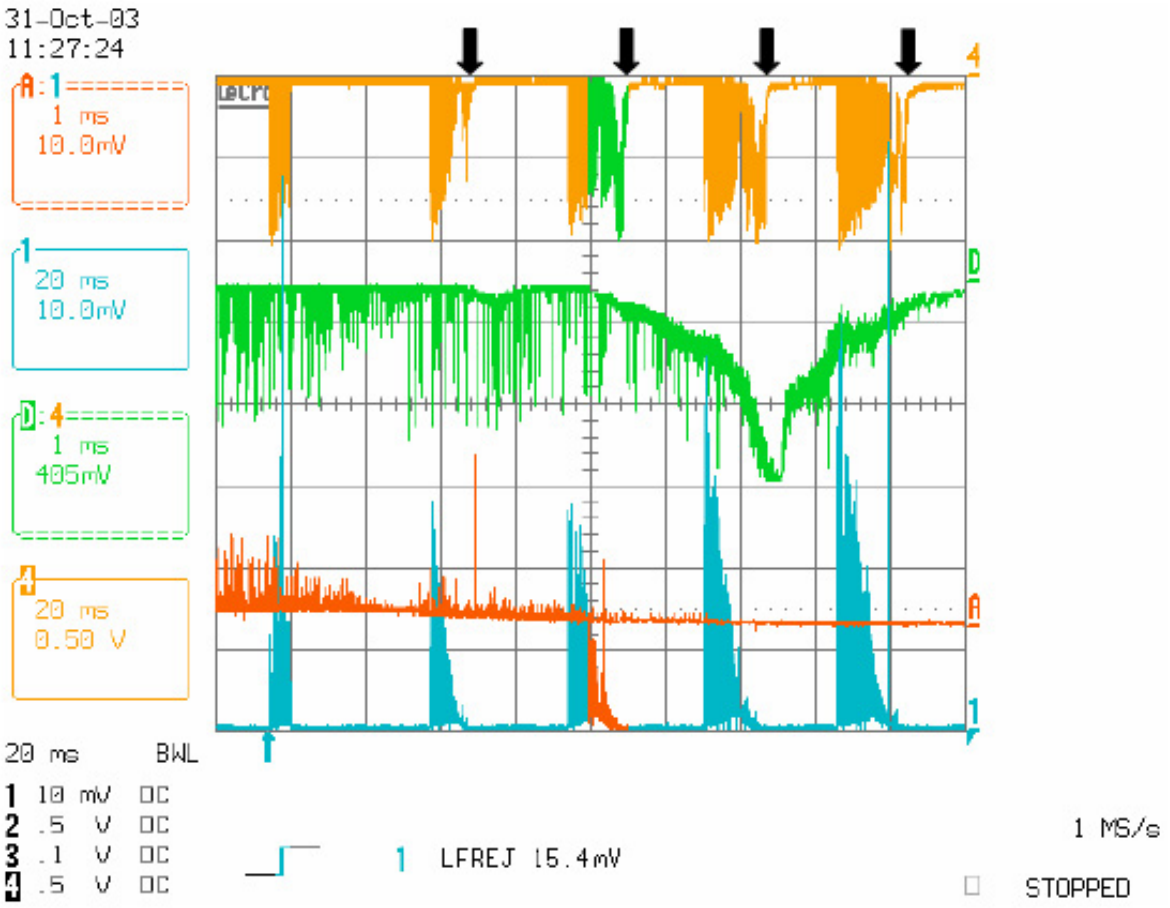

Figure 4.21: Light emission (top two traces) and current (lower two traces) of Trichel pulse "packets"recorded at discharge inception on a negatively charged 50 μl drop [95]. The "satellite"light pulses (↓) signify the passage of a charged droplet towards the anode. The middle two traces are synchronous $\times$20 expansions made to show that no significant current is associated with those light signals. The expand photomultiplier current trace corresponds to an instant as indicated by an arrow at the top.

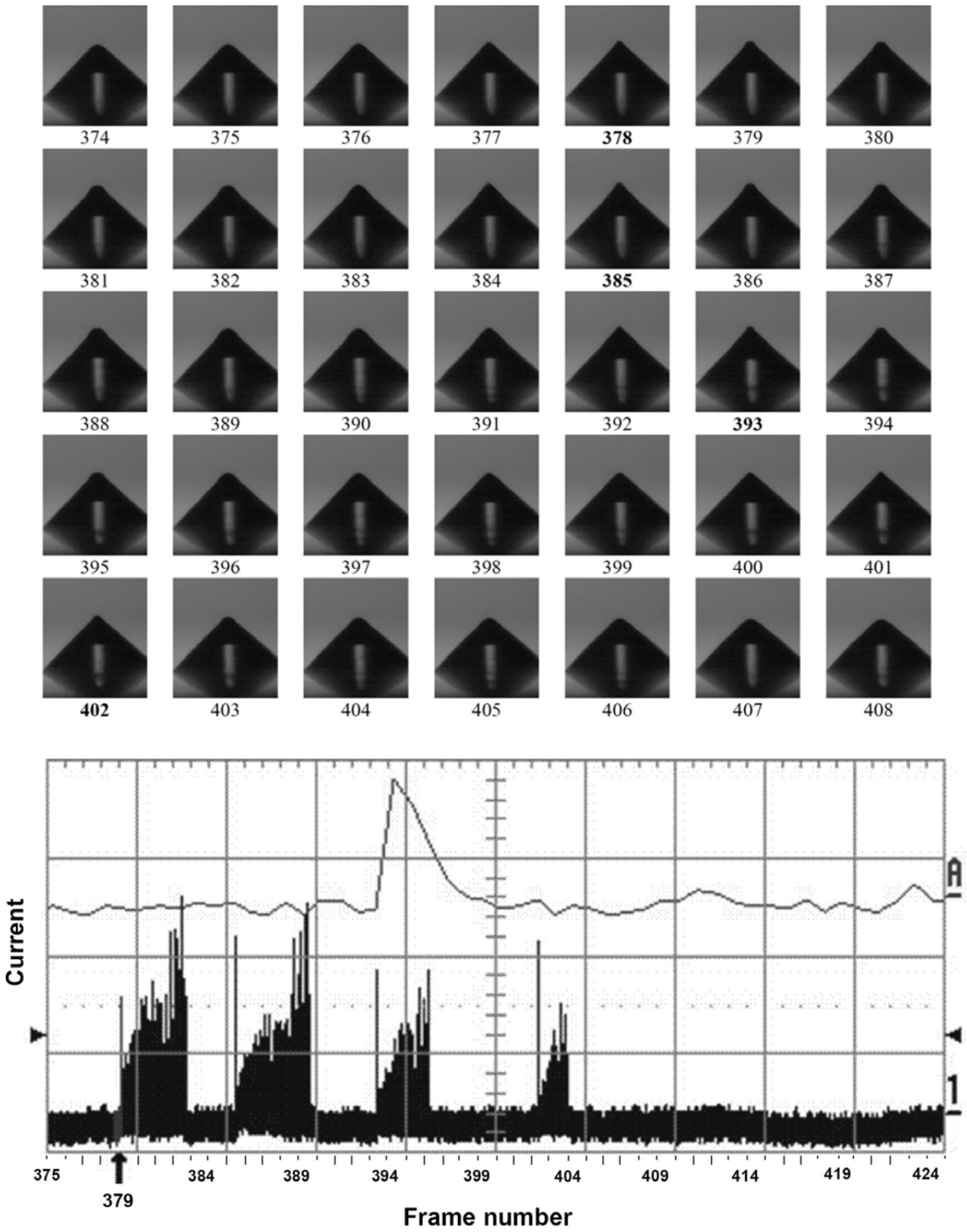

Figure 4.22: Temporary instabilities of a 20 μl sessile water drop in a 10 mm discharge gap. Current and tip shape records taken at 5000 frames/s, 0.6 mA and 1 ms per unit (upper trace A: first pulse current expansion to 100 ns/unit), 'Fast' Trichel pulse group sequence. Observe the change in tip shape following after frames 378, 385, 393, 402.

In the literature some characteristics of the 'fast' group in Figure 4.22 have been adequately described [63]. In the record shown here, each pulse group is initiated by a current pulse of the order of 1.2 mA corresponding to a charge of 60 pC. After this current pulse occurs, a sequence of individual Trichel pulses is seen initially small and closely spaced, eventually reaching a similar amplitude as the initiating pulse, with a spacing gradually increasing to about 4 ms (25kHz repetition). As the sequence breaks off, each subsequent group is reduced in charge content. The video recording in Figure 4.22 was triggered by the first current pulse in the sequence; the corresponding frame (379) follows immediately on the frame showing the most pointed tip of the 20 μl drop. Subsequent frames show a significant and progressive change of the shape of the tip until the current pulse sequence breaks off (383) when the Taylor cone again starts to form (385), (393), (402). After frame (404) the sequence breaks off altogether and the drop returns to a more ellipsoidal form (late frames not shown). In the experiment with model conductors under DC and AC 'fast' Trichel pulse groups have been observed to occur in just the same way with single water drops [25].
The interpretation of the occurrence of slow sequences with spacing 20-40 ms of Trichel pulses groups (Figure 4.22) is less well established. In an attempt to elucidate this, a flat UV light beam was passed centrally across the gap between drop apex and anode to intercept any ejected liquid, producing scattered light to be picked up by the same fast photomultiplier which registers the UV light from the discharge. Except with the first group of the slow sequence, a pronounced light emission not associated with any discharge current can be seen to follow each light pulse group of the discharge, close to the end of the current pulse group (Figure 4.22). The actual instant of ejection can not yet be given here. It appears that the repetition of 'slow' pulse groups is linked to oscillation of the drops, the frequency of which is connected with drop size: 50 μl/28 Hz; 1.6 μl/110 Hz. These frequencies correspond roughly to those measured optically by Corcoran [61] in a similar setup.

4.3.2 Positive water drops

With positive drop polarity, behaviour appears to be similar, with burst pulse corona in place of the far more regular but lower amplitude Trichel pulses. Positive discharges take the form of filamentary onset streamers which may - or may not - initiate a transition to a glow. While onset streamers have been observed in all three configurations mentioned, the glow transition has so far only been looked for and observed in the 10 mm parallel plate gap. Two or three consecutive streamer pulses were leading to a transition typically within 5 to 50 μs. In all configurations, the positive pulses have a much greater

charge content than the negative ones in the same setup (e.g. 2.7 nC as against 60...80 pC), greater pulse duration of the light emission (e.g. 120 ns as against 40) and a much lower repetition rate (mostly not very regular repetition from 10/s to 9000/s as against the quite regularly repeating Trichel pulses at about 25000/s).
The ratio of charge content of the fast component of current pulses (which is also reflected in the UV light emission) of positive and negative polarity is typically 30...40 with water drops as well as with a 60° metal cone. It has been pointed out [99] that metal points should not be considered as equivalent to water drops as regards the resulting discharges.

4.3.3 Resonance phenomena of single water drops under an AC electric field

It has already been said that drop instability and discharge behaviour are intimately linked. Mechanical resonance frequencies are connected with drop dimensions and also with contact angle [100], as explained in Section 2.4. In the previous sections and in the papers [96, 95] it has been seen that the global electric field strength causing drop instability and discharges at a given drop volume is more than halved when the contact angle increases from near 0° to 90° (Figure 4.20).
Drop resonances have been studied in a 10 mm parallel plate discharge gap configuration (120° Rogowski profile electrodes, see Figure A.2 in Appendix A) .

Oscillation frequencies of water drops

It has been seen that resonant Taylor cone formation coincides with sequences of Trichel pulse packets [95]when the sessile drop is negative; the sequences cease eventually due to liquid loss from the drop which in turn is responsible for a consequential increase in inception voltage. Resonance frequencies inferred from the spacing of Trichel pulse packets from negative drops correspond well with those found with AC for large oscillation amplitudes near or at Taylor cone occurrence and with a relatively hydrophilic substrate (contact angle $\approx 45°$); they are also quite compatible with those measured by Corcoran [61] who observed the oscillation frequencies close to droplet breakup in a DC field (Table 4.2 and Figure 4.23).

V $[\mu l]$	Drop radius [mm]	DC from Trichel pulse [Hz]	AC large ampl. $\alpha \approx 45^\circ$	AC small ampl. $\alpha \approx 90^\circ$	DC Corcoran drop destruction [Hz]
0.45	0.60	-	-	-	120
0.88	0.75	-	-	-	95
2.09	1.00	-	-	-	87
2.60	1.08	81	-	-	-
4.00	1.23	-	-	160	-
4.30	1.27	-	-	-	80
5.00	1.35	69	-	-	-
7.00	1.48	-	-	100	-
8.56	1.60	-	-	100	-
10.00	1.71	52	44.6	85/68	-
12.00	1.79	-	-	-	59
15.00	1.91	-	-	68	-
17.20	2.02	-	-	-	52
20.00	2.17	38	-	52	-
30.00	2.50	30	25.3	54	-
40.00	2.68	-	22.4	40	-
50.00	2.95	28	21	-	-
70.00	3.30	-	-	31	-
100.00	3.70	-	14.8	33	-

Table 4.3: Resonant oscillation frequency [Hz] of sessile water drops against radius and volume.

With larger volume drops (20-100 μl) higher mode oscillations are also observed: they take the form of a seesaw motion. Selected frames from a 1000 f/s sequence are presented in Figures 4.24, 4.25 and 4.26.

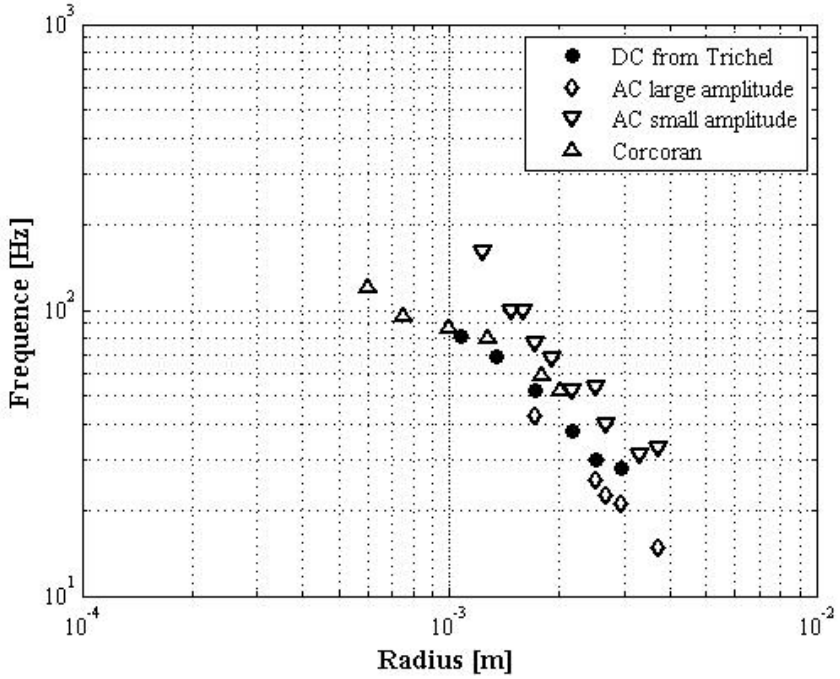

Figure 4.23: Resonance frequencies of sessile water drops in DC and AC electric fields in dependence upon actual drop volume represented here in terms of a fictive radius which would be that of a *hemispherical drop* of just that volume. Very small amplitude *resonant* oscillation (∇) occurs at higher frequencies than large amplitude oscillation close to or at instability ($\bullet\diamondsuit\triangle$ [61]) which is tied up with discharges from the drop, that means with the process involved in sound emission. The small amplitude oscillations are irrelevant from point of view of sound emission.

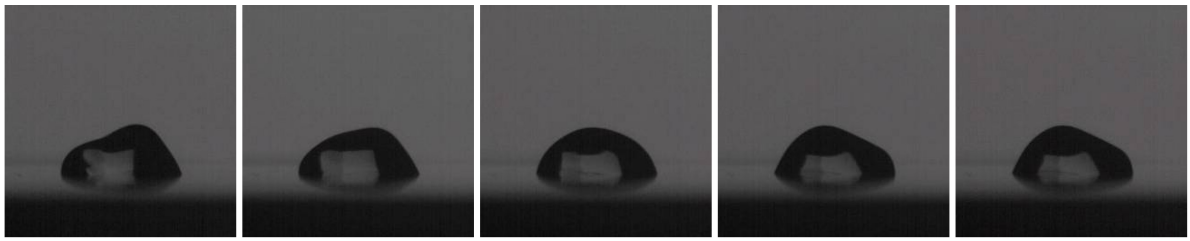

Figure 4.24: Oscillation of a 100 μl water drop by a 50 Hz AC voltage of 25 kV. Time interval Max-Min is $\sim$ 20 ms, i.e. the frequency of deformation is $\sim$ 25 Hz.

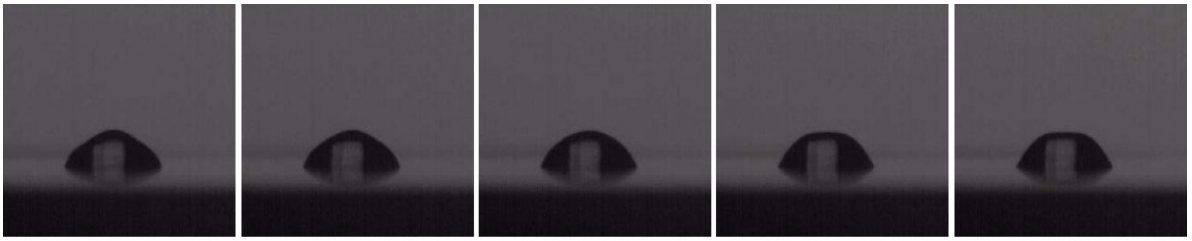

Figure 4.25: Oscillation of a 50 μl water drop by a 50 Hz AC voltage of 27.5 kV. Time interval Max-Min is $\sim$ 10 ms, i.e. the frequency of deformation is $\sim$ 100 Hz.

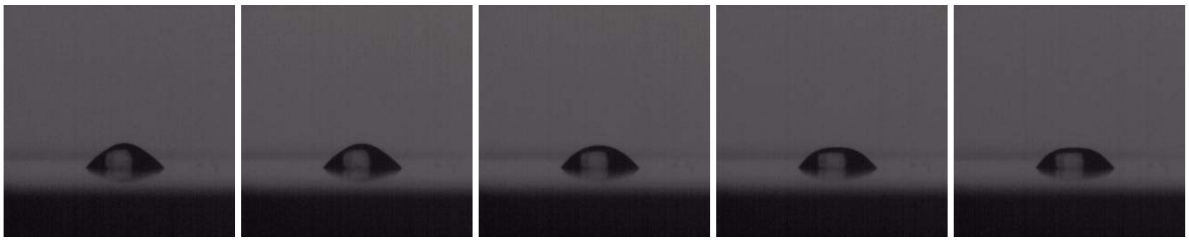

Figure 4.26: Oscillation of a 20 μl water drops by a 50 Hz AC voltage of 35 kV. Time interval Max-Min is $\sim$ 12 ms, i.e. the frequency of deformation is $\sim$ 80 Hz.

Clearly the voltage at which the higher modes of oscillation occur depends on the drop size. In fact a higher voltage value (typically 30 kV_{rms} on a 30mm gap) is needed to see oscillations if the drop is small.

4.3.4 Summary on the behaviour of water drops in a DC and an AC field

For the development of a method to quantify the effectiveness of the use of some coatings to cover high voltage transmission lines, the first step is the analysis of the behaviour of single water drops on coatings of the type envisaged. The deformation and instability of water drops in an electric field and their dependence on applied voltage, size of water drops and surface properties were described for four different surface conditions: untreated, hydrophobic, moderately hydrophilic and hydrophilic. A new set-up for detailed optical investigation of drop instability development at up to 10000 frames per second was used and has proved its capability to yield significant information on the parameter dependence of deformation of water drops in an electric field. Investigations showed that the voltage at which a water drop elongates in the direction of the electric field increases strongly with a reduction in zero-field

contact angle and decreases with increasing drop volume. In order to measure the change in contact angle values, a software which permits hands-free measurements with an uncertainty of about $\pm 2^{\circ}$ was developed.
In AC fields, droplet motion is found to be subject to different oscillation modes and resonances in the frequency range of particular interest (100 Hz), dependent on droplet size and electrical field strength. All ionization phases of current pulses are associated with UV light emission, so optical observation of light emission was a valid method to map all ionization generating processes. Records of motion sequences for different size drops in an AC field on an untreated stainless steel surface demonstrated that the oscillation of drops of smaller size is rotationally symmetric, while that of the bigger drops can be seesaw. On a hydrophilic surface, these oscillations are quite reduced.
In order to assess the quality of a coating, tests with single water drops under DC and AC electric fields are therefore recommended for checking the quality of hydrophilicity of the coating under high voltage. All investigations emphasized that surface condition determines instability field and thus, as will be seen in the next chapter, it is expected that it controls size of droplets surviving on a conductor.

5 Drop population on high voltage conductors

As the ensemble of water drops usually forms the most important source of charge injection from a high voltage conductor and as drop oscillation and drop instability in the electric field depend on drop size, drop populations and their development on model and real conductors have been investigated in order to deliver a tool for the evaluation of coatings to be applied to high voltage lines. Water droplets of different sizes and shapes and in different positions on the conductors may produce a different discharge behaviour and thus merely assuming a uniform drop size population seems to be inadequate. With constant intensity of rain the drop population eventually reaches an equilibrium steady state representing where inflow and outflow of water are in balance. When the inflow of rain is stopped and the drying phase starts, the drop population undergoes a steady change.
In order to set up a model which satisfactorily represents the population of the droplets on conductors after rain, an evaluation of the behaviour of drop numbers and sizes as function of time, geometry, electric field at the conductors, contact angle and thus surface properties has been carried out.

5.1 The analysis of the drop population

5.1.1 Laboratory set-up

The general technical description can be kept short, since details of the laboratory equipment can be found in Appendix A.3. In brief, in the high voltage laboratory 150 cm long tubular model conductors of 10 mm radius first robbed down with ethyl alcohol and then prepared to show different surface conditions were set up at a distance of 74 cm from the ground. The surface conditions analyzed were: untreated, hydrophobic coated (SiO_2) and hydrophilic coated (SiO_2). With an applied AC voltage of $100\,kV_{rms}$, this corresponds to a geometrical electric field strength on the surface of $20\,kV_{eff}/cm$. The centre section of the model conductors has been exposed to a spray of deionized water from a nozzle, typically at the rate of 100 mm/h representing heavy rain, for e.g. 4 minutes followed by a drying period of 30 minutes. Diagnostics in-

cluded optical observation of deformation of water drops on the conductors by means of either a high speed camera capable of up to 10000 frames/sec, or by recording the change of drop population using a web-cam with 1 picture/min and sound pressure level detection with third-octave band filter centred on 100 Hz.

5.1.2 Methods to analyze drop population pictures

To check size and number of drops on conductors, two ways have been used. For hydrophilic conductors, characterized by a low number of persisting drops all hanging on the underside, drops were measured and counted manually. For hydrophobic and untreated conductors, characterized by a much higher number of small and big drops on the top and the sides of conductors, the manual evaluation is extremely time consuming and thus an automatic evaluation was desired. So far, a general method for the automated estimation of the size and the distribution of water drops on a surface had not been available, as already mentioned in Section 2.5. A tool to automatically count and size water drops on the conductors was developed. This tool, a Matlab script (see Appendix B.2 for details), allows hands-free measurements using image acquisition and image processing techniques. As reported in Section 2.5, automated processing of drops pictures is in general not easy because it needs as input high-quality pictures of droplets. Therefore, several different ways to obtain high-quality pictures have been explored.
A first attempt to provide suitable illumination and trying to reduce reflexes on the drops has been undertaken by means of a indirect lighting. However, the resulting pictures were still not good enough to be analyzed automatically. Another attempt consisted of using different kinds of pigments (black, yellow and red) to improve the contrast of drops on the conductors. The problem here was that the pigments change the properties of water a little and the obtained pictures were still not free from reflexes as had been hoped. This condition has been properly met only by means of adding a very small quantity of a fluorescent substance to water and then illuminate by a UV source. Even if the sodium salt of fluorescein does not change the properties of water significantly, it had at the time been considered physiologically problematic by some people, so that only a reduced number of experiments have been performed using this substance, although it gave superior pictures of the water drops.

5.2 Determination of the drop population on high voltage conductors

Drop populations on high voltage conductors depend on several parameters, namely the nature of the conductor's surface, the voltage applied and the rain rate. In order to set up a methodology to show the possible ageing of a coating applied to high voltage lines, the statistics of water drops in dependence upon these parameters are needed.

5.2.1 The influence of the nature of conductor's surface on the drop population

In Chapter 4, the influence of surface properties on the deformation and instability of water drops in an electric field was investigated in detail. In this section the populations of water drops during and after a period of rain on different surfaces carrying various coatings (untreated, hydrophobic and hydrophilic) are investigated.
Investigations showed that a hydrophobic surface is characterized by harbouring numerous small sessile drops on the top and a second mode of larger sessile and pendant drops. A bimodal population can be observed if the surface is hydrophobic (see Figure 5.1 bottom and Figure 5.2). In contrast, a hydrophilic surface leads to an aqueous film (50-100 μm thick) lagging the conductor and large pendant drops on the underside, as one can see in Figures 5.1 top and 5.2. For neighbouring drops, there may be just one deformed pointed drop which produces discharges, while the another is flat, then the discharge activity may jump between the drops back and forth. The maximum number of discharge-active drops on the underside of the conductor can be approximated to circa 30-40 per meter. Typical distance between two active drops is of the order of 4-6 cm.

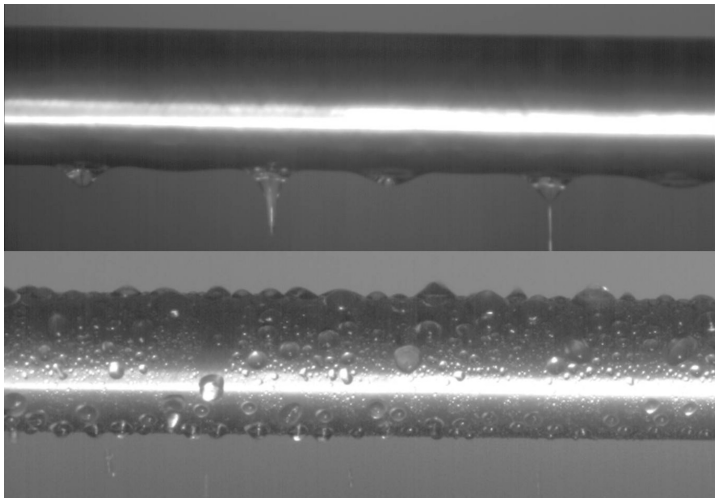

Figure 5.1: Appearance of drop populations during rain (rate 100 mm/h) on different conductors: for (top) hydrophilic SiO_2 surfaces and (bottom) a hydrophobic SiO_2 surface.

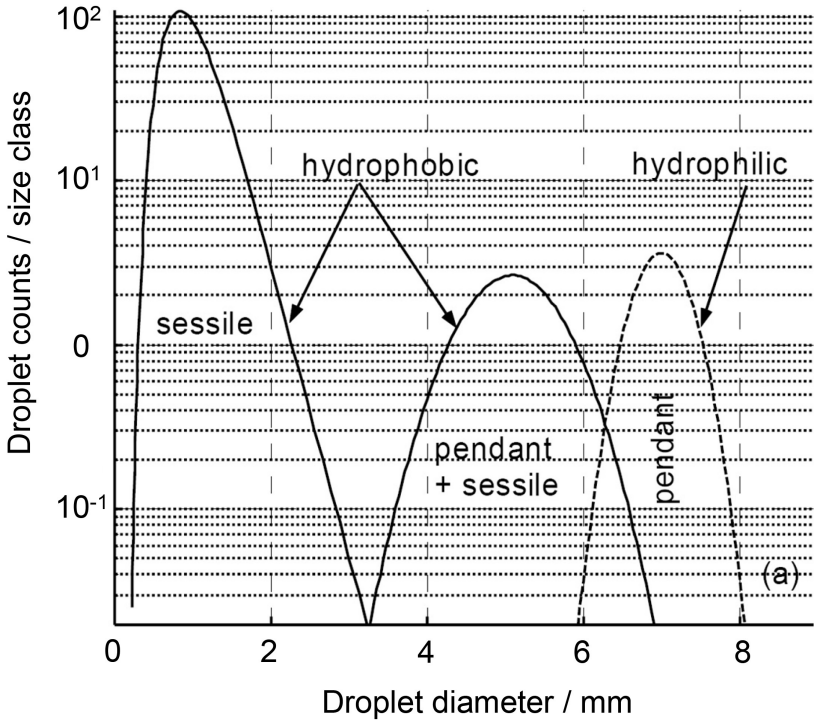

Figure 5.2: Drop population on different conductors: schematically for (dashed line) hydrophilic SiO_2 surfaces and (solid line) hydrophobic SiO_2 surfaces [101].

5.2.2 The influence of rain rate on the drop population

In Section 2.5 a model for the identification of the drop population on a surface in dependence upon the rain rate has been described. However, additional

investigations about the drop population on cylindrical surfaces such as model conductors with different rain rates are needed. To evaluate the number and size of drops, the conductors have here been azimuthally divided into four zones (from top to bottom: 1, 2, 3 and 4) (Figure 5.3) since the drops have different shapes in each of these zones.
An example of a picture of a model conductor wetted by rain rates of 4.1mm/h and 7.7 mm/h is given in Figure 5.4.

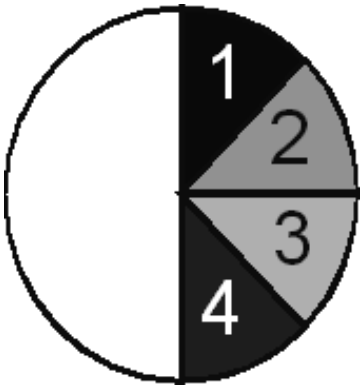

Figure 5.3: Partition of a model conductor into four zones: 1 (top), 2 (half top), 3 (half bottom) and 4 (bottom). Each segment corresponds to an angle of 45°. The camera frames only one half of the conductor, therefore a symmetric distribution on the back side of the conductor has been assumed.

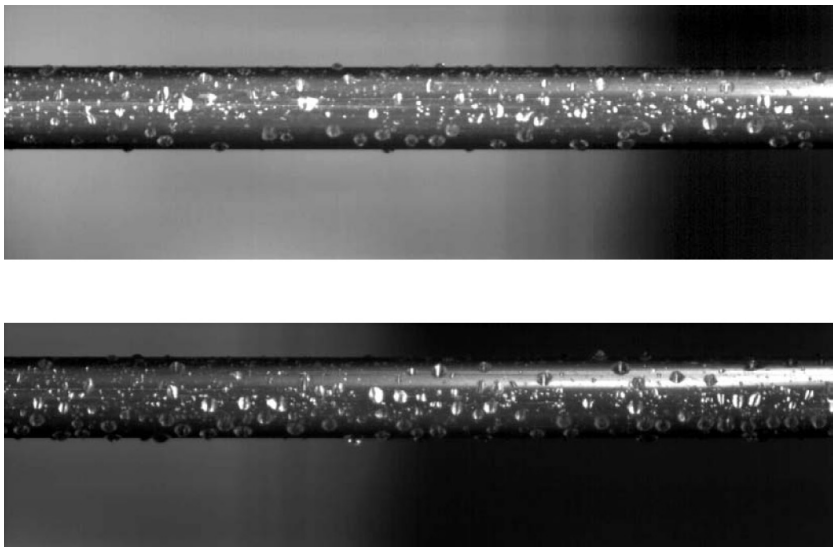

Figure 5.4: Population of water drops on a hydrophobic aluminium model conductor under high voltage (100 kV) by a rain rate of 4.1 mm/h (top) and of 7.7 mm/h (bottom).

In the zone 1, there are sessile drops directly as originated from rain from the nozzle. In the zones 2 and 3, there are not only drops from the nozzle,

but also drops that on the way to flow to the underside of the conductor. The zone 4 is characterize only by hanging drops. It has been observed that the number of drops versus the drop size in the zone 1 is log-normally distributed. In the half top position, drop numbers versus drop size show also a log-normal distribution. For the half bottom position, one can observe a log-normal distribution for the small droplets and a normal distribution for the big ones. On the underside of the conductor, drops present a gamma distribution. The marked decay of the number of drops bigger than 4.5 mm is due to the fact that water drops in an electric field become unstable and deform to a conical shape and thus lose water. The distribution of drop number versus drop diameter with different rain rates of 0.3, 1.2, 4.1, 7.7 and 15.4 mm/h is presented in Table 5.1 and represented in graphics in corresponding Figures C.1, C.2, C.3, C.4 and C.5 in Appendix C.

Rain rate [mm/h]	**figure**	**sect.1**	**sect.2**	**sect.3**	**sect.4**	**big drops in sect.4**
0.3	Fig.C1	lognormal 4.4 mm	lognormal 2.4 mm	lognormal 1.6 mm	gamma 2.7 mm	normal 5.0 mm
1.2	Fig.C2	lognormal 2.2 mm	lognormal 1.5 mm	lognormal 2.0 mm	gamma 3.6 mm	normal 2.7 mm
4.1	Fig.C3	lognormal 1.8 mm	lognormal 0.9 mm	lognormal 1.3 mm	gamma 4.2 mm	normal 3.0 mm
7.7	Fig.C4	lognormal 1.6 mm	lognormal 1.1 mm	lognormal 1.1 mm	gamma 3.9 mm	normal 3.0 mm
15.4	Fig.C5	lognormal 1.9 mm	lognormal 1.1 mm	lognormal 0.9 mm	gamma 4.0 mm	normal 3.3 mm

Table 5.1: Drop populations at different rain rates: distribution and mean diameter. Voltage: 100 kV_{rms}.

This table clearly shows tendencies of sectorial drop diameters with increasing rain rate and indicates that the assumption made in Section 2.5 that the mean diameter of drops increases with increasing rain rate does not apply. Although at higher rain rates there is more water on the conductor, this manifests itself not in an increase of the mean size, but in an increase of the number of drops.

5.2.3 The influence of applied electric field on the drop population

The effect of the application of an electric field on the drop population need also to be shown. The statistical distribution of drop sizes on hydrophobic or untreated model conductors shows a significant reduction of the drop volume of the order of 40% after a 20 minute high voltage application (100 kV_{eff}) and 1 min rain (100 mm/h). It can be observed that after the application of high voltage the size and number of big drops does not show significant changes, while the small drops largely disappear (see Figure 5.5) and thus the character of the distribution changes with time.

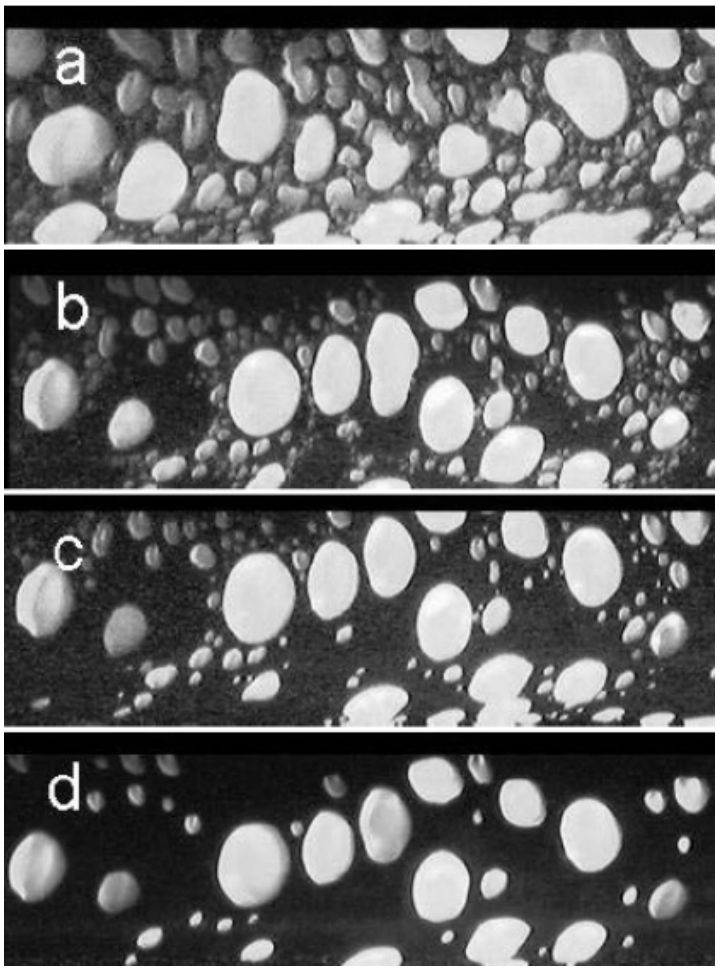

Figure 5.5: Drop population on an untreated model conductor after 1 min rain, high voltage 100 kV_{eff}. a) 0 min after rain b) 5 min after rain c) 10 min after rain d) 20 min after rain. Improvement of the contrast by addition of fluorescein and illumination by a UV source.

The different appearance of drop population during rain by different electric field strength (0 to 20 kV/cm) is shown in Figure 5.6. The analysis of the size distribution of water drops with respect to different electric field shows that as voltage increases there is a shift to smaller sizes. The size distribution is approximately lognormal with all electric field strengths.

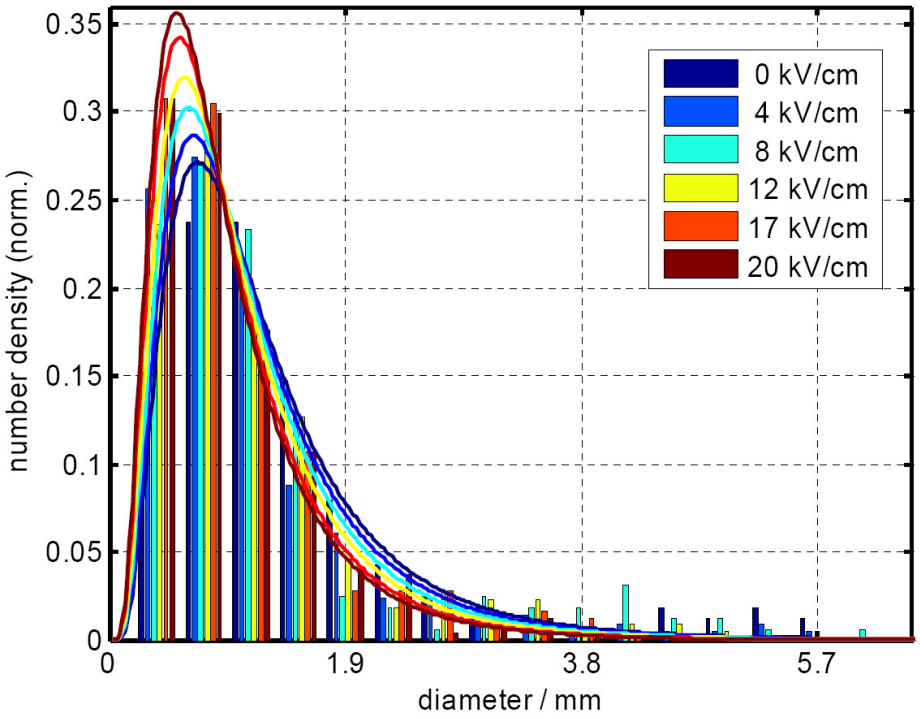

Figure 5.6: Drop population on a 20 mm untreated Al model conductor during rain, high voltage 100 kV_{eff}.

5.3 Summary on the study of drop population on high voltage lines

Drop populations depend on several parameters from which the most important is probably the nature of the conductor's surface. It has been observed that the number of discharge-active drops is smaller than the total number of drops on the conductors (typical values for untreated conductors: 30-40 vs.. 70-80 large drops; there is a significantly lower number for hydrophilic coated conductors). It has also been observed elsewhere [99] that only a limited number of the existing drops take part in the discharge activity. A hydrophilic surface leads to an aqueous film (50-100 μm thick) around the conductor and large pendant drops on the underside which are the only sources of discharge and thus of noise emissions. Some investigations show that the presence of an

electric field leads to a reduction in the number of small droplets as compared to a population without electric field.

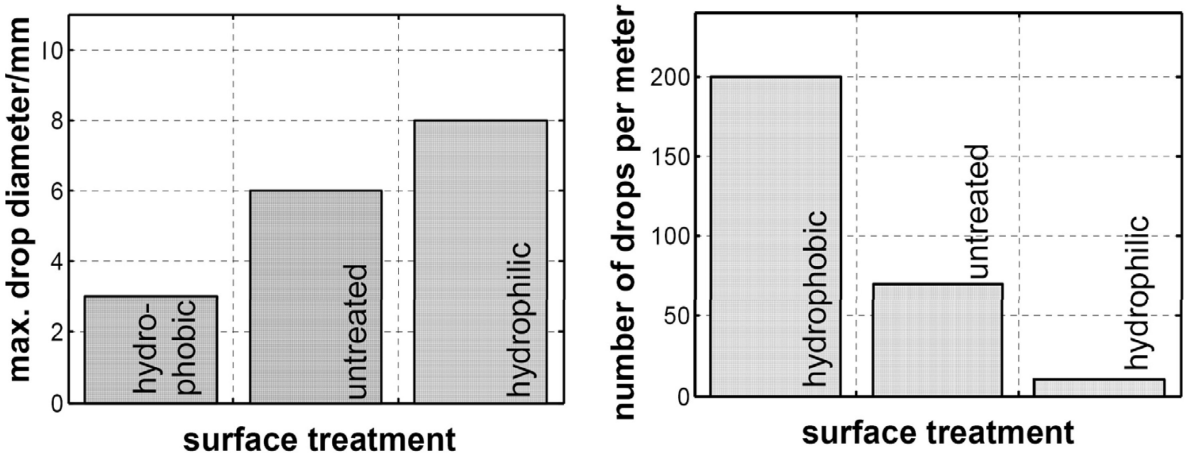

Figure 5.7: Left) Maximum drop diameter on different conductor surfaces during rain. Right) Total number of drops on different conductor surfaces immediately after 4 min rain at 100 mm/h.

To summarize, the maximum drop diameter is much higher with hydrophilic surfaces than with hydrophobic ones (Figure 5.7 left), while the number of drops per meter during periods of rain is significantly higher with hydrophobic surfaces compared to the situation with hydrophilic ones (see Figure 5.7 right). These results underscore the characteristics that hydrophilic coatings suitable for high voltage lines must have. In particular, a good hydrophilic coating will have no water drops remaining on the upper side of the conductor and just pendant drops forming on the underside which proceed to the lowest point when the conductor is only slightly inclined (3°-6° or even less), as will be shown in the next chapter.

6 The evaluation of the durability of coatings

Experiments presented in Chapter 4 showed that the instability voltage of drops increases with a reduction of the contact angle. This emphasizes the fact that a remedy against tonal emission after precipitation is the use of hydrophilic conductors to reduce the discharge activity. Hydrophilic coatings provide runoff and drying of the conductors and thus the reduction of the population of deformable water drops.

After having assessed the behaviour of single drops and of populations of drops on high voltage conductors, a major aim of this investigation is to deliver a method to identify and quantify robust coatings for conductors which will persistently show hydrophilic behaviour. A potentially good coating should display a satisfactory stability of its characteristics as regards different temperatures, different atmospheric conditions, but above all with increasing age. For assessment, coating materials and coated samples (flat and tubular) have been obtained from commercial and institutional sources. Some samples were hydrophobic, which means that the surface has low surface energy and water drops with contact angles of 90° or greater will form. Superhydrophobic surfaces have contact angles greater than 150°, showing almost no contact between the liquid drop and the surface; this is referred to as the "Lotus effect". Some samples were hydrophilic, which means the surface has a high surface energy or surface tension and a drop will spread, or wet, the surface. Some other samples were titanium dioxide (TiO_2) photocatalyst with the desired property of superhydrophilicity.

When *moderately* hydrophobic coatings are applied to a tubular conductor, there are numerous drops of all sizes on the top and pendant drops on the underside. So far, the effect produced by these coatings appears to be more or less the same as with new untreated conductors, and thus they do not produce any useful effect with respect to quick drying of HV lines. When *superhydrophobic* coatings are applied to a conductor, only quite small drops with large contact angles form on the top. Since drops with larger contact angles start discharges at lower voltage than drops with smaller contact angles, it is expected (and well known in the literature [102, 103, 83], as described in Section 2.6) that discharge activity significantly affects the properties of such coatings. Applied to a tubular conductor, moderately *hydrophilic* coatings show

good wettability only on the top, while hanging drops on the underside run off with an inclination $\sim 10^{\circ}$). With strongly hydrophilic coatings, drops appear *only* on the underside of the conductor and run off with quite a small inclination, as seen in Chapter 5. So far, there has been no evidence that corona discharge activity will change the properties of *hydrophilic* coatings applied to high voltage conductors.

6.1 The properties of coatings and surface treatments properties applied to HV lines

6.1.1 Characteristics of coatings

The collection of coating materials or coated samples available in the laboratory for assessment included:

- Anatase pulver (A - provided by the company Tioxide Ltd.);
- Silica based hydrophobic coating (VP12 - provided by the company Nanocare);
- Silica based hydrophilic coating (H12 - provided by the company Nanocare)
- Thin-film deposition titania CVD coating (TC - provided by the company Titam);
- Thin-film deposition titania Sol-gel coating (TS - provided by the company Titam);
- Thin-film deposition titania Sol-gel coating (H - provided by the University of Hannover);
- Titania and silica based coating (TT - provided by the company TOTO).

The VP12 coating is conceived in such a way that dirt particles have only a small contact area with surfaces. By hydro- and oleophobic effect, dirt particles like fat and oily materials, lime and materials from environmental impacts, have little adhesion to the substrates, and thus they do not need the application of abrasive methods to be removed. Due to its inorganic reticulation the coating is extremely tough. VP12 is a soil-resisting coating formulation suitable for application on glass substrates. VP12 is dissolved in ethanol and it contains a bi-functional bonding: the silicon-functional groups contained in it link with oxides, hydroxy- and carboxyl groups of the glass substrate surface to form a permanent chemical bond. The other functional groups give an

extremely low surface energy to the substrate surface glass. This coating is relatively easy to apply; the big advantage is that the application can be done by everyone, without having specialized facilities. The coating needs only 24 hours drying time. Then it can be used immediately with all temperatures and without requiring any additional energy or ultraviolet light irradiation for activation. Other coatings (H12) having according to the manufacturer a similar formulation but show hydrophilic (or anti-fog) effect and have been used for experiments. Due to their easy applicability in comparison with certain photocatalytic coatings, they have been chosen for most of the experiments presented here.
Titania based samples were also used for investigations TC, TS, H and TT). They are expected to show photocatalytic behaviour, showing at first contact angles of several tens of degrees, and then, by the irradiation with ultraviolet (UV) light, contact angles decrease gradually, reaching at last 0 degrees, as seen in in Section 2.6, when a photocatalyst TiO_2 captures ultraviolet light (UV). With their photocatalytic properties, these super-hydrophilic coatings have been seen as possible coatings for high voltage conductors. In fact, the super-hydrophilic surface dries quickly utilizing the property that the water flatly spreads on it. This effect can be applied to preventing drops forming on the conductors. Some photocatalytic coatings and samples have been obtained from one of Japan's largest manufacturers of sanitary ware (TT-TOTO).
Thin-film deposition has also been used in the preparation of some samples provided by external sources. In particular they used CVD (Chemical vapor deposition), sputtering (PVD) and Sol-gel methods for the thin-film deposition. Some CVD (CVD-Titam) and Sol-gel (Sol-Titam) samples annealed at elevated temperature have been provided by a German company, Titam. Some other Sol-gel samples (Sol-Hannover) were provided by the University of Hannover.

6.1.2 Factors affecting the stability of coatings

The hypothesis made here is that there are some factors which can affect the durability of hydrophilic coatings applied to high voltage lines. These factors could be: degradation by ultraviolet light, elevated or low temperature, moisture and the combination of these factors with the discharge activity. The stress factors which could affect coatings on high voltage conductors are listed and explained in Table 6.1. It is common to ascribe these stress factors as one of four causes; namely discharge activity, defective application of the coating, mechanical stress and dirtiness and exposure to environmental pollutants.

Parameters	Typical range	Remarks
UV irradiation	295 to 380 nm	UV light can cause substantial damage to organic coatings. Photo-degradation of coatings is caused by the absorption of energetic UV light, which either breaks chemical bonds directly, or results in the formation of free radicals, which can subsequently result in bond breaking or bond formation. Either process will result in changes in the physical properties of the coating, usually for the worse.
Air temperature and conductor heating	-20°C to 40°C and more	Air temperature is rarely the same as the conductor temperature, since the conductor also absorbs infrared radiation and suffers Joule heating.
Rain	800 to 1200 mm/year	Rain could wash away the coating.
Partial discharges	0,1 to 10...W/m	Discharge activity can lead to 'hot spots' due to localized discharges which could destroy the surfaces.

Table 6.1: Stress factors which could affect coatings applied to high voltage conductors in use extending over several years.

While it is true and well known in the literature that coating failures fall into one of the last three categories, or perhaps into a combination of them, it is still to be assessed if discharge activity can significantly affect the properties of hydrophilic coatings applied to high voltage transmission lines.

6.1.3 Criteria to assess the ageing of a coating

To verify whether the coating failed or not, a specific method has been developed. An accurate analysis is required of the contact angle, runoff angle, partial discharge activity and acoustical emissions after every exposure to the ageing factors mentioned above. In particular, the different steps of the method include:

1. Surface preparation, inclusive cleaning and possibly sandblasting;
2. Application of the coating;
3. Drying of the coating, typically it takes 24 to 48 hours;

4. Preliminary measurement of contact angle, to be able to assess changes in the properties of the coating;
5. Positioning of the coating outdoors for several days or months;
6. Accurate analysis of the contact angle and runoff angle after every exposure to the ageing factors mentioned above to see if the surface has retained its properties;
7. Repeated measurement of noise level and corresponding partial discharge activity with model conductors at 1 m distance from the conductor for an applied voltage of 100 kV and rain rate of 100 mm/h to assess whether the conductor has maintained its drying properties (this part of the analysis will be described in detail in Chapter 7).

6.2 Methods to analyze the efficacy of different coatings types

To characterize the coatings described in Section 6.1, a preliminary analysis of the wettability of the materials and their resistance to different environmental conditions has been carried out. In particular, contact angle was used to characterize surface properties before and after exposure to atmospheric conditions. For the analysis of wettability of materials, the measurements of contact angle have been made using the software explained in the previous chapter when possible, otherwise using the goniometer method and the common sessile-drop technique.

6.2.1 Method to analyze non-photocatalytic coatings

The hydrophilic commercial coating (H12) which is neither based on titania nor relying on UV irradiation has been initially applied to a 10 cm by 10 cm sandblasted aluminium sheet to assess the durability of its desirable property under environmental stress. Initial contact angle has been measured and found to be $10^\circ \pm 2.0^\circ$.
The metal sheet covered with H12 was then positioned outdoors for over six months and thus subjected to various kinds of environmental stress (rain, fog, snow, ice). A contact angle measurement has been made every month and no significant change of its hydrophilic property has been noticed. Since good hydrophilicity of this sample has persisted for six months or more with or without any exposition to additional ultraviolet light, the conclusion was that this coating could be potentially a good material to cover high voltage transmission lines. However, additional investigations of the ageing of the coating

had to be carried out with respect to different electric field strengths, different discharge levels, variation in substrate and increasing age (contamination, corrosion). Part of these investigations are reported in the next chapter, while a long-term stability study of the coating is still missing.

6.2.2 Methods to analyze photocatalytic coatings

CVD or a Sol-gel technique had been used in the preparation of a set of eight different samples by the company Titam (TC and TS). The samples investigated with respect to contact angle were 10 cm by 10 cm aluminium sandblasted sheets half coated with photoactive material, annealed at different temperatures. It was immediately noticeable that they were not homogeneously covered, since they presented a clear change in the color and many scratches on their surface. This means that in the following analysis it has to be taken into account that the comparisons of the surface characteristics before and after the ultraviolet exposition may be affected by relatively large errors.

Sample No.	**Annealing temperature**	**Treated half**	**Untreated half**
2892	400°C	40°	58°
2893	450°C	53°	74°
2894	500°C	55°	69°
2895	550°C	54°	64°

Table 6.2: Contact angle values of a 50 μl water drop positioned on the treated and untreated halves of the samples.

After the first assessment of contact angle (see Table 6.2), the samples were put outdoors for the first time. Further contact angle measurements have been done changing the duration of exposure to sunlight and the time of resting in the dark. The complete history for all samples is presented in Table 6.3.

Expos. to UV	Temp. °C	2892		2893		2894		2895	
		T	U	T	U	T	U	T	U
1 h out	40	29°	44°	39°	55°	41°	52°	53°	61°
16 h in	20	35°	53°	51°	65°	45°	58°	57°	52°
2 h out	32	25°	48°	29°	49°	37°	51°	45°	57°
48 h in	20	42°	54°	55°	62°	41°	52°	57°	52°
4 h out	39	0°	35°	0°	39°	29°	43°	34°	45°
1 h in	20	10°	39°	15°	44°	32°	47°	39°	45°
3 h in	20	28°	41°	23°	48°	33°	50°	40°	51°
6 h in	20	32°	44°	24°	51°	35°	52°	48°	55°
24 h in	20	39°	52°	33°	57°	38°	56°	53°	55°
2 d out	18-41	0°	32°	0°	38°	31°	42°	45°	56°
4 h in	20	23°	49°	26°	47°	51°	67°	57°	58°
24 h in	20	34°	52°	50°	54°	52°	68°	61°	65°
48 h in	20	44°	60°	53°	61°	52°	65°	62°	66°

Table 6.3: History and contact angle values of 50 μl water drop placed indoors (in) and outdoors (out) (T = treated, U = untreated) on the samples.

After one hour of exposure of the samples to sunlight, the treated half of samples 2892, 2893 and 2894 showed a small reduction of contact angle values, while the treated half of samples 2895 did not show a reduction in contact angle. That even the untreated halves of samples 2892-4 show a contact angle reduction after UV exposure may be due to a very slight contamination with traces of titania during and after preparation. This means that an exposition to UV light of only an hour is not enough to have large enough decrease of contact angle. In order to obtain a greater reduction of contact angle, samples have been put outdoors in the sunlight for 2 hours, reaching a temperature of about 32°C. Results showed a further reduction in contact angle for samples 2892 and 2893, with a lesser effect for samples 2893 and 2894, but a satisfactory wettability was not yet achieved with any sample. For this reason they have been further exposed to sunlight for 4 hours. Finally, the treated half of the samples annealed at the lower temperatures (2892, 2893) attained a contact angle of almost zero degrees, while the remaining samples annealed at higher temperatures showed only a modest further reduction in contact angle without, however, becoming completely wettable. This effect persisted only for a limited time: the contact angle of the droplet becomes already 10° or more only few hours after the end of the UV exposure, reaching again $33° - 53°$ after one day. This means that the analyzed surfaces recover their original state after less than one day.
In addition to contact angle measurements, a sequence of pictures of a 50μl

water droplet before and after the sunlight exposure is presented in Figure 6.1. To get additional information on behavior of water on the surfaces, measurements of the inclination angle of the samples at which the drop runs off the samples have been done. These measurements showed that before the exposition to UV light an inclination of the samples 2892 and 2893 of about 10° is needed for the run-off, while after the UV exposure this angle reduces to about 5°.

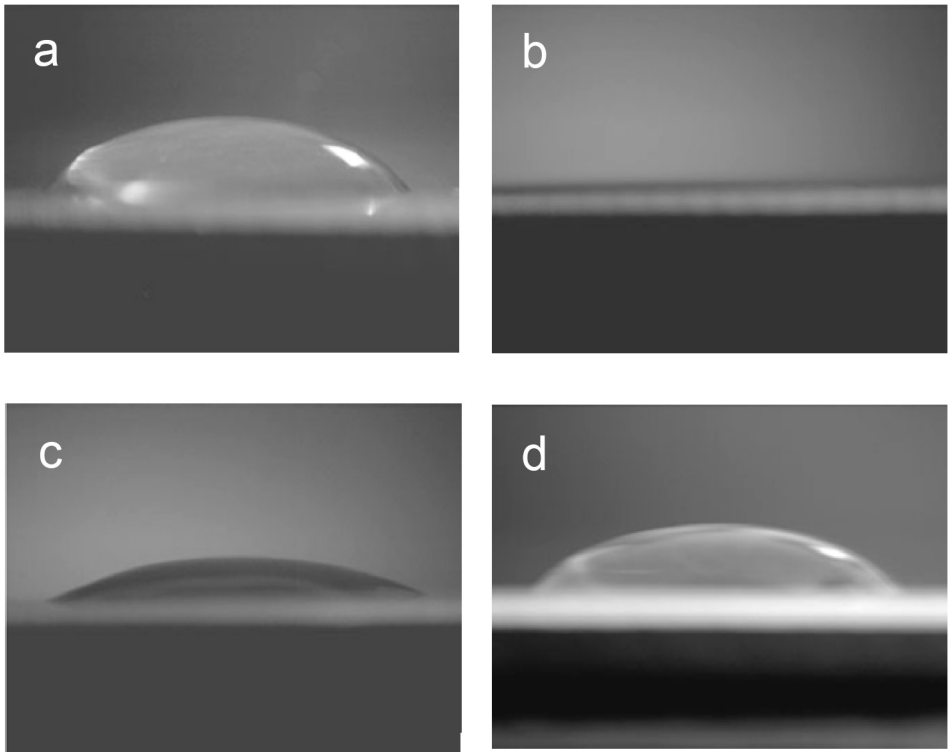

Figure 6.1: 50 μl water drop on the treated half of the sample annealed at 400°C (2892) before (a) and 0 (b), 16 (c) and 24 (d) hours in the dark after 48 hours of UV exposure.

The samples have been then positioned outdoors for 2 days and again samples 2892 and 2893 showed complete wettability but only for a short time. The samples have also been exposed outdoors when the weather was partially overcast and temperature was around 25°C. In fact the samples showed a reduction in contact angle value of only few degrees, which could be linked to the reduction in the ultraviolet incident on the surface as well as to the no-uniformity of the treatment.
In conclusions, it can be said that sunlight exposure had to be extended to at least four hours to obtain good hydrophilicity - and this was only achieved with samples 2892 and 2893 (annealing temperatures 400°C and 450°C, respectively). However, with these samples there is a relatively fast loss of

hydrophilicity/increase in contact angle after the cessation of exposure to sunlight. Even a longer exposure to sunlight could not guarantee a longer persistence of the hydrophilicity. This would, however, have to be achieved to make the coating really useful in the envisaged application. Days of uninterrupted sunshine are not all that frequent in the North of Switzerland and adjoining territory.

The other Titania coatings (H) made by a Sol-gel technique on a set of four metal tubes had been kindly provided by the University of Hannover. As a pre-treatment, the aluminium tubes had been washed and sponged with detergent and afterwards cleaned with dichloroethylene. The dipping solution was composed of titaniumtetraisopropoxide, n-propanol, acetylacetonate and water. After coating, the tubes had been tempered for 40 minutes at 400°C. After four hours of sunlight exposure, the tubes showed a fairly good wettability (contact angle $< 10°$) and this was achieved with all tubes. However, after only few hours, the surfaces started already to show a contact angle of more than tens of degrees. As in the case of coatings TS and TC, there is a relatively fast loss of hydrophilicity/increase in contact angle after the cessation of exposure to sunlight.
Some Japanese assessment of TiO_2-coated facade elements (TT) seemed to indicate that natural activation would tie over hydrophilicity from one day to the next. Earlier hydrophilic treatment of a model conductor [5] had been based on this titania coating.

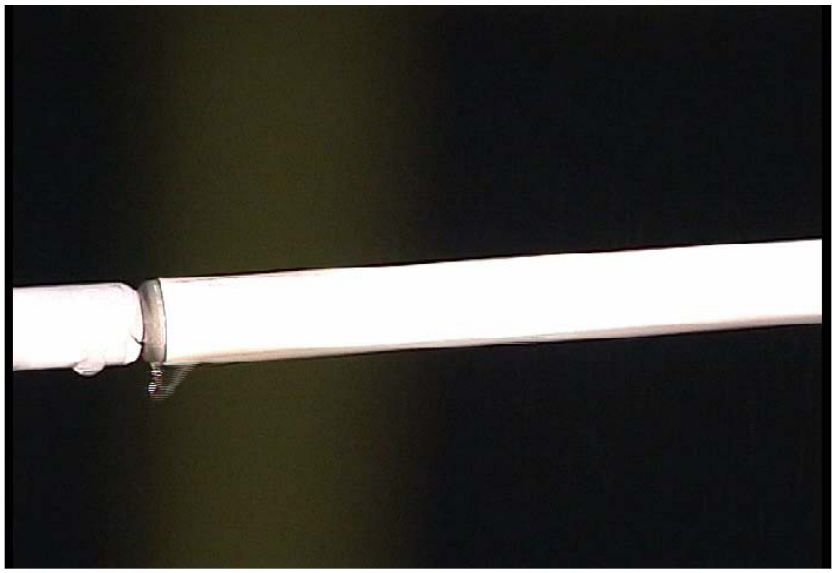

Figure 6.2: Properties of super-hydrophilic coating (T) sprayed massively with water. With only a slight inclination just one single drop runs along the underside and drips off at the boundary of the coated surface.

As this showed promise, commercial titania-based coating on tubular con-

ductors has been obtained from the Japanese company TOTO (see Figure 6.2). This has by now been exposed to the elements (rain, ice, snow) for a number of years and was found to retain perfect wettability also indoors for several days without further exposure to light. With this coating there are no water drops remaining on the upper side of the conductor (Figure 6.2); if the conductor is slightly inclined (3° to 6°), drops forming on the underside progress to the lowest point. When the samples were manually sprayed it has been seen that only a single initial drop runs along the underside, from then on water reaches the low end without forming any conspicuous drops until it drips off at boundary of the coated area.

6.3 Summary on the methods used here to assess hydrophilic coatings

A major aim of the present investigations was to present a methodology to identify robust coatings for conductors which persistently show hydrophilic behaviour. Through the many international contacts with different companies and institutions it was hoped to identify the most stable and suitable coating. So far, investigations showed that in terms of permanent hydrophilicity, the silica-based coating (H12) and a titania-based photo-activated coating (T) proved more satisfactory than the other coatings. Comparisons proved that the hydrophilicity of the T coating is significantly superior compared to that of the H12 coating. The properties and efficiency of all coatings analyzed are represented in Table. 6.4.

Name	Art	Self-applicable	Hydro-phobic	Hydro-philic	Months outdoors	Run angle	Observations
A	Anatase powder	+	-	+++	-	1°	Without binders not weather-resistant
VP12	nano-SiO_2	+	++	-	-	$> 30^\circ$	
H12	nano-SiO_2	+	-	++++	6	$< 6^\circ$	
TC/TS	nano-TiO_2 Sol-Gel	-	-	++	6(+)	$< 10^\circ$	annealed
U	Sol-Gel SiO_2	-	-	++	6(+)	$< 10^\circ$	annealed
T	SiO_2+ TiO_2	–	-	++++	30(++)	1°	self-cleaning commercially applied

Table 6.4: Properties of all coatings analyzed. The run angle is considered after outdoor exposure.

7 The evaluation of measures against tonal noise emission

To evaluate a coating and the durability of its hydrophilic properties completely, coated high voltage model and real conductors have to be tested with electrical stresses applied. The roles of parameters that influence tonal emission during and after precipitation have to be clarified [104, 105]: several parameters (e.g. type, age, stranding of the conductor) had to be looked at in detail to identify parameters with strong impact on the emitted tonal noise levels. Earlier work [6, 5] had indicated that hydrophilic coating, particularly with inclined sections of line, could alleviate the situation after cessation of heavy rain by assisting runoff, eliminating drops except on the underside of conductors and generally speeding up the drying of the line. As the initial type of coating (A) successfully used in the laboratory could not be expected to stand up to the elements, the stability of various other coatings has here been assessed in terms of acoustical emissions.

7.1 Laboratory investigations to assess the success of measures against noise

In line with earlier practice [1, 16, 49, 18, 106] a single-phase model line with tubular conductors (typically diameter 20 mm) has been set up with variable conductor-ground distance in a fully screened laboratory. Details of the laboratory equipment are found in Appendix A.3.

7.1.1 Differences between model and real conductor

In the laboratory, model conductors as well as 'real' conductors (standard and 'Z' type) can be used for investigations.
Model conductors (Figure 7.2 top) are rigid straight tubes or rods with a macroscopically smooth surface. They have been chosen for experiments, since their cylindrical shape and their rigidity generate, under voltage, a fairly uniformly distributed electric field around the conductor. 'Real' conductors

(Figure 7.2 bottom) are stranded, in standard form composed of round aluminum wires arranged around a core; in 'Z'-type conductors the outer strands are shaped to give a less undulating outer contour.
The classification of all model and real conductors used for these investigations is given in Table 7.1.

Figure 7.1: Top: Model conductors. N.1) Stainless steel C_rN_i N.2) Aluminium N.3) Stainless steel C_rN_i sandblasted N.4) Aluminium sandblasted. Bottom: 'Stranded real' conductors, Aldrey or Aluminium steel cored (Al/St).

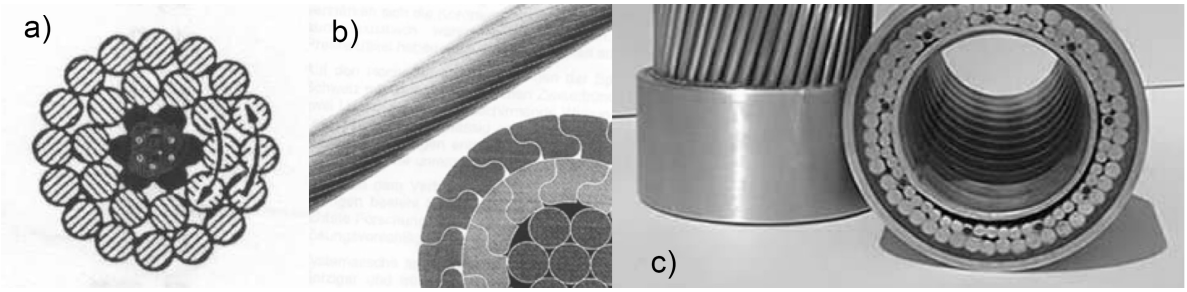

Figure 7.2: Cross section of a)Standard real, b) Z and c) Hollow conductors.

Name	Nominal cross section (mm^2)	∅ (mm)	Material	State	Source
model	176.6	15	Al	new	ETH
245-2Z	241.9	18.9	Al/St	new	Illwerke
265-2Z	261.34	19.6	Al/St	new	Illwerke
model	314	20	Al	new	ETH
240/40	282.5	21.8	Al/St	new	EnBW
257/60	n.a.	n.a.	Al/St	new	Illwerke
257/60	n.a.	n.a.	Al/St	used	Illwerke
285/35	297.8	22.4	Al/St	new	EnBW
340-2Z	345.6	22.4	Al/St	new	Illwerke
380/50	431.2	27.0	Al/St	new	EnBW
435/55	490.6	28.8	Al/St	new	EnBW
536-2Z	538.0	28.3	Al/St	new	Illwerke
490/65	553.8	30.6	Al/St	new	EnBW
Aldrey	601.0	30.2	Aldrey	new	EWZ
Aldrey	601.0	30.2	Aldrey	used	EWZ
560/50	611.2	32.2	Al/St	new	EnBW
710-2Z	704.9	32.4	Al/St	new	Illwerke
926-3Z	928.4	36.8	Al/St	new	Illwerke

Table 7.1: Classification of model and 'real' conductors used for experiments.

7.1.2 The choice of coatings for high voltage lines

Numerous coatings have been applied to model and real conductors for assessment. A detailed description and analysis of the utilized coatings is provided in chapter 6.

The silica based coating (H12) has been used to cover model and real conductors. For comparisons, also the commercial silica based coating which shows hydrophobic behavior (VP12) has also been used. Other conductors were coated with TiO_2 and thus expected to show photocatalytic behaviour. Compared to the silica based coatings, the photocatalytic ones available at the time of the earlier tests had the disadvantage that they required special procedures and techniques to prepare the conductors that could only be done by the manufacturers and not just in every laboratory. Some conductors were coated using CVD and Sol-gel techniques described in Chapter 6.

The major aim of this investigation was to find a robust coating for conductors which persistently shows hydrophilic behaviour. In chapter 6 preliminary investigations on the stability of coatings with respect to weather stress have

been presented. The next step is to determine the success of coatings with respect to acoustical emissions and eventually partial discharge measurements.

7.1.3 Procedure and measurements

In general, high voltage (70 to 100 kV, resulting in a surface field strength of 14 to 20 kV_{rms} on the dry conductor) was applied before "rain"commenced. The conductor could be horizontal or inclined to e.g. 3.5°. Typical experiments involved spraying the central section of 1.5 m long conductors by means of a nozzle for 4 minutes followed by a drying period of 30 minutes or more. To determine the drying properties of each conductor and thus the effectiveness (or lack of it) of the measures to reduce tonal noise, the time needed for the recovery of quiet conditions (decay time) has been measured (see Figure 7.3).

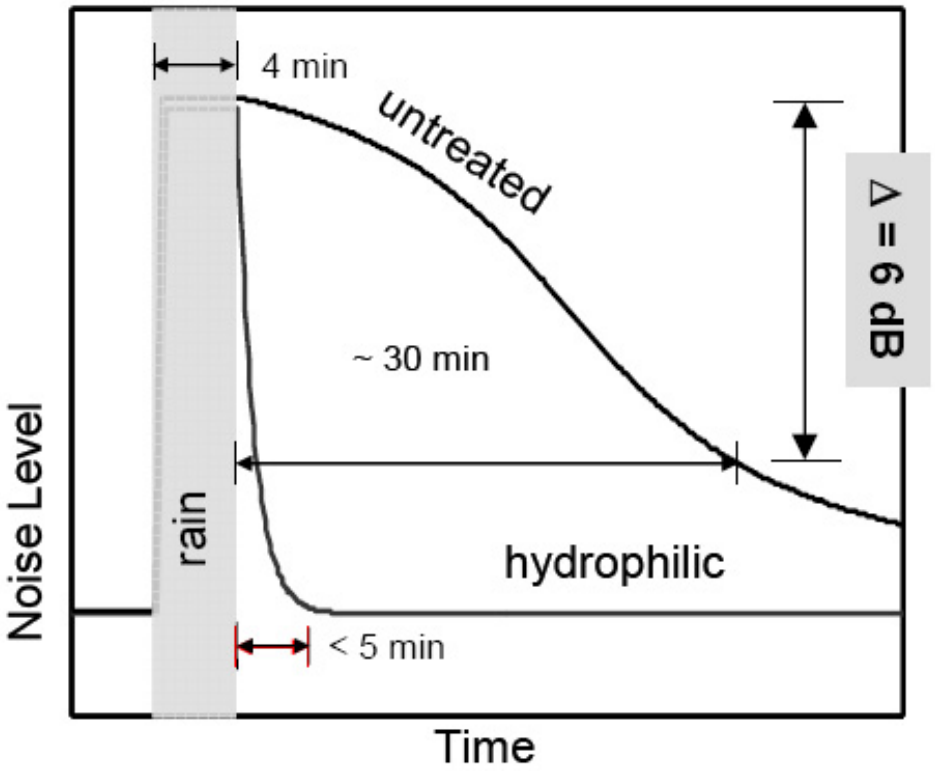

Figure 7.3: Assignation of the decay time in a typical experiment (-6 dB). In the case of the hydrophilic model conductor, a noise reduction of 6 dB was often observed within about a minute after cessation of rain, as it will be seen in the next section.

7.2 Evaluation of coatings as measure to reduce tonal noise

Tonal noise is associated with electrical discharges from protrusions such as are constituted by water drops [95, 25]. Thus, the basic strategy for the reduction of the $2f$ emissions must be to eliminate or at least reduce the number and severity of such sites and to keep field strengths low to avoid discharge inception. In this context, for the evaluation of such strategies conductor arrangements, bundle configurations, conductor geometry and surface properties have to be considered [104].

7.2.1 Evaluation of coatings applied to model and real conductors

To confirm the assumption that one can achieve a significant reduction of sound emission by using a suitable hydrophilic treatment of the conductors, a series of surface preparations (untreated, sandblasted, hydrophobic and hydrophilic coated) on model aluminum conductors as well as on real stranded conductors have been investigated.
The case of a 20 mm diameter aluminium model conductor is reported here to compare the effect of different treatments/coatings with respect to persistence of drops on the conductors and to noise emissions (see Figure 7.4 where conductors are inclined by a angle of $0°$). All the results refer to 4 minutes 'mean rain', a quantity which here corresponds to $0.39\,\mathrm{mm/min}$ at the conductor centre.

As one can see, the decay of acoustical noise is much more rapid for the conductor covered with hydrophilic coating than for the hydrophobic one. One can observe that for the sandblasted conductor the acoustical noise decays already noticeably (1 dB) during the time of rain. Much more impressive is the behaviour of the TOTO (TT) coating: tonal sound emission falls to near the background level almost within seconds of the rain ceasing (15 dB decrease). This is due to the fact that during rain only one initial drop runs along the underside of the TOTO (TT) coated conductor, from then on water reaches the low end without forming any conspicuous drops on the way. These results suggested the idea to further reduce tonal noise by combining the hydrophilic coatings with one or more so-called drip-off sites separating the water from the cable as discharge-free as possible. A possible prototype of such drip-off sites and their noise reducing effect have been presented in [4].
It should also be emphasized that an important property of hydrophilicity is also its promotion of water runoff along inclined underside surfaces. Drops will run along the undersides, often hardly visible, until they reach a suitable

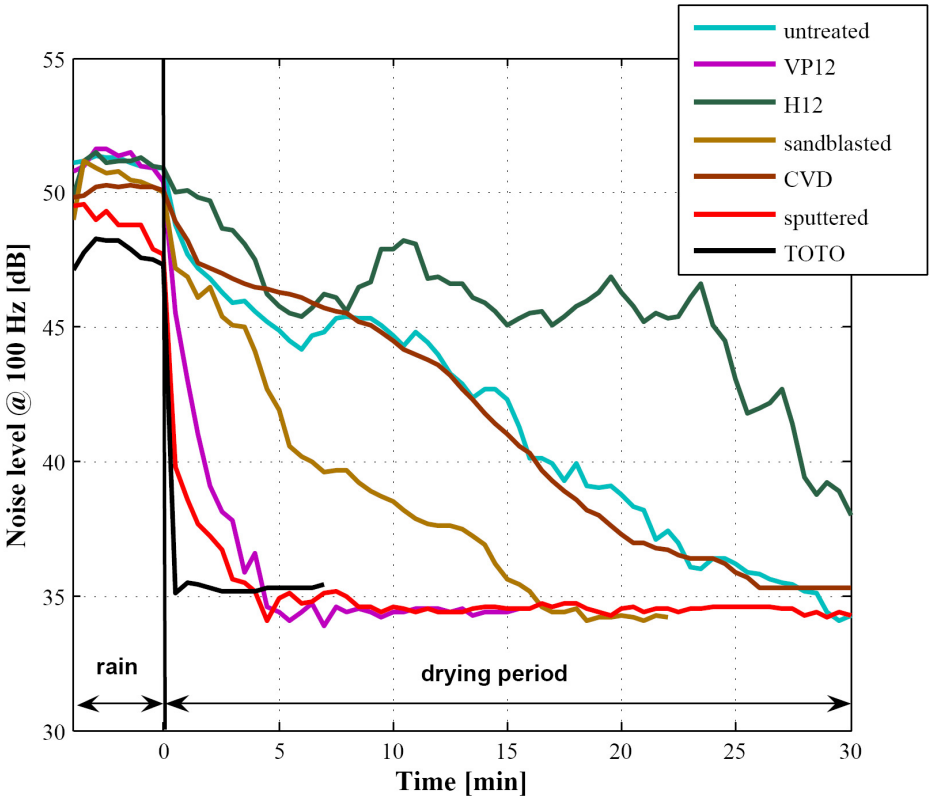

Figure 7.4: Decay of sound level during and after a rain period of 4 minutes for a 20 mm aluminium model conductor with different coatings/treatments. Applied voltage: 100 kV_{eff}

drip-off sites, this is effective with quite modest inclinations and is then causing an even faster decay of sound emission. In real cable installations a major part of the line tends to be inclined, even above level ground due to the sag of the suspended cable. The sequence in Figure 7.5 shows the persistence of water for a hydrophilic aluminium conductor and a hydrophilic sandblasted conductor. Quite impressive is that with an inclination of the conductor of only 3.5°, immediately after the cessation of precipitation there is complete drying and thus the decay of sound emissions takes place in a very short time, compared to a horizontal conductor.

The case of a 32.4 mm diameter *real* cable is reported in Figure 7.6 to compare the effect of different treatments/coatings with respect to noise emissions. The application of the silica based hydrophilic treatment to some Z-type real conductors showed a significant and useful effect regarding acoustical 100 Hz emissions after cessation of rain (Figure 7.6 bottom trace). During heavy rain, the use of a hydrophilic coating showed a decrease in tonal emission of few decibel, which the human ear could hardly perceive. Whit the hydrophilic horizontal conductor, the main discharge sources are large water drops more or less stationary on the underside.

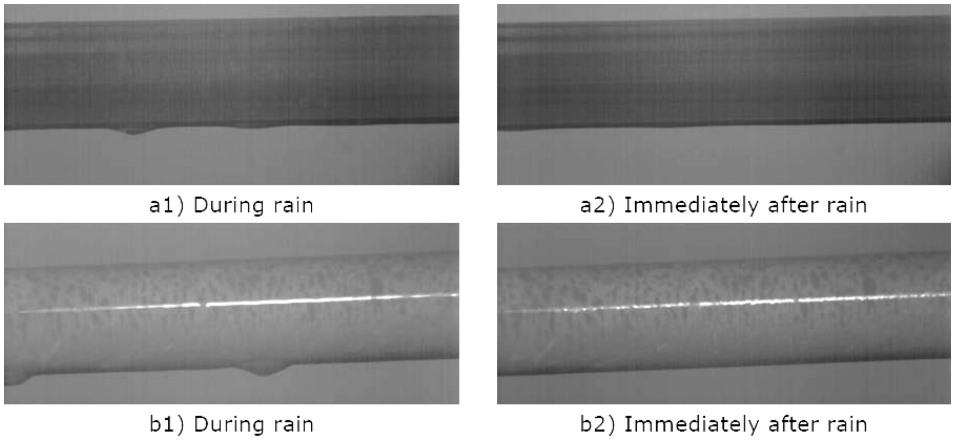

Figure 7.5: a1) Aluminium model conductor 3.5° inclined, hydrophilic coated, during and a2) immediately after rain. b1) Aluminium sandblasted model conductor 3.5° inclined, hydrophilic coated during and b2) immediately after rain.

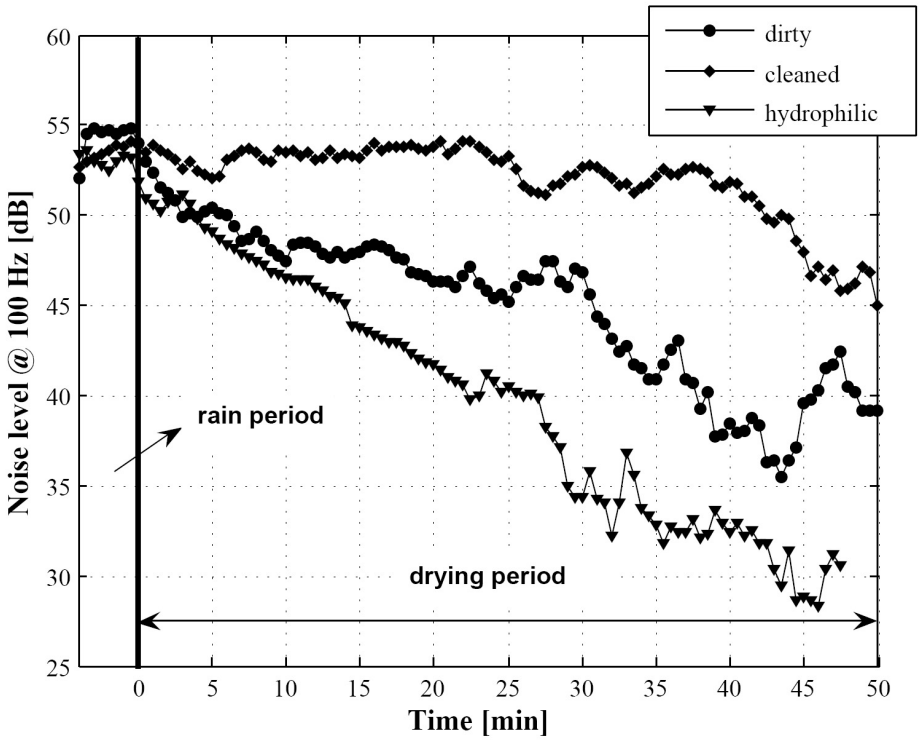

Figure 7.6: Z type real trapezoidally stranded conductor, 32.4 mm diameter. Tonal emissions during and after a rain period of 4 min, heavy rain and at constant voltage (100 kV_{eff}), with the conductor in its original ex-stock state (’dirty’, middle curve), after cleaning (top) and after hydrophilic coating (bottom).

The effectiveness of hydrophilic coatings applied to real conductor cables

are also confirmed by partial discharge measurements (see Figure 7.7). This emphasizes the beneficial effects of hydrophilic coating in its significant reduction of corona loss.

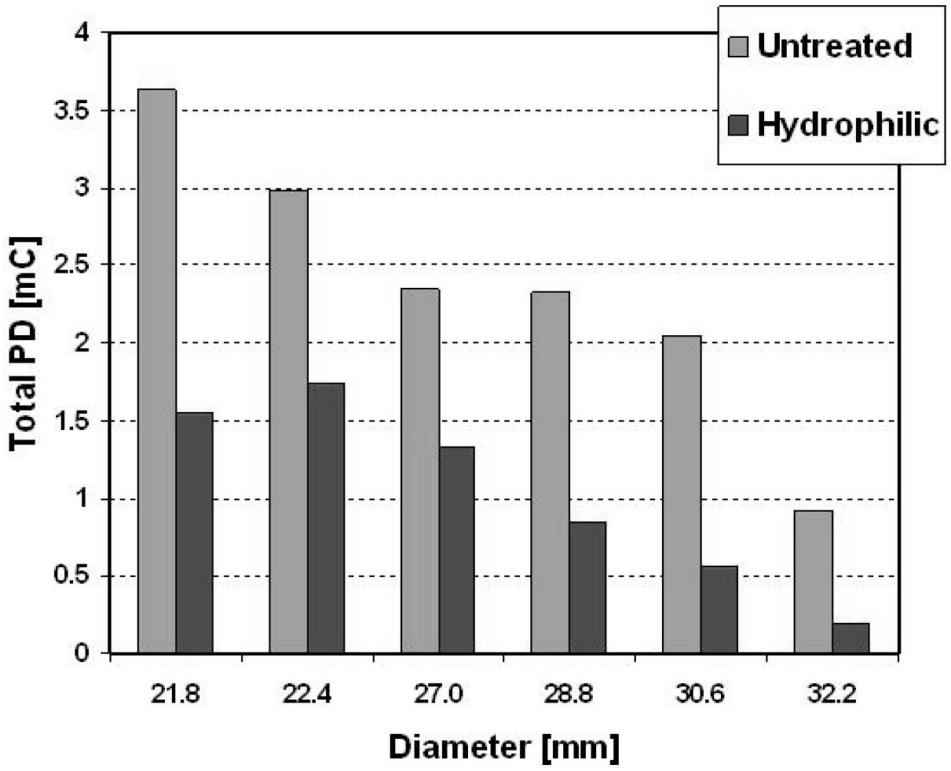

Figure 7.7: Total charge transport in pulses carrying between 0.6 and 12.4 nC each for HV real stranded conductors of different diameters at $100kV_{eff}$, as accumulated in 600 minutes.

7.2.2 The influence of rain rate on the success of hydrophilic coatings

Hydrophilic coatings that successfully shorten the duration of emission after the rain stopped seemed to have only very little effect during the period of heavy precipitation [107]. Additional experiments, however, showed that the noise-reducing effect of this proposed remedy against tonal noise also depends on the rain rate as shown in Figure 7.8.

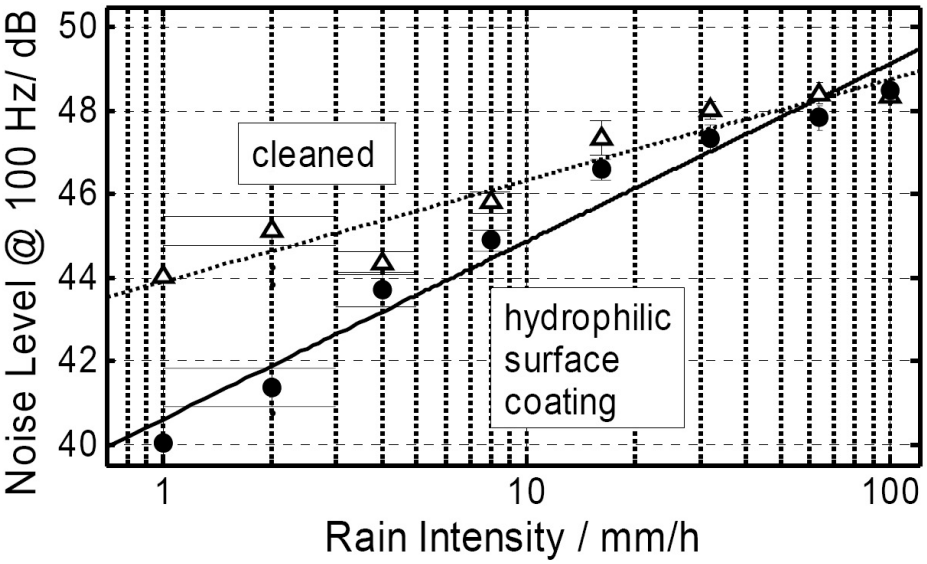

Figure 7.8: Tonal noise at 0.6 m distance from a single ACSR cable (type: Al-St 680/85), *during* continuous rain over a range of intensities from 1 to 100 mm/h: with different surface treatments: step 1: cleaned with ethanol; step 2: hydrophilic coating applied. Surface field strength: 13.1 kV/cm [108].

In the figures it is illustrated that with decreasing rain intensity the noise reduction increases. The positive effect of coatings during rain had been missed so far due to the severity of the rain ($>$ 100 mm/h) mostly used in the early experiments. The drawback that water drops are predominantly collected on the underside, where they can be most efficient emitters of tonal noise, is more than compensated by the draining properties of coated conductors.
The reduction of tonal noise during rain (as calculated utilizing the model of Kirkham and Gajda [27] as presented in Chapter 2) for a conductor without and with hydrophilic coating is presented in Table 7.2:

Conductor type	1 mm/h	10 mm/h	100 mm/h
340/10	-5.0 dB	-3.7 dB	-2.4 dB
680/85	-3.3 dB	-1.4 dB	+ 0.5 dB

Table 7.2: Fitted results for the rain rate parameter based on the model of Kirkham and Gajda [27, 28].

7.2.3 The influence of electric field strength on the success of hydrophilic coatings

A straightforward way to reduce corona losses and thus tonal emission during and after precipitation consists of reducing the electric field strength [17]. The variation of noise level with respect to different electric field strength values is represented in Figure 7.9.

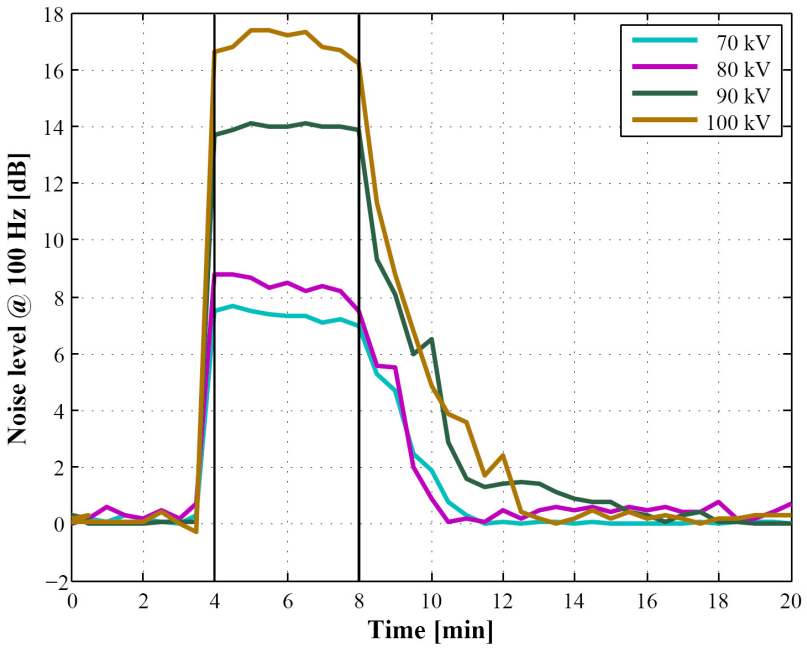

Figure 7.9: Hydrophilic model conductor with different electrical surface field strengths proportional to voltages given (note the shorter time scale). Background level taken as 0 dB. Rain 4 min at 100 mm/h. The voltage has been changed to have a range of surface field strengths (geometrical field strength).

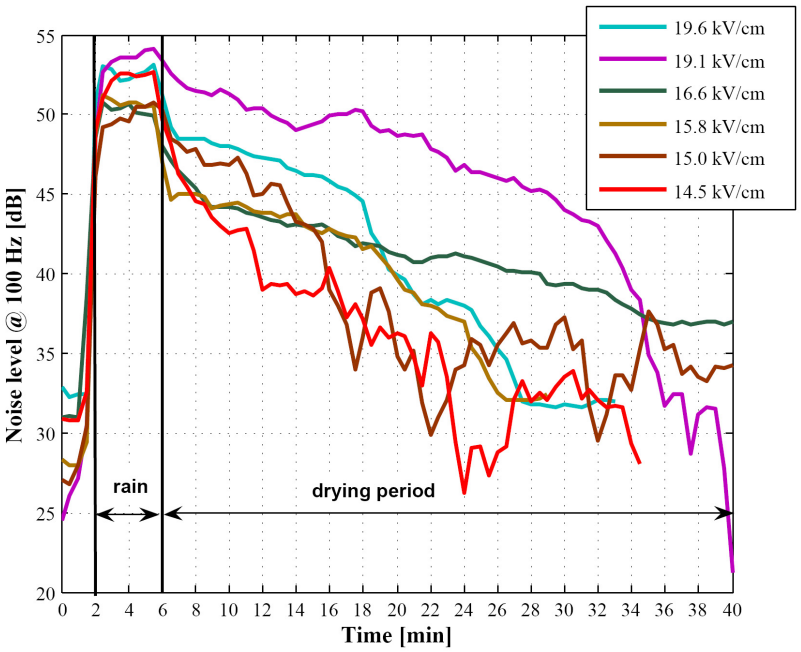

Figure 7.10: Noise level at 1 m distance with a series of stranded conductors of different nominal diameters at a constant applied voltage of 100 kV_{RMS} and after 4 min of heavy rain of 100 mm/h. The diameters are reflected in the surface field strengths listed. The increase of surface field strength due to stranding is conventionally assumed to be 1/0.82.

As an example, the case of a 20 mm diameter aluminium model conductor covered with a hydrophilic coating is taken, in addition to the results obtained with the hydrophobic coating and a sandblasted sample. It is clearly evident that the decay of tonal emission is rather rapid for all the field strength values and that the initial return to the baseline typically takes place with a rate of about 5 dB/ min.

At 100 kV (20 kV/cm), the noise decay with the hydrophobic conductor is much slower at than with the lower voltages. An explanation could be that at the higher voltage a larger number of small droplets goes into instability. With the sandblasted conductor one can observe a considerable noise reduction during the rain period as the wettability changes with the amount of rain, which has flowed over the surface to the underside of the conductor.

When the applied *voltage* is kept constant, conductors with larger diameter emit less tonal noise as compared to smaller diameter specimens (see Figure 7.10). For larger diameter cables the noise-reducing effect of the lower surface field strength dominates over the noise intensifying effect of an increased surface area, holding more water.

7.2.4 Surface properties of conductors of various geometries as reflected in the success of hydrophilic coatings

The tonal noise emissions from *untreated* Z, standard and hollow real conductors at given electric field strengths showed no noticeable difference during precipitation (Figure 7.11), despite the different surface structure. In combination with hydrophilic coatings, and in particular in the drying phase, the type (geometry) of the conductor might, however, play a role.

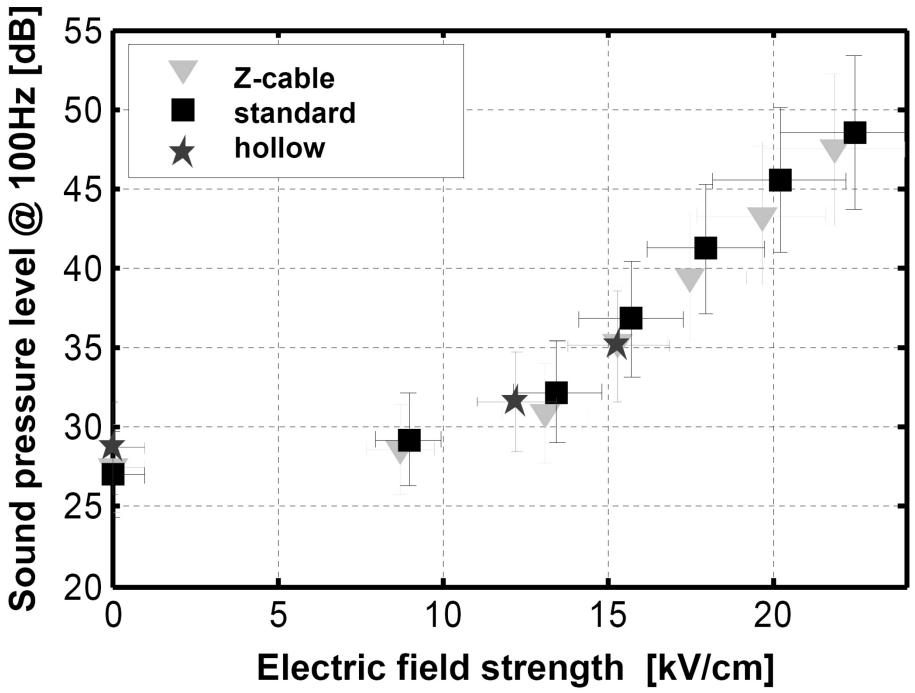

Figure 7.11: Noise level at 1 m distance for a number of untreated Z, standard and hollow real HV cables hydrophilic coated for different nominal electric field strengths. Applied voltage: 100 kV_{eff}. Rain rate: 100 mm/h. [108]

From the operators, there is no clear information regarding the ageing state of the untreated cables supplied and the noise emissions which had been associated with these types. Laboratory experiments showed that, in general, and in agreement with common perception, aged conductors are quieter than new ones (Figure 7.12). The differences, however, were here only few decibels and are, therefore, not always perceptible for the human hear.

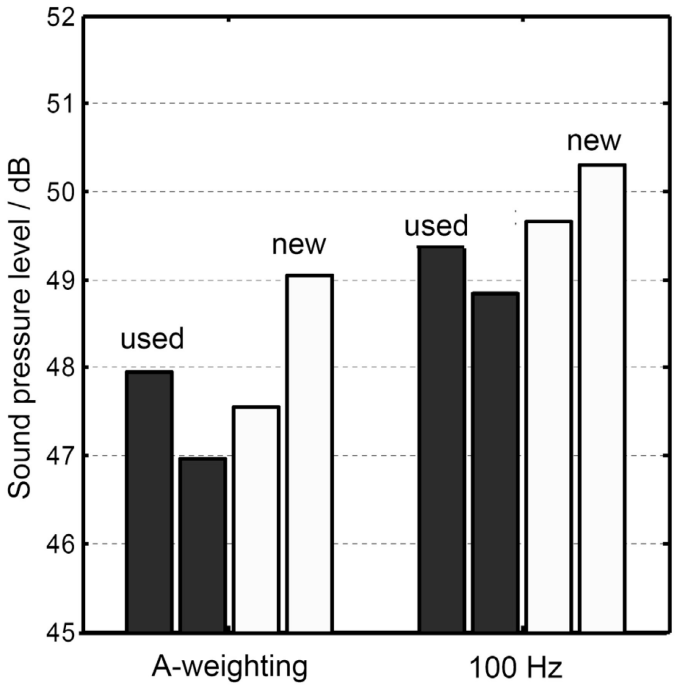

Figure 7.12: A-weighted and 100 Hz noise level at 1 m distance for different uncoated new and used HV cables. Applied voltage: 100 kV Electric field strength: 14.3 kV/cm. Rain rate: 100 mm/h.

7.2.5 Accelerated ageing tests of coatings

The analysis presented in Chapter 6 had indicated that the silica based coating showed perfect wettability for six months or more and might therefore serve as an easily applied robust coating for high voltage conductors. To see if discharge activity on the surface of the conductor is one of the stress factors which could affect coatings on high voltage cables, investigations of the ageing of the coating with respect to different electric field strengths, discharge levels and substrates have been carried out. The assumption made here is that any damage to the coating would be related to the cumulative amount of charge passed [105]. Diagnostics included as usual sound pressure level measurement, PD events displayed against AC waveform (ICM system) and the total charge flowing to the conductor.
To reveal the aging of the coating mentioned, a hydrophilic aluminium model conductor of 20 mm diameter has been exposed to 4 minutes rain, rate 100 mm/h, followed by a drying period of 20 min, under an electric surface field strength of 21 kV/cm. The same experiment has been repeated several times, charge cumulatively passed in large amplitude partial discharges was typically 12 mC in 600 minutes each time and the resulting 100 Hz and A-weighted noise level trends gave no evidence of any obvious damage to the coating (see

Figure 7.13).

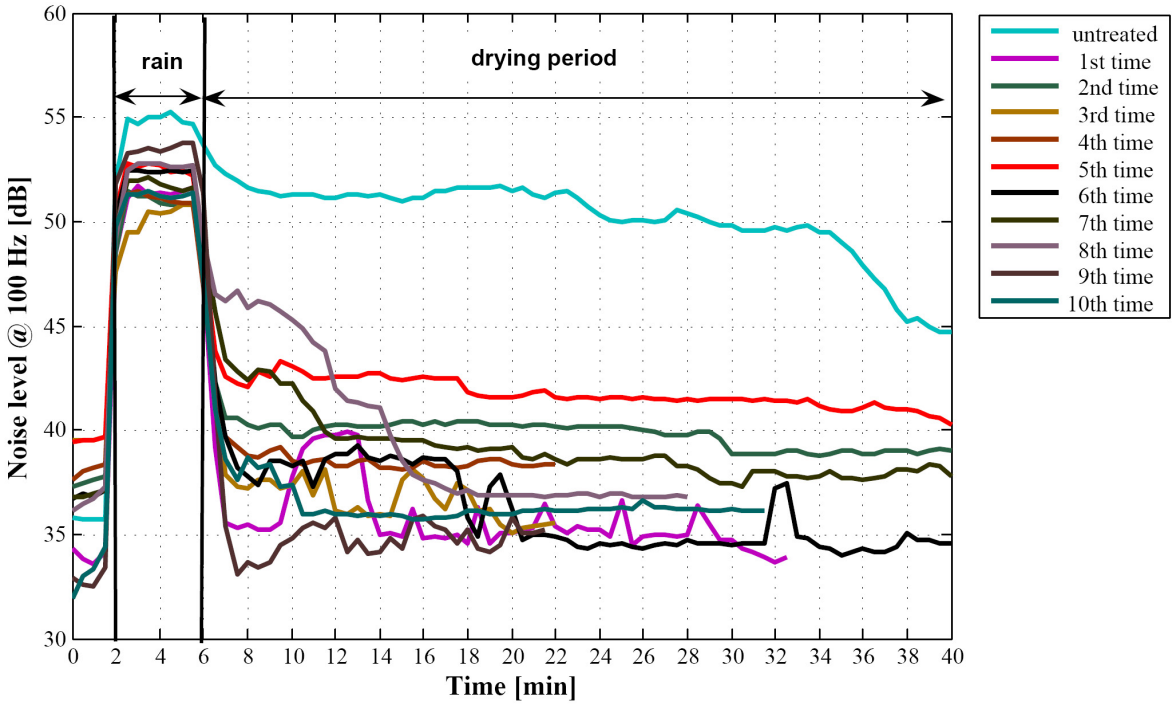

Figure 7.13: Repeated measurements of tonal noise from a 20 mm diameter model conductor coated with a hydrophilic coating. Surface field strength: 21 kV/cm.

To increase the PD charge amount, the subsequent experiment has been made with another coated aluminum conductor of smaller diameter (15 mm), and thus with the much higher electric field strength of 26.5 kV/cm, and, in consequence, a total charge passed of 20 mC each time.

Acoustical and PD measurements still showed no noticeable ageing of the coating. This is, of course, still a modest amount of ageing compared to that encountered by a conductor in active use over many years. Further acoustical and PD measurements using also real conductor cables did again not show any kind of evidence that would make one suspicious that a detrimental ageing of the coating had taken place.

7.3 Summary on the evaluation of measures against tonal noise emission

The effect of hydrophilic coatings applied to a range of different conductors (model, Z and standard) has been evaluated and corresponding results are listed in Table 7.3. Conditions applied were 100 kV_{rms} and 4 minutes of very heavy rain (100 mm/h) followed by a drying period.

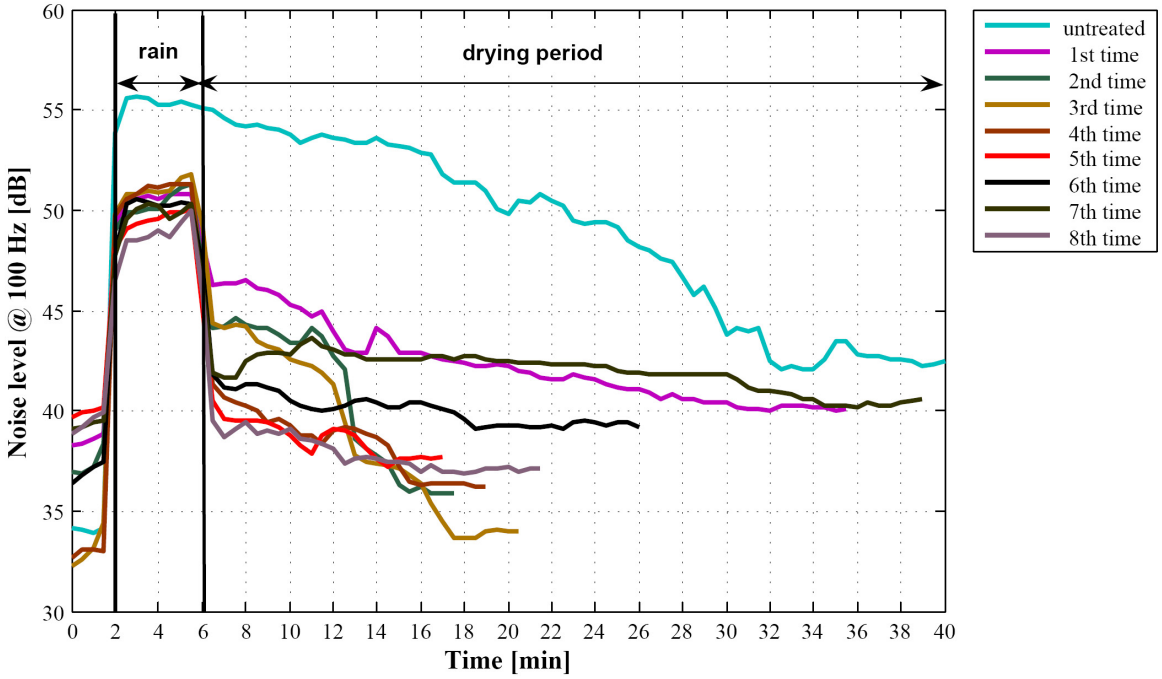

Figure 7.14: Repeated measurements of tonal noise from a 15 mm diameter model conductor with a hydrophilic coating. Surface field strength: 26.5 kV/cm. 4 minutes of 100 mm/h rain and subsequent drying.

Investigations showed that during rain at this high rate the coating has little influence on sound emission (see Figure 7.8). After the cessation of rain, the effect is very variable with the different conductors; with the model conductors (inclined by 3°) the sound emission drops drastically within half a minute. Some 'real' cables suffer heavy water loading at this high rain rate and thus a rather extended drying period, even when the peripheral surfaces of the outer wires have been coated. Other experiments with a wide range of rain rates had shown that the hydrophilic coating is generally much more beneficial when the rain rate is more realistic, i.e. drastically lower than the rare rate of 100 mm/h.

	Noise levels during rain		Decay time after rain	
Type of conductor	100 Hz (dB)	A-weighted (dB)	$T_{(\sim 6dB)}$ untreated	$T_{(\sim 6dB)}$ hydrophilic
Al (∅15 mm)	-5.2 ± 0.8	$+4.9 \pm 0.7$	17 min	0.5 min
Al (∅20 mm)	-3.3 ± 0.8	-2.6 ± 0.4	30 min	0.5 min
Al-sandblasted (∅20 mm)	-2.2 ± 0.8	$+0.5 \pm 0.8$	0.5 min	0.5 min
Mean value	$\mathbf{-3.6 \pm 1.4}$	$\mathbf{+0.9 \pm 1.1}$	**15 min**	**0.5 min**
245-2Z (∅18.9 mm)	$+0.9 \pm 0.6$	-2.2 ± 0.3	28 min	25 min
265-2Z (∅19.6 mm)	-4.0 ± 0.5	-3.3 ± 0.3	39 min	28 min
340-2Z (∅22.4 mm)	-3.5 ± 0.9	-3.3 ± 0.8	21 min	2.5 min
536-2Z (∅28.3 mm)	-0.5 ± 0.5	-2.6 ± 0.3	16 min	9 min
710-2Z (∅32.4 mm)	-2.5 ± 1.3	-5.2 ± 0.4	2.5 min	2 min
926-3Z (∅36.8 mm)	-2.6 ± 0.9	-4.9 ± 0.2	2 min	2 min
Mean value	$\mathbf{-2.0 \pm 2.0}$	$\mathbf{-3.6 \pm 1.6}$	**18 min**	**11 min**
240/40 (∅21.8 mm)	-1.4 ± 0.5	-0.7 ± 0.3	14 min	10 min
285/35 (∅22.4 mm)	-1.6 ± 0.5	-1.7 ± 0.6	17 min	14 min
380/50 (∅27.0 mm)	-0.1 ± 0.5	-1.7 ± 0.6	13 min	9 min
435/55 (∅28.8 mm)	$+2.1 \pm 0.5$	$+1.6 \pm 1.7$	4 min	6 min
490/65 (∅30.6 mm)	$+0.9 \pm 0.7$	-3.1 ± 0.5	9 min	12 min
560/50 (∅32.2 mm)	-2.7 ± 0.7	-1.6 ± 0.4	1.5 min	1 min
Mean value	$\mathbf{-0.5 \pm 1.4}$	$\mathbf{-1.2 \pm 2.0}$	**9 min**	**8 min**

Table 7.3: Reduction of noise level during rain 100 mm/h for 4 minutes in each case and subsequent drying period for return of sound emission to a level lower by 6 dB for different model and real conductors/treatments. Applied voltage: $100\,\mathrm{kV_{eff}}$.

	Coating	**Type & State**	**Bundle**	**Drip-off points**
+	- reduces noise levels and shortens noise duration - application to existing line	- influences effect of coating - no additional maintenance	- permanent effect, no ageing - no additional maintenance	- add to effect of hydrophilic coating - implementation on existing line possible
-	- long term ageing / life time not yet known - development of application robot desiderable	- no or at most small effect without coating - change of conductor cost - large variability (short samples)	- probably replacement of masts, isolation or supports needed (far too costly)	- potentially problems with ice or snow load - many unknowns, e.g. effect without coating

Table 7.4: Advantages and disadvantages of remedies against noise.

In conclusion, it can be stated that, besides the rain intensity, the most important parameters that control tonal noise emission during and after rain are the surface field strength and the surface properties of the conductor. Noise reduction can be achieved by large diameter cables or an optimized bundle geometry. Mechanical and cost constraints, however, draw tight limits to practical implementation of inherently low tonal noise overhead transmission lines, coating may be the cheapest remedy.

The different surface states of the conductors analyzed showed different appearance and persistence of water drops and thus different effects on acoustical emissions on both model and real conductors. Results demonstrated that hydrophilic coatings on model conductors show properties which could lead to a significant suppression of sound emission and reduction of corona loss during and particularly after rain. Corresponding treatments of real conductors showed a significant and useful effect regarding acoustical emissions after cessation of rain, while their efficacy during very heavy rain is quite small, although corona loss appears also to be significantly reduced (Figure 7.7). To summarize, an overview of the advantages and disadvantages of the analyzed measures to reduce noise from high voltage lines is given in Table 7.3.

8 Summary and conclusions

In this work, a methodology to assess measures to mitigate tonal and other acoustic emission from high voltage lines is presented. In particular, this work is concentrated on describing a method to quantify the effectiveness of the use of such hydrophilic coatings and to provide a classification of properties that a suitable coating for high voltage lines must have. From the results gained, the following conclusions are made:

- The periodic water drop deformation in dependence on the surface properties has been assessed to improve the understanding of the ageing phenomenon of coatings applied to high voltage lines. It has been found that such deformation is the source of charge injection into the immediate surroundings of conductors and thus a source of tonal noise emission [95, 25]. Through the record of all stages of water drop instability development at up to 10000 frames per second, as well as other measurements it has been possible to demonstrate how instability voltage is highly dependent on the surface conditions. In particular, the instability voltage at which a water drop elongates in the direction of the electric field was demonstrated to increase strongly with a reduction in zero-field contact angle and to decrease with increasing drop volume.

- A small-scale setup has been used to expose single sessile water drops to globally homogeneous or moderately inhomogeneous DC electric fields aiming to study the effect of the surface property and of the drop sizes on the resonance phenomena of water drops by measuring discharge currents and light emission. It has been observed that with negative drops, discharge onset produces a sequence of "packets"of Trichel pulse trains, each of which is terminated by droplet ejection. This confirmed that there is a link between drop oscillation and slow Trichel pulse sequences. With positive drop polarity, behaviour appears to be similar, with burst pulse corona in place of the far more regular but lower amplitude Trichel pulses.
  The oscillation frequencies of water drops of a range of volumes have been recorded using different observation techniques and found to be linked to the spacing of Trichel pulse packets from negative drops. These frequencies correspond well with those found with variable frequency

AC for large oscillation amplitudes near or at Taylor cone occurrence and with a relatively hydrophilic substrate and they are also quite compatible with those measured with DC by other researchers [61].

- Drop populations on conductors variously treated and their development during and after periods of rain have been recorded and analyzed to evaluate completely the characteristics of coatings. The investigations showed that the application of an electric field to the high voltage conductors produces a significant decrease of the drop number, particularly as far as small drops are concerned. A detailed analysis of the spatial drop size distribution on conductors during rain has revealed that only a small fraction of drops contributes at a given instant to tonal noise emissions, in particular, large drops that reside on the bottom side of the conductor. After rain, highly hydrophilic coating promotes the drying of the conductors and thus rapidly reduces the population of deformable water drops.

- Since a remedy against tonal emission after precipitation is seen in the reduction of the population of readily deformable water drops on the conductors by encouraging runoff and drying as well as attaining drop shapes less subject to deformation, a method to evaluate the effectiveness of applying a hydrophilic coating to real and model high voltage lines is proposed. Part of this work was focalized on the search of a robust coating for conductors which will persistently show hydrophilic behaviour. So far, various formulations have been analyzed under different conditions and indicated that a silica based coating and another even more promising titania based commercial coating which can claim to have photocatalytic properties, could be potentially suitable for high voltage lines. Such hydrophilic coatings applied to model conductors have demonstrated properties which could lead to a significant suppression of sound emission and reduction of corona loss after rain. Corresponding treatments of some real conductors showed also a significant but reduced effect regarding acoustical emissions after cessation of rain compared to that observed with model conductors.

- A suitable accelerated ageing test to see whether hydrophilic coated conductors become aged has been developed. Conditions leading to a higher stress were chosen by applying a stronger electric field and a rate of rainfall higher than typically expected in reality. Results based on acoustical and PD measurements showed no noticeable ageing of the analyzed coatings.

- Hydrophilic coatings which successfully shorten the duration of emis-

sion after rain has stopped seem to have no positive effect during a period of *heavy* precipitation. Results showed that their noise-reducing effect depends on the rain rate: with decreasing rain intensity the noise reduction improves. Furthermore, hydrophilic coating is particularly advantageous at low surface gradients, say 16 kV/cm or less.

- Since conductor arrangements, bundle configurations and conductor geometry are also possible methods to keep the total annoyance at a minimum, their efficacy alone and combined with the use of hydrophilic coatings has been investigated. It has been demonstrated that reduction of tonal noise *during rain* can be achieved by lowering the surface field strength, while the duration of tonal noise emission after the end of precipitation and with low rain rates can be significantly reduced by suitable hydrophilic coating of the conductor.

A Experimental setups

A.1 Set-up and equipment for DC single drop analysis

A small-scale setup was used to expose single sessile water drops to globally homogeneous or moderately inhomogeneous DC electric fields. The experimental arrangements consisted of two parallel metal plates of defined dimensions and shapes (6.5 cm diameter, 90° Rogowski profile) arranged typically with 1 cm gap spacing. The upper electrode was always stainless steel without any treatment, while the lower one was varied to test different surfaces and coatings available.
The arrangement of Figure A.1, supplemented by the use of a framing camera, has been used to study drop deformation and instability.

In particular, the following diagnostics were provided:

1. High series resistance of 140 M Ω to have some protection for the current recording amplifier.

2. MotionPro high-speed digital imaging system (up to 10000 fps) which includes:

   - A compact light-weight camera containing a sensor with 1280 × 1024 active pixels and the electronics that capture and transmit images,
   - Camera cable, which provides power as well as data and control Signals,
   - PCI Controller Board,
   - F_{Mount}Adapter,
   - Redlake MiDAS software operates in Windows 2000,
   - The software displays.

3. Bertan high voltage power supply, from which a wide range of stable outputs up to 50 kV are available. It contains a DC power supply to convert the AC line power to low voltage DC and a DC/DC converter which generates the high DC voltage.

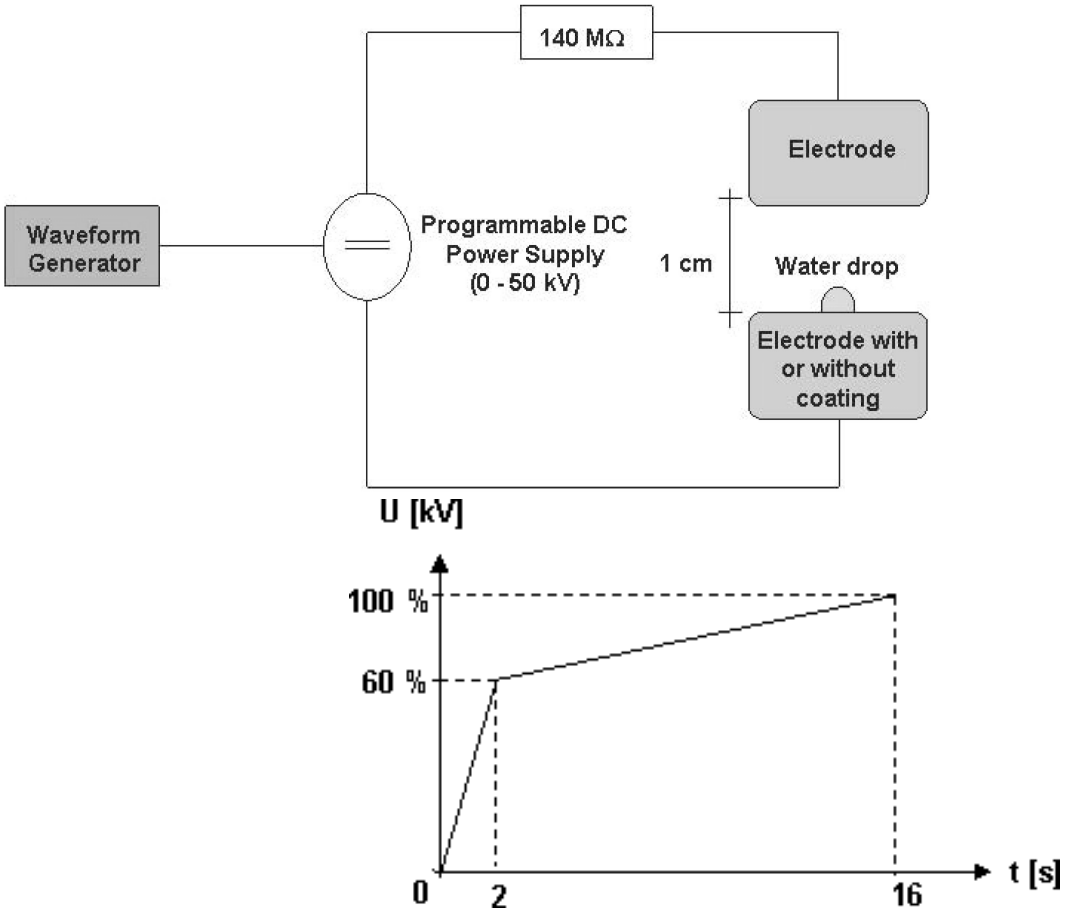

Figure A.1: Experimental configuration: up) The sessile drop in a parallel-plate electrode arrangement was exposed to a ramped electric field; down) the voltage at the instant of instability was recorded as it manifests itself as a load current on the supply.

4. Function generator for any signal shapes connected with the power supply. To have the time to record water drops sequences up to instability, a special function with voltage linearly increasing with time has been programmed as represented in Fig. A.1. With the function chosen, 60% of the chosen maximum voltage amplitude (U) is reached in 2 s, and then the voltage is increased slowly up to the breakdown voltage in typically 14 s.

5. A precision digital oscilloscope LeCroy 9430 to capture, analyze and display electrical current and voltage waveforms.

A.2 Set-up and equipment for AC single drop analysis

To study drop resonances a 30 mm parallel plate discharge gap configuration (120° Rogowski profile electrodes), in the arrangement of Fig. A.2 was used.

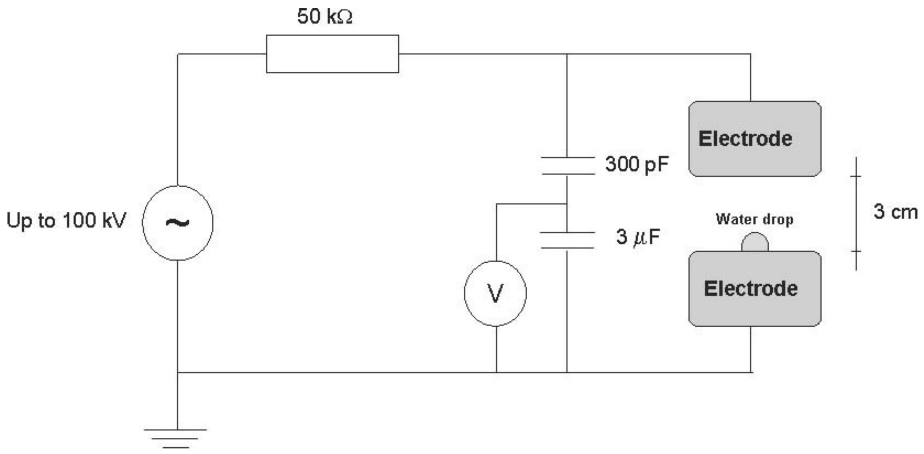

Figure A.2: Circuit diagram of the AC measurements.

Drop resonances have been observed by three different techniques:

1. "Natural"drop oscillation to instability manifesting itself in repetitive Trichel pulse packets (as with DC) observed by current measurement.

2. Variable frequency AC excitation with optical observation at small amplitudes (resonances only just perceptible) and at large amplitudes leading to instability.

3. Optical observation of resonant drop breakup [61].

A.3 Experimental set-up to test measures to reduce tonal emissions

The laboratory set-up consisted of the high voltage electric circuit, the measurement devices and the rain simulator system. The high voltage elements were positioned inside a Faraday cage, while the voltage control units were located in the adjacent room in order to offer low RI, light and sound backgrounds. The laboratory set-up is presented in Figure A.3.

In Figure A.4 the equivalent electric circuit is shown. It is essentially composed of the resistance R of 50 kΩ, to provide protection for the AC source, the voltage divider to obtain the effective value of the voltage (in the figure,

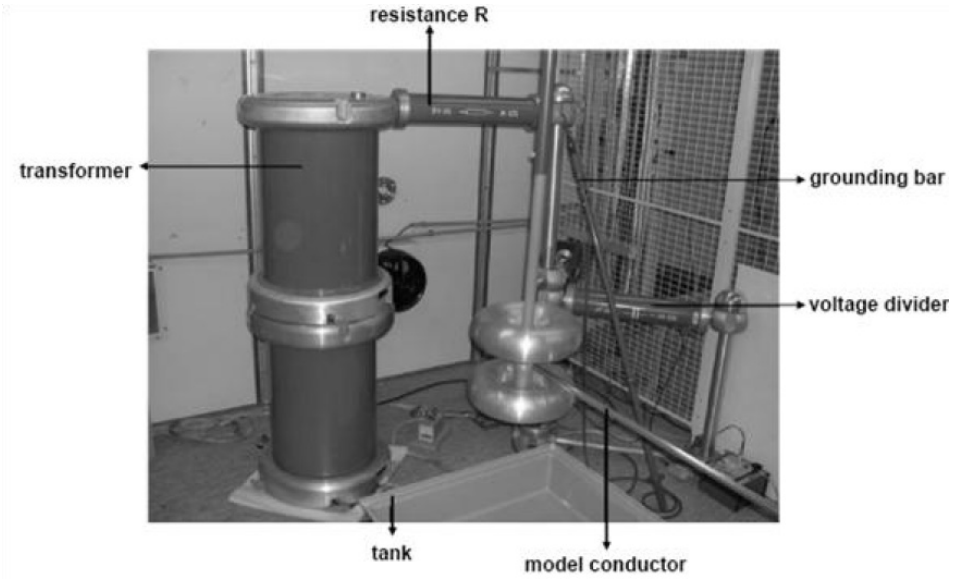

Figure A.3: Laboratory overview.

$C_1 = 300\text{pF}, C_2 = 3\mu\text{F}$ and $R_V = 1.3\text{M}\Omega$) and the capacitance C_E of 13 pF representing the capacitance between the conductor and the ground.

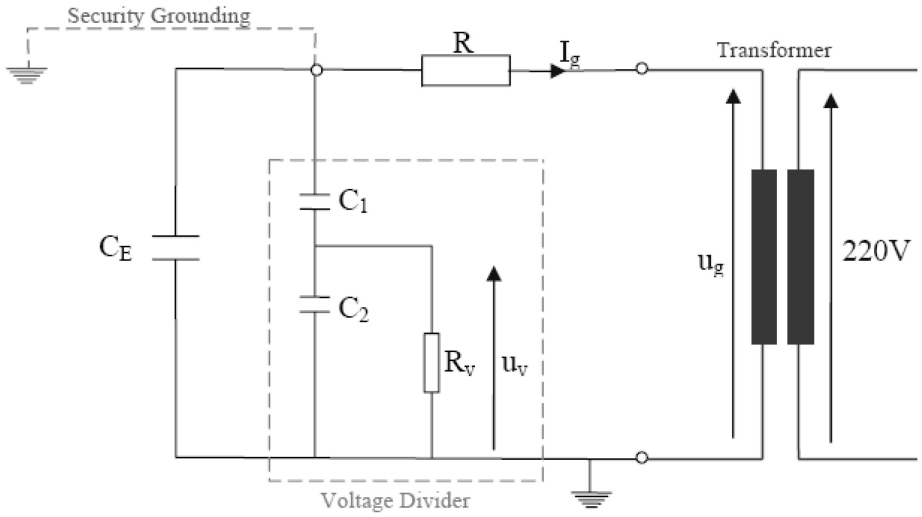

Figure A.4: Equivalent electric circuit.

For a typical distance from ground of 78 cm, this results in electric field strengths on the surface of less than 20 $\text{kV}_{\text{rms}}/\text{cm}$ at an applied voltage of 100 kV_{rms} (see Fig. A.5).

The 1.5 metre long, 20 mm diametre model conductor has been exposed to rain from a nozzle with deionized water sprayed by compressed air at constant pressure, typical rate 100 mm/min, and representing heavy rain, followed by a drying period. Before spraying commenced it was always ascertained that the

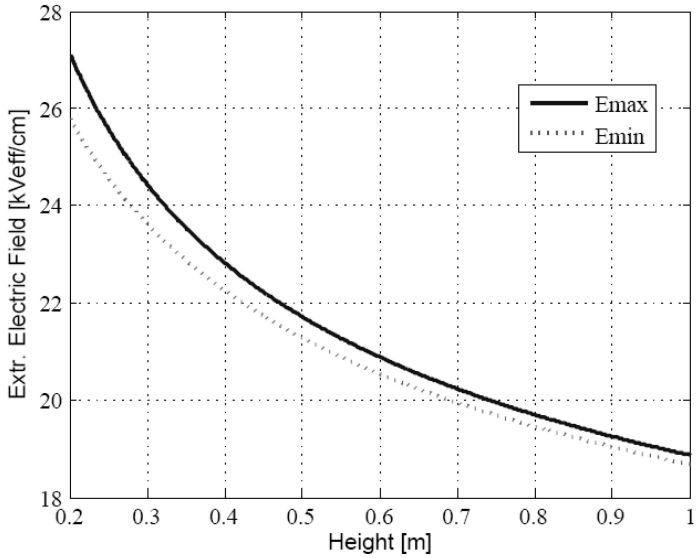

Figure A.5: Electric field strengths for a 20 mm diameter tubular conductor at an applied voltage of 100 kV_{rms} for different conductor-ground distances.

set-up was- in the dry state - totally free from partial discharges (< 1 pC) at the intended operating voltage. The microphone used for AN measurements was located at the conductor-to-ground distance of 78 cm above the floor and 1 m from the centre section of the conductor.
Diagnostics included:

1. Sound pressure level Lp(r) detection with third-octave band filter (Nor118 Sound Level Meter).

2. PD emission recorded and displayed against AC waveform (ICMsystem, PD System GmbH).

3. Visual observation of discharges on the conductor by means of UV image converter

4. Up to 10000 fps framing camera (MotionPro) to record deformation of water drops on the conductors. In order to have sufficient light intensity for fast framing, the center section of the conductor and the background had to be intensely illuminated by means of a high pressure mercury vapour arc lamp.

B Programs for the evaluation of the data

B.1 Evaluation of contact angle

B.1.1 Sample image treatment

In the routine image processing of a single drop picture, the following steps are utilized :

- the image of the water drop is acquired;
- the area of interest is identified and optimized first;
- a threshold transformation yields the picture in a binary matrix;
- before the required morphological operations could be performed the matrix values are inverted;
- a pruning cycle on the dark boundaries onto the contiguous white pixels follows;
- the creation of a skeletized image of the drops is generated.

B.1.2 Contour of a drop

```
I = imread('f.jpg');
imshow(I);
start_row = 220;
start_col = 50;
cropRGB = I(220:350, 50:350);
imshow(cropRGB)
offsetX = start_col-1;
offsetY = start_row-1;
threshold = graythresh(cropRGB);
bw = im2bw(cropRGB,threshold);
bw = ~bw;
% complement the image (objects of interest must be white)
imshow(bw)
% remove all object containing fewer than 30 pixels
bw = bwareaopen(bw,30);
```

```
% fill a gap in the pen's cap
se = strel('disk',2);
bw = imclose(bw,se);
% fill any holes, so that regionprops can be used to estimate
% the area enclosed by each of the boundaries
bw = imfill(bw,'holes');
imshow(bw)
% trace only the contour of the droplet
hy = fspecial('sobel');
hx = hy';
Iy = imfilter(double(bw), hy, 'replicate');
Ix = imfilter(double(bw), hx, 'replicate');
A= sqrt(Ix.^2 + Iy.^2);
imshow(A,[])
res=A;
```

B.1.3 Calculate the contact angle

```
% Calculate the angle of a droplet
% assumptions: x axis is horizontal-> the second biggest a angle
% is the one of the tangent, the first biggest is 90
% idea the angle in every point is the product of the gradient
% multiplied by the vector with coordinates (-1,0) if we consider
% positives the angles at the right of the droplet
% method: compute partial derivatives, calculate angle of gradient,
% remove the maximum and take the arcos of the second maximum
% the calculation of partial derivatives should be verified!! And the
% whole method tested with empirical observations
% usage: dangle('droplet','jpg') if the file is 'droplet.jpg'
function res = dangle(file,type)
% read image
A=imread('Copy of 1-100ul_00000V.bmp');
% convert image to gray
B=rgb2gray(A);
% do contourn detection! May be not necessary, test different methods
% like reberts,sobel,prewitt, etc;
%B=edge(B,'roberts');
%define masking matrixes for partial derivative calculation
dx=[-1 0 1; -1 0 1;-1 0 1]; dy=dx';
% compute partial derivatives using convolution (VERIFY!!
% that the formula is OK)
Ix=conv2(B,dx,'same'); Iy=conv2(B,dy,'same');
% magic formula: project the gradient to x axis
% and calculate cosinus of angle
G = [ Ix ./ (sqrt(Ix.^2 .* Iy.^2))];
% !handle warning division by zero!
% find angle in radiants
Gr=acos(G);
% remove the maximum angle (should be 3.14), set the maximum
% to -1.0 and verify that the maximum is always pi !!
% compute maximum
m=max(max(Gr));
for i = 1:size(B,1)
    for j=1:size(B,2)
        if (Gr(i,j)==m) F(i,j)=-1.0;
```

```
            else F(i,j)=Gr(i,j);
        end
    end
end
% convert the maximum angle from radiants to grads
res=max(max(F))*90/pi;
```

B.1.4 The tangent method

```
% Trace horizontal line, tangent on the right and output angle
% input has to be an image with WHITE countours!!
function angle = drangle(A);
R=sum(A')';
[a,b]=max(R);
res=b;
figure imshow(A);
hold on;
line([1 size(A,2)], [res res], 'color',[1 0 0]);
% compute tangent on the right
% first invert colors, since need to find black points!!
A=~A;
% this part is tricky, try with more points!! The parameter is res-i
% first intersection point
p1=boundary(A,[size(A,2);res-1],'W');
% second intersection point
p2=boundary(A,[size(A,2);res-12],'W');
% third intersection point
p3=boundary(A,[size(A,2);res-18],'W');
% fourth intersection point
p4=boundary(A,[size(A,2);res-22],'W');
l=polyfit([p1(1);p2(1);p3(1);p4(1)],[p1(2);p2(2);p3(2);p4(2)],1);
%trace line, find coordinates
x1=1; x2=size(A,2); y1=dot(l,[x1;1]); y2=dot(l,[x2;1]);
line([x1 x2],[y1 y2],'color',[0 0 1])
% compute angle
% tangent to form positive angle
v1=-[1 l(2)]
%horizontal axis
v2=[-1 0];
% find norm of the v1 and v2
nv1=sqrt(sum(v1.^2)); nv2=sqrt(sum(v2.^2));
%angle
angle=acos(dot(v1,v2)/(nv1*nv2))*(180/pi);
%plot result
```

B.1.5 The fitted-curve method

```
% fit circle using polinomial regression
% input:Matrix A
%function angle=circle(A)
filter=fspecial('average');
% invert,
```

```
B=conv2(A,filter,'same');
%B=im2bw(B,0.31);
%empirical finding, threshold is 14 times the average pixel density
%B=im2bw(B,mean(mean(B)*14));
%compute the boundary
% invert B
B=~B;
n=6; %number of splits
inf=round(size(B,2)/n); sup=(n-1)*inf; R=[]; t=1; for i=inf:sup
    b=boundary1(B,[i;1],'S');
    R(t,1)=b(1);
    R(t,2)=b(2);
    t=t+1;
end
% fit polinom
l=polyfit(R(:,1),R(:,2),8);
% trace polinomium
eval=polyval(l,[1:size(B,2)]); figure B=~B;
%imshow(B);
imshow(A); hold on;
%plot circle
plot([1:size(B,2)],eval,'m','LineWidth',3);
% now plot line
origin=hline(B)
% evaluate angle of intersection
% new polinom is
l2=l l2(1,size(l,2))=l(1,size(l,2))-origin
%derivate of the polinomial
derivate=polyder(l)
%evaluate derivate in roots
tang=polyval(derivate,roots(l2));
%the angle is the atan
angles=atan(tang);
% convert in degrees
angles=angles.*(180/pi);
angle=angles;
hold on;
angle
```

B.2 Evaluation of water drops population

B.2.1 Image processing

To analyze an image of water drops, the following steps are utilized:

- Use a command that counts and measures objects in binary or thresholded images. It works by scanning the image or selection until it finds the edge of an object.
- The command outlines the object using a tool that creates a selection by tracing objects of uniform colour or thresholded objects.

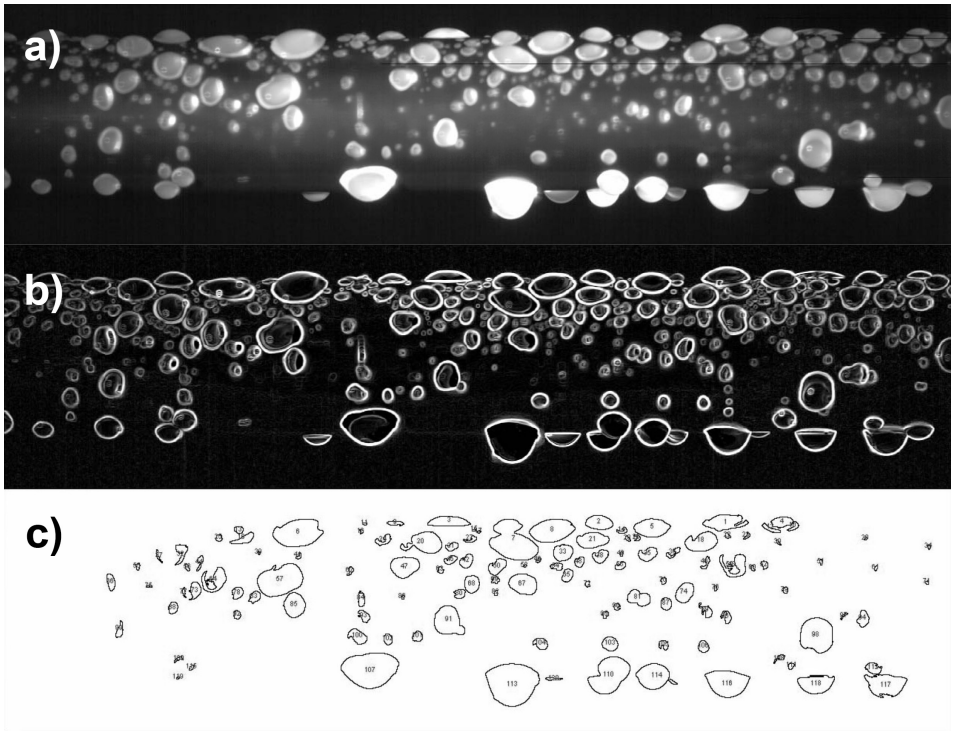

Figure B.1: a) Original image; b) finding the edges of drops; c) applying the function 'threshold'.

- The command fills in the object to make it invisible, then resumes scanning until it reaches the end of the image or selection.

B.2.2 Edge detection of drops using different filters

```
%  I0 - original picture
clear; Filename = 'picture.jpg'; Filetype = 'jpg';
%
I0 = imread(strcat(Filename,'.',Filetype),Filetype);
imshow(I0);title('Original Image'); [nvert,nhoriz]=size(I0);
%%%%%%%%%%%%%%%%%%%%%%%%%%%%%%%%%%%%%%%%%%%%%%%%%%%%%%%%%%%%%%%%%%%
%  conversion: color -> black and white
%  I0 = rgb2gray(I0);
%%%%%%%%%%%%%%%%%%%%%%%%%%%%%%%%%%%%%%%%%%%%%%%%%%%%%%%%%%%%%%%%%%%
%  I0 -> I1: contrast improving
threshold=150; contrast_gamma=1;
%
I1 = imadjust(I0,[threshold/255 max(max(double(I0)))/255],[0
1],contrast_gamma); figure; imshow(I1); title('Contrast
Enhancement');
%%%%%%%%%%%%%%%%%%%%%%%%%%%%%%%%%%%%%%%%%%%%%%%%%%%%%%%%%%%%%%%%%%%
%  I1 -> I2:  noise suppression using the Wiener filter
mit_Wiener=logical(0); I2=I1;
%
if mit_Wiener, I2 = wiener2(I1);
     I2 = imadjust(I2,stretchlim(I2),[]); I2 = wiener2(I2);
```

```
     figure; imshow(I2);
     title('2x Noise Filter (Wiener)'); end;
%%%%%%%%%%%%%%%%%%%%%%%%%%%%%%%%%%%%%%%%%%%%%%%%%%%%%%%%%%%
%  I2 -> I3:  detection of contour
%  possible filter:
filtermethod=char('log','sobel','canny','roberts','prewitt',
'zerocross');
%   [1] Laplace-Gauss
%   [2] Sobel
%   [3] Canny
%   [4] Roberts
%   [5] Prewitt
%   [6] Zerocross
edge_detection=logical(1); I3=I2; fm=1; edge_thresh=0.5;
%
if edge_detection, [I3,thresh] = edge(I2,filtermethod(fm,:));
thresh;
    I3 = edge(I2,filtermethod(fm,:),thresh*edge_thresh);
    figure; imshow(imcomplement(I3));title(filtermethod(fm,:));
    title('Edge Detection from Greylevel Image'); end;
% figure; imshow(imcomplement(I3))
%%%%%%%%%%%%%%%%%%%%%%%%%%%%%%%%%%%%%%%%%%%%%%%%%%%%%%%%%%%
%  working with I2: background detection
for j=1:nvert,
[count(j),pix(j)]=max(hist(double(I2(j,:)),0:1:255)); end; figure;
hold on; plot(pix);
%  fit function for the background:  y = -(x+a)^n
%  Bimodal
nstart=logical(1); nend=logical(0); k=1; for j=2:nvert,
    if nstart, if pix(j)>1, x1(k)=j-1; nstart=logical(0);
    nend=logical(1); end;
    if nend, if pix(j)==1, x2(k)=j; nstart=logical(1);
    nend=logical(0); k=k+1; end; end;
    end;
%  warning: correction by hand is necessary
%          : region 1: x1(1) -> x2(1)
%            region 2: x1(2) -> x2(3) ... almost two together ...
nc2=3; fun = inline('a(2)*(x-a(1)).^2.+a(3)','a','x');
[b1,resnorm] =
lsqcurvefit(fun,[80,-0.1,250],x1(1):1:x2(1),pix(x1(1):x2(1)));
[b2,resnorm] =
lsqcurvefit(fun,[80,-0.1,250],x1(2):1:x2(nc2),pix(x1(2):x2(nc2)));
%
%  background vector:
bg(1:nvert)=0; for i=x1(1):x2(1), bg(i)=b1(2)*(i-b1(1)).^2.+b1(3);
end; for i=x1(2):x2(nc2), bg(i)=b2(2)*(i-b2(1)).^2.+b2(3); end;
plot(1:1:nvert,bg,'r-'); xlabel('Line Number'); ylabel('Average
Greyvalue');
```

C Identification of the drop population

C.1 The influence of rain rate on the drop population

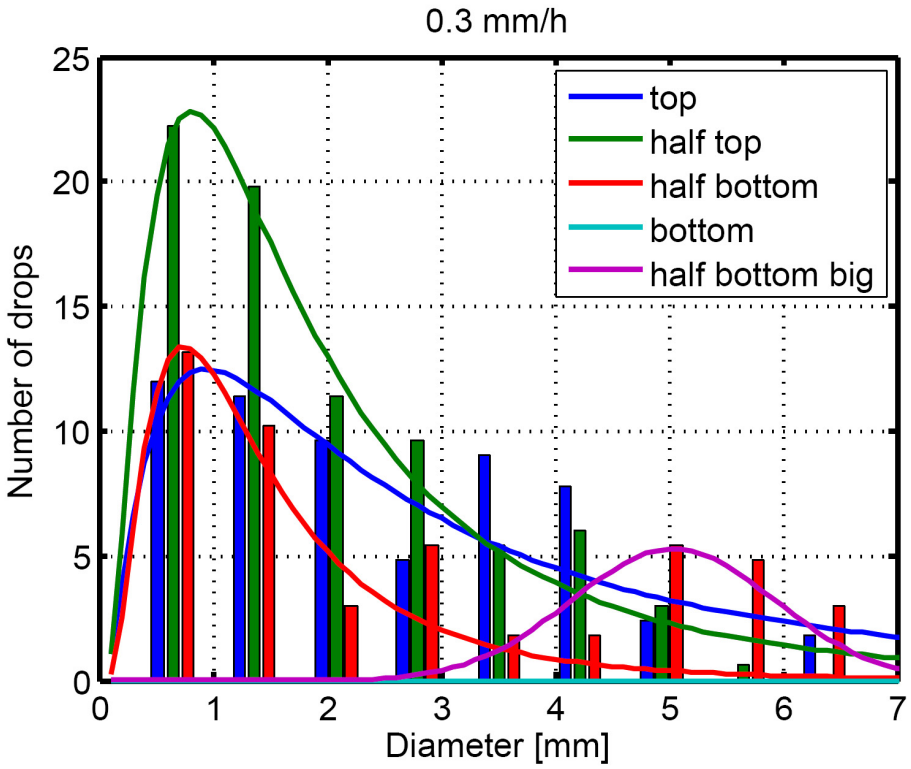

Figure C.1: Drop population on an untreated aluminium model conductor with a rain rate of 0.3 mm/h. Top: distribution: lognormal, mean diameter: 4.4 mm. Half top: distribution: lognormal, mean diameter: 2.4 mm. Half bottom: distribution: lognormal, mean diameter: 1.6 mm. Bottom: distribution: gamma, mean diameter: 2.7 mm. Only big drops half bottom: distribution: *normal*, mean diameter: 5.0 mm.

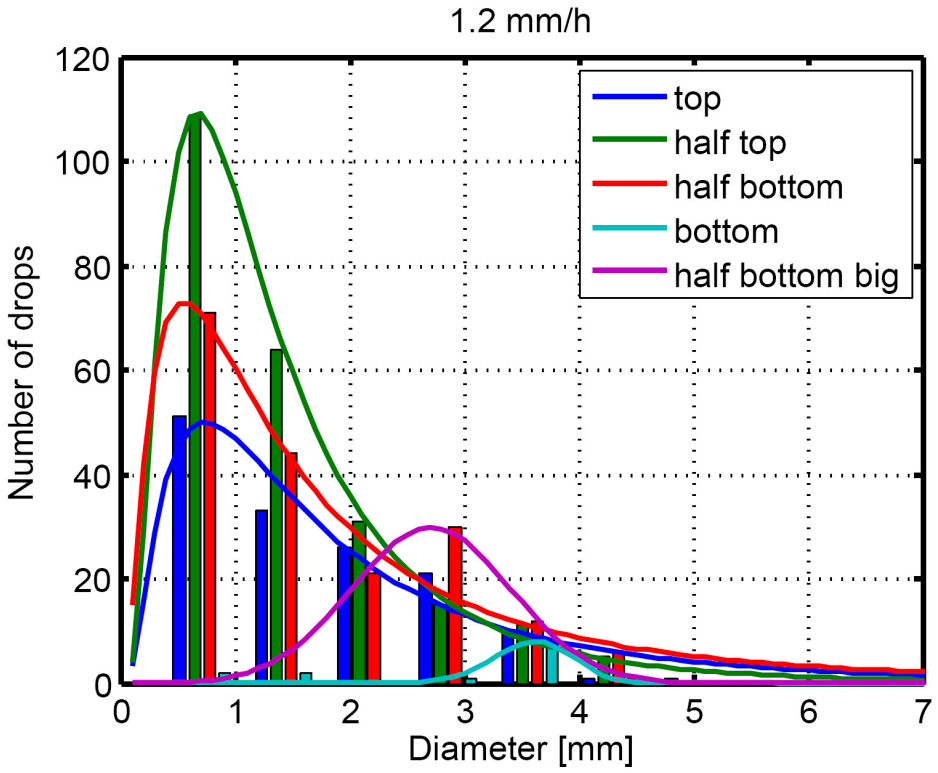

Figure C.2: Drop population on an untreated aluminium model conductor with a rain rate of 1.2 mm/h. Top: distribution: lognormal, mean diameter: 2.2 mm. Half top: distribution: lognormal, mean diameter: 1.5 mm. Half bottom: distribution: lognormal, mean diameter: 2.0 mm. Bottom: distribution: gamma, mean diameter: 3.6 mm. Only big drops half bottom: distribution: *normal*, mean diameter: 2.7 mm.

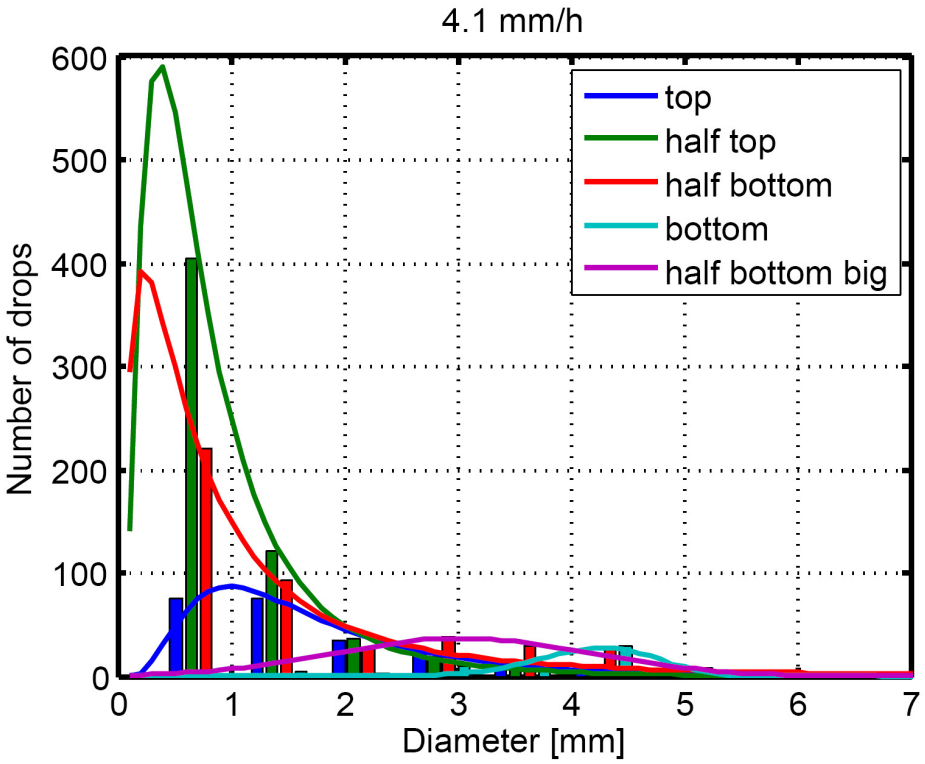

Figure C.3: Drop population on an untreated aluminium model conductor with a rain rate of 4.1 mm/h. Top: distribution: lognormal, mean diameter: 1.8 mm. Half top: distribution: lognormal, mean diameter: 0.9 mm. Half bottom: distribution: lognormal, mean diameter: 1.3 mm. Bottom: distribution: gamma, mean diameter: 4.2 mm. Only big drops half bottom: distribution: *normal*, mean diameter: 3.0 mm.

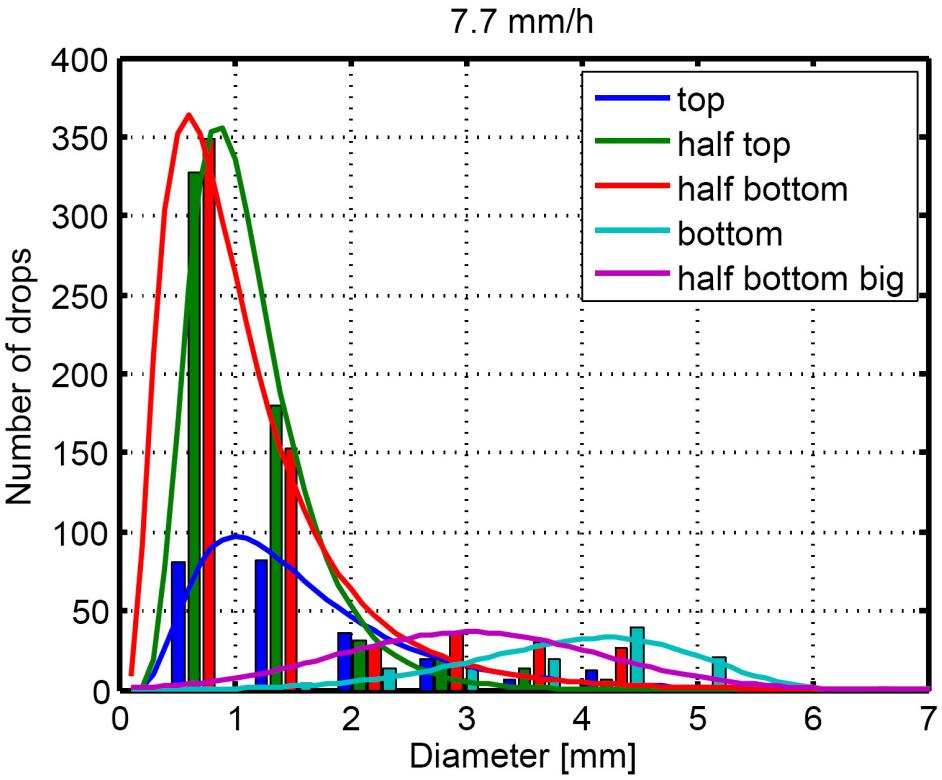

Figure C.4: Drop population on an untreated aluminium model conductor with a rain rate of 7.7 mm/h. Top: distribution: lognormal, mean diameter: 1.6 mm. Half top: distribution: lognormal, mean diameter: 1.1 mm. Half bottom: distribution: lognormal, mean diameter: 1.1 mm. Bottom: distribution: gamma, mean diameter: 3.9 mm. Only big drops half bottom: distribution: *normal*, mean diameter: 3.0 mm.

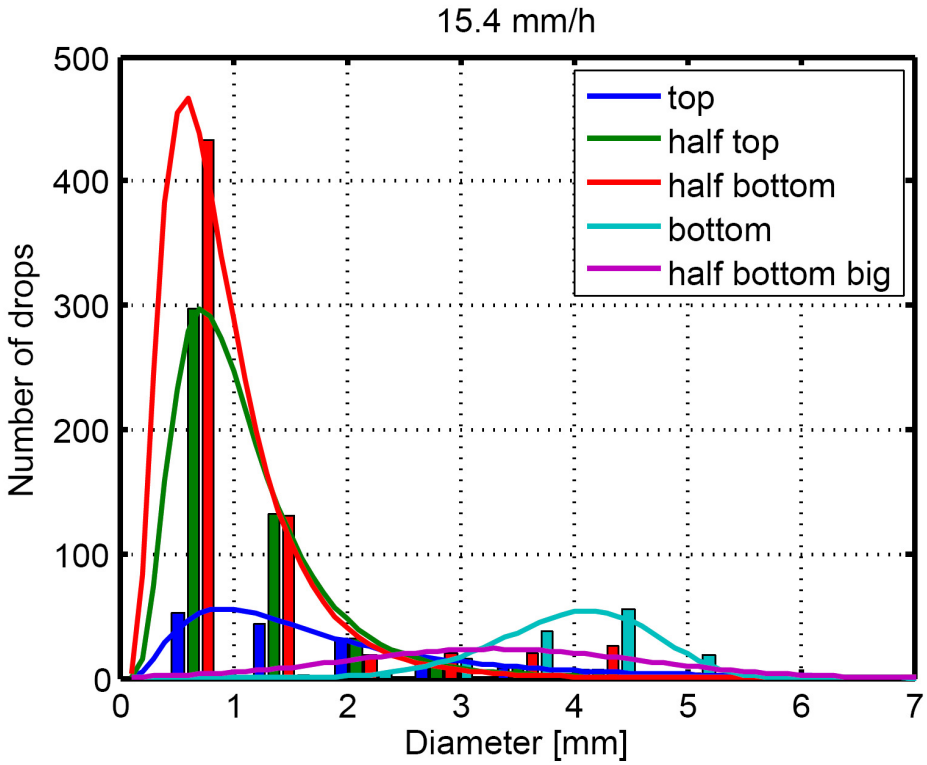

Figure C.5: Drop population on an untreated aluminium model conductor with a rain rate of 15.4 mm/h. Top: distribution: lognormal, mean diameter: 1.9 mm. Half top: distribution: lognormal, mean diameter: 1.1 mm. Half bottom: distribution: lognormal, mean diameter: 0.9 mm. Bottom: distribution: gamma, mean diameter: 4.0 mm. Only big drops half bottom: distribution: *normal*, mean diameter: 3.3 mm.

D Abbreviations and symbols

Abbreviations

AN	Audible Noise
AC	Alternate Current
DC	Direct Current
CONOR	COrona NOise Reduction
UV	Ultra Violet
PD	Partial Discharges
WC	Wettability Class
CVD	Chemical Vapour Deposition

Symbols

δ [-]	relative air density
γ [kg/s^2 = N/m]	surface tension
γ_{LV} [kg/s^2 = N/m]	surface tension between the liquid and the air
γ_{SL} [kg/s^2 = N/m]	surface tension between the liquid and the solid surface
γ_{SV} [kg/s^2 = N/m]	surface tension between the surface and the air
ε_0 [$A^2 \cdot s^4/(kg \cdot m^3 = A \cdot /(V \cdot m))$]	permittivity of free space
ε_r [-]	relative dielectric constant
θ [°]	contact angle
θ_a [°]	advancing contact angle
θ_r [°]	receding contact angle
ρ [mm/h]	rain rate
τ [s]	drop lifetime
A_b [m^2]	water drop base aerea
a_{sub} [mm]	radius of the subconductor in a bundle

A_s [m^2]	water drop area
b_r [mm]	radius of the bundle
d [mm]	common for diameter (conductor or water drop)
E_0 [$kg \cdot m/(A \cdot s^3) = V/m$]	original electric field strength
E_c [$kg \cdot m/(A \cdot s^3) = V/m$]	critical electric field strength (corona inception)
E_{cr} [$kg \cdot m/(A \cdot s^3) = V/m$]	critical electric field strength
$E_{cr_{charged}}$ [$kg \cdot m/(A \cdot s^3) = V/m$]	critical electric field strength for a charged drop
F [Hz]	Trichel pulse frequency
G [V/m]	average maximum gradient
h [mm]	height of the water drop
I [A]	time-averaged corona current
n [-]	number of subconductors in a bundle
P [dB]	generated acoustic power
P(d)[-]	distribution of water drops
Q [$A \cdot s = C$]	charge
Q_R [$A \cdot s = C$]	Rayleigh charge
r [mm]	common for radius (conductor or water drop)
S [mm]	needle-to-plane spacing
v [m/s]	drop fall velocity
V_l [m^3 or l]	water drop volume
V [$kg \cdot m^2/(A \cdot s^3) = V$]	applied voltage
V_0 [$kg \cdot m^2/(A \cdot s^3) = V$]	threshold voltage

List of Figures

List of Tables

Bibliography

[1] P. S. Maruvada. *Corona performance of high voltage transmission lines*, chapter 6.6, pages 164–165. Research Studies Press Ltd. Bardock, Hertfordshire, England, 2000.

[2] E. R. Taylor, V. L. Chartier, and D. N. Rice. Audible noise and visual corona from HV and EHV transmission lines and substation conductors - laboratory tests. In *IEEE Trans. PAS*, volume 88(5), pages 666–679, 1969.

[3] D. E. Perry. An analysis of transmission line audible noise levels based upon field and three-phase test line measurements. In *IEEE Trans. PAS*, volume 91(3), pages 857–865, 1972.

[4] U. Straumann. *Berechnung und Reduktion der tonalen Geräuschemission von Hochspannungsfreileitungen*. PhD thesis, Eidgenössische Technische Hochschule, Nr.17408, Zürich, Switzerland, 2007.

[5] T. H. Teich and H. J. Weber. Tonal emission from high voltage lines. In *XIVth International Conference On Gas Discharges and Their Applications*, volume 1, pages 259–262, Liverpool, England, 2002.

[6] T. H. Teich and H. J. Weber. Origin and abatement of tonal emission from high voltage transmission line. In *Elektrotechnik und Informationstechnik e&i*, volume 119(1), pages 103–113, 2002.

[7] B. Parmigiani and A. Lanfranconi. *Above-ground conductor unit with corona noise reducing covering comprising a conductive material and a hydrophilic material*. Cavi Pirelli S.p.A., United States Patent No.4’358’637, Milan, Italy, 1982.

[8] K. Saruwatari, T. Saito, A. Okazato amd K. Kounosu, T. Inoue, T. Hita, and M. Maejima. *Aluminum conductor of low audible noise transmission*. United States Patent No.4’759’805, Japan, 1988.

[9] N. G. Trinh. Partial discharge XIX: Discharge in air. part I: Physical mechanisms. In *IEEE Electrical Insulation Magazine*, volume II(2), pages 23–29, 1995.

[10] N. G. Trinh. Partial discharge XIX: Discharge in air. part II: Selection of line conductors. In *IEEE Electrical Insulation Magazine*, volume II(3), pages 5–11, 1995.

[11] Q. Vuhuu and R. P. Comsa. Influence of gap length on wire-plane corona. In *IEEE Trans. PAS*, volume 88(10), pages 1462–1471, 1969.

[12] R. T. Waters, T. E. Richard, and W. B. Stark. Electric field measurements in d.c. corona discharge. In *IInd International Conference On Gas Discharges IEE Conference Publication, No. 90*, pages 188–190, London, England, 1972.

[13] N. G. Trinh and B. J. Jan. Modes of corona discharges in air. In *IEEE Trans. PAS*, volume 87(5), pages 1207–1215, 1972.

[14] R. T. Waters, T. E. S. Richard, and W. B. Stark. Direct measurement of electric field at line conductors during a.c. corona. In *Proc. IEE*, volume 119(6), pages 717–723, 1972.

[15] Z. Engel and T. Wszolek. Audible noise of transmission lines caused by the corona effect: Analysis, modelling, prediction. In *Applied Acoustics*, volume 47(2), pages 149–163, 1996.

[16] F. Ianna, G. L. Wilson, and D. J. Bosack. Spectral characteristics of acoustic noise from metallic protrusions and water droplets in high electric fields. In *IEEE Trans. PAS*, volume 93(6), pages 1787–1796, 1974.

[17] G. W. Juette and L. E. Zaffanella. Radio noise currents and audible noise on short sections of uhv bundle conductors. In *IEEE Trans. PAS*, volume 89(5/6), pages 902–913, 1970.

[18] M. Akazaki. Corona phenomena from water drops on smooth conductors under high direct voltage. In *IEEE Trans. PAS*, volume 84(1), pages 1–8, 1965.

[19] G. W. Juette and L. E. Zaffanella. Radio noise, audible noise and corona loss of EHV and UHV transmission lines under rain: predetermination based on cage tests. In *IEEE Trans. PAS*, volume 89(6), pages 1168–1178, 1970.

[20] M. G. Comber and L. E. Zaffanella. Audible noise reduction by bundle geometry optimization. In *IEEE Trans. PAS*, volume 92, pages 1782–1791, 1973.

[21] W. C. Pokorny, R. H. Schlomann, H. C. Barnes, and C. J. Miller. Investigation of corona effects from wet bundle conductors for application to UHV configurations. In *IEEE Trans. PAS*, volume 91(1), pages 211–222, 1972.

[22] R. L. Tremaine and A. R. Jones. Corona loss at extra-high voltages. In *Westinghhouse Engineer*, volume 11(5), pages 144–150, 1951.

[23] R. Bräunlich. Psel (Projekt- und Studienfonds des Elektrizitätswirtschaft). S. 34-35, Projekt Nr. 194, Tätigkeitsbericht, 2000.

[24] M. Friedmann. Luft-Ionenmessung bei der Hochspannungsleitung Obersielach-Kainachtel, Lärmmesstelle Klein Preding. Technical report, Arsenal Research. Projekt M1231/1. S.30, Vienna, Austria, April 2000.

[25] U. Straumann and M. Semmler. About the mechanism of tonal emission from high voltage transmission lines. In *XVth International Conference On Gas Discharges and Their Applications*, volume 1, pages 363–366, Toulouse, France, 2004.

[26] N. D. Lerner J. A. Molino, G. A. Zerdy and D. L. Harwood. Use of the acoustic menu in assessing human response to audible (corona) noise from electric transmission lines. In *Journal of the Acoustical Society of America*, volume 66, pages 1435–1445, 1979.

[27] H. Kirkham and W. J. Gajda. A mathematical model of transmission line audible noise, part 1. In *IEEE Trans. PAS*, volume 102(3), pages 710–717, 1983.

[28] H. Kirkham and W. J. Gajda. A mathematical model of transmission line audible noise, part 2. In *IEEE Trans. PAS*, volume 102(3), pages 718–728, 1983.

[29] M. Semmler. Tonal noise during period of rain. In *ETH Power Systems and High Voltage Laboratories*, pages 58–60, Annual Report 2004.

[30] P. de Gennes, F. Brochard-Wyart, D. Quéré, and A. Reisinger. *Capillarity and Wetting Phenomena: Drops, Bubbles, Pearls, Waves*. Springer, ISBN 0387005927, 2004.

[31] A. Adamson and A. Gast, editors. *Physical Chemistry of Surfaces*. Wiley, ISBN 0471610194, New York, 1997.

[32] T. Young. An essay on the cohesion of fluids. In *Philosophical Transactions of the Royal Society of London*, volume 95, pages 65–87, 1805.

[33] J. C. Berg. *Wettability*. Marcel Dekker, ISBN 0824790464, New York, 1993.

[34] O. I. Del Rio, D. Y. Kwok, R. Wu, J. M. Alvarez, and A. W. Neumann. Contact angle measurements by axisymmetric drop shape analysis and an automated polynomial fit program. In *Colloids Surfaces A: Physicochemical and Engineering Aspects*, volume 143(2), pages 197–210, 1998.

[35] P. Dalet, E. Papon, and J.-J. Villenave. Surface free energy of polymeric materials: relevancy of conventional contact angle data analyses. In *Journal of Adhesion science and Technology*, volume 13, pages 857–870, 1999.

[36] IEC TS 62073. *Guidance on the measurement of wettability of insulator surfaces*. 1 edition, 2003-06.

[37] J. D. Malcolm and H. M. Paynter. Simultaneous determination of contact angle and interfacial tension from sessile drop measurements. In *Journal of Colloid and Interfacial Science*, volume 82(2), pages 269–275, 1981.

[38] F. Exl and J. Kindersberger. Messung von Tropfenrandwinkeln auf Isolierstoffoberflächen. In *ETG-Fachtagung, Diagnostik elektrischer Betribsmittel*, pages 67–72, Köln, Germany, 2004. VDE Verlag GmbH Berlin.

[39] S. Keim and D. Koenig. The performance of electrically stressed droplets on insulating surfaces observed with an optical measuring system. In *IEEE Conference on Electrical Insulation and Dieletric Phenomena (CEIDP)*, pages 792–795, Victoria BC, Canada, 2000.

[40] T. Yamada and T. Sugimoto. Resonance phenomena of a single water droplet located on a hydrophobic sheet under ac electric field. In *IEEE Trans. on Industry App.*, volume 39(1), pages 59–65, 2003.

[41] K. S. Birdi and A. Winter. A study of the evaporation rates of small water drops placed on a solid surface. In *Journal of Physical Chemistry*, volume 93(9), pages 3702–3703, 1989.

[42] L. Muszynski, D. Baptista, and J. G. Douglas. A geometrical model to predict the evaporative behavior of spherical sessile droplets on impermeable surfaces. *Journal of Contact Angle, Wettability and Adhesion*, 4:165–176, 2006.

[43] H. Janssen and U. Stietzel. Contact angle measurement on clean and polluted high voltage polymers insulators. In *10th International Symposium on High Voltage Engineering (ISH)*, volume 13, pages 149–152, Montreal, Canada, 1997.

[44] L. Rayleigh. On the equilibrium of liquid conducting masses charged with electricity. In *Philosophical Magazine*, volume 14, series 5, pages 184–186, 1882.

[45] A. J. Phillips, I. R. Jandrell, and J. P. Reynders. Consideration of corona onset from a water drop as a function of air pressure. In *Science, Measurement and Technology, IEE Proceedings*, volume 143(2), pages 125–130, 1996.

[46] W. A. Macky. Some investigation on the deformation and breaking of water drops in strong electric fields. In *Proceedings of the Royal Society of London*, number 133, pages 565–587, 1931.

[47] C. T. R. Wilson and G. I. Taylor. The bursting of soap bubbles in a uniform electric field. In *Mathematical Proceedings of the Cambridge Philosophical Society*, volume 22, part 5, pages 728–730, 1925.

[48] J. Zeleny. Instability of electrified liquid surfaces. In *Physical Review Series 2*, volume 10(1), pages 1–6, 1917.

[49] Sir Geoffrey Taylor. Disintegration of water drops in an electric field. In *Proceedings of the Royal Society of London. Series A, Mathematical and Physical Sciences*, volume 280(1382), pages 383–397, 1964.

[50] P. R. Brazier-Smith, S. G. Jennings, and J. Latham. An investigation of the behaviour of drops and drop-pairs subjected to strong electrical forces. In *Proceedings of the Royal Society of London. Series A, Mathematical and Physical Sciences*, volume A 325, pages 363–376, 1971.

[51] D. Windmar. *Water drop initiated discharges in air*. PhD thesis, University of Uppsala, Sweden, 1994.

[52] M. A. Abbas and J. Latham. The disintegration and electrification of charged water drops falling in an electric field. In *Quarterly Journal of the Royal Meteorological Society*, volume 95, pages 63–76, 1969.

[53] M. A. Abbas and J. Latham. The instability of evaporating charged drops. In *Journal of Fluid Mechanics*, volume 30, part 4, pages 663–670, 1967.

[54] L. B. Loeb. *Electrical Coronas*. University of California Press, Berkeley, page 299, 1965.

[55] M. Hara, S. Ishibe, and M. Akazaki. Corona discharge and electrical charge on water drops dripping from d.c. transmission conductors - an experimental study in laboratory. In *Journal Electrostatics*, volume 6(3), pages 235–257, 1979.

[56] W. N. English and L. B. Loeb. Positive and negative point-to-plane corona in air. In *Physical Review*, volume 74(1), pages 170–178, 1948.

[57] Y. Satoh, Y. Tsunoda, and K. Arai. Corona pulses from a water drop on a cylindrical conductor surface. In *Electrotechnical Journal of Japan*, volume 8(1/2), pages 19–23, 1963.

[58] G. A. Dawson. Electrical corona from water-drop surfaces. In *Journal of Geophysical Research*, volume 75(12), pages 2153–2158, 1970.

[59] J. A. Crabb and J. Latham. Corona from colliding drops as a possible mechanism for the triggering of lightning. In *Quarterly Journal of the Royal Meteorological Society*, number 100, pages 191–202, 1974.

[60] H. A. Elghazaly and G. S. P. Castle. The charge limit of liquid droplets due to electron avalanches and surface disruption. In *7th Conference of Electrostatics*, number 85, pages 121–126, Oxford, England, 1987.

[61] M. Corcoran and J. A. Bicknell. Behaviour of water drop in a uniform electric field. Technical report, Private communication, 2001.

[62] J. A. Robinson, M. A. Bergougnou, G. S. P. Castle, and I. Inculet. The electric field at a conducting liquid surface stressed by an ac voltage. In *1999 IEEE-IAS meeting*, volume 3, pages 1811–1816, 1999.

[63] T. Sugimoto, K. Asano, and Y. Higashiyama. Negative corona discharge at a tip of water cone deformed under dc field. In *Journal of Electrostatics*, volume 53, pages 25–38, 2001.

[64] W. L. Lama and C. F. Gallo. Systematic study of the electrical characteristic of the "trichel"current pulses from negative needle-to-plane corona. In *Journal of Applied Physics*, volume 45(1), pages 103–113, 1974.

[65] A. Rawle. The basic principles of particle size analysis. Technical report, application note MRK038, Malvern Instruments, Malvern, England.

[66] T. Allen. *Particle Size Measurement*. Chapman & Hall, London, England, 1990.

[67] R. Cadle. *Particle Size Theory and Industrial Applications*. Reinhold, New York, USA, 1965.

[68] A. Kuma. *Hydrodynamics and mass transfer in Kühni extractor*. PhD thesis, Eidgenössischen Technische Hochschule, Nr. 7806, Zürich, Switzerland, 1985.

[69] M. Laso. *A model for the dynamic simulation of liquid-liquid dispersions*. PhD thesis, Eidgenössischen Technische Hochschule, Nr. 8041, Zürich, Switzerland, 1986.

[70] A. N. Dingle and H. F. Schulte. A research instrument for the study of raindrop size spectra. In *Journal of Applied Meteorology*, volume 1.

[71] H. E. Green. A sensor for detecting and sizing moving water drops. In *Journal of Electrical and Electronics Engineering*, volume 18(1), pages 1–10, Australia, 1998.

[72] C. Mundo, M. Sommerfeld, and C. Tropea. Droplet-wall collisions: Experimental studies of the deformation and breakup process. In *International Journal of multiphase flow*, volume 21(2), pages 151–173, 1995.

[73] Dwight G. Weldon. *Failure Analysis of Paints and Coatings*. John Wiley & Sons, ISBN 0471490725, Chichester, England, 2005.

[74] Arthur A. Tracton. *Coatings Technology Handbook*. CRC Press, ISBN 1574446495, 3rd edition, 2001.

[75] D. Stoye and W. Freitag. *Paints, Coatings and Solvents*. Wiley-VCH, ISBN 3527288635, Chichester, England, 1998.

[76] A. Fujishima, K. Hashimoto, and T. Watanabe. *TiO_2 Photocatalysis: Fundamental and Applications*. BKV Tokyo, ISBN 493905103X, 1999.

[77] R. E. Kirk D. F. Othmer A. Seidel Kirk-Othmer, J. I. Kroschwitz. *Encyclopedia of Chemical Technology: Vol. 1*. Wiley-Interscience, ISBN 0471485225, 5th edition, 2007.

[78] Teil 1 DIN 50035. *Begriffe auf dem Gebiet der Alterung, Grundbegriffe*. 1989-03.

[79] F. Exl and J. Kindersberger. Contact angle measurement on insulator surfaces with artificial pollution layers and various surface roughnesses. In *14th International Symposium on High Voltage Engineering (ISH)*, page D 47, 2005.

[80] A. Krivda and D. Birtwhistle. Breakdown between water drops on wet polymer surfaces. In *IEEE Conference on Electrical Insulation and Dieletric Phenomena (CEIDP)*, pages 572–579, 2001.

[81] A. N. Jahromi, E. A. Chernery, and S. H. Jayaram. Ageing characteristics of RTV silicone coating materials by corona discharge. In *IEEE Conference on Electrical Insulation and Dieletric Phenomena (CEIDP)*, volume 15(2), pages 444–452, 2008.

[82] A. Moukegengue Imano and A. Beroual. Behavior of water droplets on surface of solid insulator in electric field. In *14th International Symposium on High Voltage Engineering (ISH)*, page D 56, 2005.

[83] S. Keim and D. Koenig. The dynamic behavior of water drops in an ac field. In *IEEE Conference on Electrical Insulation and Dieletric Phenomena (CEIDP)*, pages 613–616, 2001.

[84] L. G. Mallinson. *Ageing Studies and Lifetime Extension of Materials*. Springer, ISBN 0306464772, 2001.

[85] IEC 60216-1. *Electrical insulating materials. Properties of thermal endurance. Part 1: Ageing procedures and evaluation of test results.* 5th edition, 2001-07.

[86] IEC 60216-2. *Electrical insulating materials. Properties of thermal endurance. Part 2: Determination of thermal endurance properties of electrical insulating materials. Choice of test criteria.* 4th edition, 2005-08.

[87] D. R. Maidment. *Handbook of Hydrology*. McGraw-Hill, ISBN 0070397325.

[88] Baudirektion Kanton Zürich. *Umweltbericht für den Kanton Zürich / hrsg. von der Baudirektion Kanton Zürich im Auftrag des Regierungsrates des Kantons Zürich*. 2004.

[89] Meteo Schweiz. *Niederschlagsdaten Stadt Zürich der Jahre 1982-2003*. Source: personal communication from Micha Semmler.

[90] T. N. Daniel and E. B. Whittaker. The reduction of audible corona discharges on A.C. transmission lines. In *IInd International Conference On Gas Discharges and Their Applications*, number 90, pages 197–199, London, England, 1972.

[91] Updating the EPRI transmission line reference book (red book). Technical report, EPRI Project Manager, Palo Alto, USA, http://www.epriweb.com/public/000000000001001763.pdf, 2004.

[92] R. Cortina and M. Sforzini. Effect of audible noise on EHV and UHV line design. In *CIGRE 1972*, pages discussion, group 36.

[93] R. Bartenstein and A. Rachel. "Korona", part II, 400 kV Forschungsgemeinschaft. Sections 6 and 7, Heidelberg, Germany, 1958.

[94] F. W. Peek. *Dielectric Phenomena in High Voltage Engineering*. McGraw-Hill Book Company, New York, London, 2nd edition, pages 38-78, 1920.

[95] C. Roero, T. H. Teich, and H-J. Weber. Mechanical and associated discharge behaviour of sessile water drop. In *XVth International Conference On Gas Discharges and Their Applications*, volume 1, pages 335–338, Toulouse, France, 2004.

[96] C. Roero and T. H. Teich. Contact angle measurements of sessile drops deformed by a dc electric field. In *Journal of Contact Angle, Wettability and Adhesion*, volume 4, pages 165–176, 2004.

[97] P. Letellier, A. Mayaffre, and M. Turmine. Drop size effect on contact angle explained by nonextensive thermodynamics. Young's equation revisited. In *Journal of Colloid and Interface Science*, volume 314(2), pages 604–614, 2007.

[98] R. J. Good and M. N. Koo. The effect of drop size on contact angle. In *Journal of Colloid and Interface Science*, volume 71, pages 283–292, 1979.

[99] P. B. Barber, D. L. V. Couchman, A. G. Morris, and D. A. Swift. Audible noise and electromagnetic radiation emitted by a.c. corona discharges from water droplets. In *VIth International Conference On Gas Discharges and Their Applications, part 1*, pages 134–137, Edinburgh, Scotland, 1980.

[100] T. Schütte and S. Hörnfeldt. Dynamics of electrically stressed water drops on insulating surfaces. In *International Symposium on Electrical Insulation (ISEI)*, pages 201–207, Toronto, Canada, 1990.

[101] M. Semmler. Tonal emission and precipitation. In *ETH Power Systems and High Voltage Laboratories*, pages 62–63, Annual Report 2003.

[102] U. Schreiber. Simulation of single water droplets on high voltage insulators. In *13th International Symposium on High Voltage Engineering (ISH)*, Delft, Netherlands, 2003.

[103] T. Braunsberger, A. Dziubek, W. Kodoll, U. Schümann, and M. Kurrat. PD between water drops influencing hydrophobic processes on SI and EP-resin system. In *13th International Symposium on High Voltage Engineering (ISH)*, Delft, Netherlands, 2003.

[104] M. Semmler, U. Straumann, C. Roero, and T. H. Teich. Tonale Schallemissionen von Hochspannungsfeileitngen: Mechanismus und Reduktionsmassnahmen. In *Bullettin SEV/VSE*, volume 96(5), pages 13–17, 2005.

[105] C. Roero, M. Semmler, U. Straumann, and T. H. Teich. Tonal noise emission from wet high voltage transmission lines. In *14th International Symposium on High Voltage Engineering (ISH)*, pages 38–45, Beijing, China, 2005.

[106] J. F. Hoburg and J. R. Melcher. Current-driven corona-terminated water jets as source of charged droplets and audible noise. In *IEEE Trans. PAS*, volume 94(1), pages 128–136, 1975.

[107] C. Roero and T. H. Teich. Water drops on high voltage transmission lines. In *Electrostatics Society of America Annual Meeting (ESA)*, pages 38–45, Edmonton, Canada, 2005.

[108] M. Semmler. Tonal noise during precipitation. In *ETH Power Systems and High Voltage Laboratories*, pages 63–65, Annual Report 2005.

Curriculum Vitae

Claudia Roero
Born on the 29th of November 1976 in Asti (Italy)
Italian citizen

Dec. 2008 to present: power lines Engineer at Nordostschweizerische Kraftwerke AG (NOK), Baden (CH)

3rd of March 2009: Degree in Advanced Studies in Finance

2nd of December 2008: Doctoral degree

Jan. 2007 - Dec. 2008: student at the Master of Advanced Studies in Finance, Zürich (Uni/ETHZ)

Apr. 2002 - March 2007: Ph.D. student and research assistant at the High Voltage Laboratory of the Swiss Federal Institute of Technology, Zürich (ETHZ), headed by Prof. Dr. K. Fröhlich

12th of July 2001: Degree in Physics University of Turin, Italy (dipl. Phys.)

1995 - July 2001: Master studies in Physics at the University of Turin, Italy

Publication

C. Roero, M. Semmler, U. Straumann and T. H. Teich
Tonal noise emission from wet high voltage transmission lines
Proceedings of the 14th International Symposium on High Voltage Engineering (ISH)
Beijing, China (August 2005)

M. Semmler, U. Straumann, C. Roero and T. H. Teich
Tonale Schallemissionen von Hochspannungsfreileitungen - Mechanismus und Reduktionsmassnahmen
Bulletin SEV/VSE (15 July 2005)

C. Roero and T. H. Teich
Water drops on high voltage transmission lines
Proceedings of the 2005 Electrostatics Society of America Annual Meeting (ESA)
Edmonton, Canada (June 2005)

C. Roero
Stability of photo-catalytic coatings on high voltage transmission lines
Proceedings of the 4th International Workshop on the Utilization and Commercialization of Photocatalytic Systems, Coatings for Clean Surfaces, and Water and Air Purification Methods
Saarbrücken, Germany (October 2004)

C. Roero, T. H. Teich and H-J. Weber
Mechanical and associated discharge behaviour of sessile water drops
Proceedings of the 15th International Conference on Gas Discharges and their Applications
Toulouse, France (September 2004)

C. Roero
Contact angle measurements of sessile drops deformed by a DC electric field
Journal of Adhesion Science and Technology (JAST) and Proceedings of 4th International Symposium on Contact Angle, Wettability and Adhesion
Philadelphia, USA (June 2004)